Last but not least -
Late cell division proteins in *Caulobacter crescentus*

WOLFGANG STROBEL

Last but not least

-

Late cell division proteins in *Caulobacter crescentus*

DISSERTATION

zur Erlangung des Doktorgrades
der Naturwissenschaften
(Dr. rer. nat.)

dem Fachbereich Biologie der
Philipps-Universität Marburg
vorgelegt von

Wolfgang Strobel
aus Bad Saulgau

Marburg, September 2016

Vom Fachbereich Biologie der Philipps-Universität Marburg (HKZ: 1180)

als Dissertation angenommen am 14.11.2016

Erstgutachter: Prof. Dr. Martin Thanbichler

Zweitgutachter: Prof. Dr. Lotte Søgaard-Andersen

Prüfungskommission: Prof. Dr. Peter Graumann

Prof. Dr. Thorsten Waldminghaus

Tag der mündlichen Prüfung am 17.11.2016

Die Untersuchungen zur vorliegenden Arbeit wurden von Oktober 2012 bis Februar 2016 am Max-Planck-Institut für terrestrische Mikrobiologie und am Fachbereich Biologie der Philipps-Universität Marburg unter Leitung von Prof. Dr. Martin Thanbichler durchgeführt.

Die während der Promotion erzielten Ergebnisse werden
in folgender Originalpublikation veröffentlicht:

Strobel, W, Schlimpert, S., Dersch, S., Thanbichler, M. A new late cell division protein involved in organizing cytokinesis under fast-growing conditions in *Caulobacter crescentus* (in Planung).

Ergebnisse aus in dieser Dissertation erwähnten Projekten sind
in folgender Originalpublikation veröffentlicht:

Strobel, W., Möll, A., Kiekebusch, D., Klein, K. E.,Thanbichler, M. (2014). Function and localization dynamics of bifunctional penicillin-binding proteins in *Caulobacter crescentus*. *J Bacteriol*, 196, 1627-1639.

Ergebnisse aus in dieser Dissertation nicht erwähnten Projekten sind
in folgender Originalpublikation veröffentlicht:

Jung, A., Eisheuer, S., Cserti, E., Leicht, O., **Strobel, W.**, Möll, A., Schlimpert, S., Kühn, J., Thanbichler, M. (2015) Molecular toolbox for genetic manipulation of the stalked budding bacterium *Hyphomonas neptunium*. *Appl Environ Microbiol* 81: 736-744.

Dedicated to my loyal companions

Der Beginn aller Wissenschaften ist das Erstaunen,

dass die Dinge so sind, wie sie sind - Aristoteles

Abstract

Bacteria display a high morphological diversity, ranging from spheres to rods and spirals that tremendously vary in size. Similarly, the bacterial envelope has evolved and adapted to different environments in response to evolutionary pressure, resulting in variations in the composition of the cell wall, type and amount of lipids and accessory proteins, thickness, and the presence or absence of an outer membrane. Despite these variations, cell division is a crucial event to generate progeny, which all bacteria have in common and perform in almost the same manner: determination of the cell division site, assembly of a multi-enzyme complex (divisome), and constriction of one or both cell membranes by the formation of a septum, which is realized by remodeling of the peptidoglycan (PG), resulting in the compartmentalization of the cytoplasm and release of the daughter cells. During cell division, PG synthesis provides the force and directionality for constriction of the cell envelope. Thus, many studies have focused over the past decade on proteins involved in PG remodeling during cytokinesis. However, these studies were mainly done in the model organism *Escherichia coli*, leading to a lack of knowledge in another model organism, such as the α-proteobacterium *Caulobacter crescentus*. In this study, we investigated the functional dynamics of bifunctional penicillin-binding proteins (bPBPs) of *C. crescentus* and focused on their role during cell division. Two out of five bPBPs, namely PbpX and PbpY, were identified to be specifically involved in septal PG remodeling. Furthermore, it was shown that their midcell localization is dependent on the late essential cell division protein FtsN, consistent with the finding that PbpX and PbpY are late recruits to the division site. Moreover, they likely interact with FtsL and the putative PG hydrolase DipM, forming a multi-enzyme complex that mediates PG remodeling. In addition, it was demonstrated that, in principle, all bPBPs, except for PbpZ, are functionally redundant and can take over the role of the others, implying that all of them have retained the ability to interact with the divisome. However, each bPBP may preferentially act in specific biosynthetic complexes but additionally be able to provide robust PG synthesis under conditions of intra- or extracellular stress.

In addition to constriction of the cell envelope, bacteria also need to ensure faithful distribution of the replicated sister chromosomes to each daughter cell. To this end, cells require a tight spatiotemporal regulation of DNA replication and segregation of each chromosome copy, to create a DNA-free division plane. Accordingly, the timing of cell division and PG remodeling must be flexible and intimately linked to chromosome dynamics. However, the temporal control mechanisms of cell division are still largely unknown, even in the well-studied model organisms. Here, I report a novel cell division protein CedC, which is a late recruit to the division site and may regulate the timing of cell division in response to the status of DNA at the division plane at the final stage of cell division. It is hypothesized that CedC could constitute a checkpoint that recognizes chromosome dimers at the division site via direct or indirect interaction with the tyrosine-recombinase XerC and FtsA, which slows down PG synthesis. In this way, cells would gain time to resolve chromosome dimers, resulting in faithful distribution of the sister chromosomes and successful division.

Zusammenfassung

Bakterien weisen eine hohe morphologische Vielfalt auf und existieren als Kugeln, Stäbchen und Spiralen, die wiederum sehr variabel in ihrer Größe sind. Ebenso vielfältig ist die bakterielle Zellhülle, die sich im Laufe der Zeit durch evolutionäre Selektion an verschiedenste Umwelteinflüsse angepasst hat. Dabei kann sich die Zellwand in ihrer Zusammensetzung und Dicke, dem Typ und der Anzahl der Lipide, sowie auch dem Fehlen oder Vorhandensein einer äußeren Membran unterscheiden. Trotz dieser Vielfalt ist Zellteilung ein entscheidender Prozess, um Nachkommen zu erzeugen, den alle Bakterien gemeinsam haben und der sich generell im Ablauf ähnelt und folgende Schritte umfasst: Festlegung der Zellteilungsebene, Aufbau eines Zellteilungsapparates, bestehend aus einer Vielzahl von Proteinen (Divisom), und letztendlich Einschnürung aller Membranen durch die Bildung eines Septums, die durch den Umbau von Peptidoglykan an der Zellteilungsebene bewerkstelligt wird. Dies führt letztendlich zur Zellkompartimentierung und Freisetzung der Tochterzelle. Während der Zellteilung stellt der Umbau des Peptidoglykans die treibende Kraft zur Einschnürung der Zellhülle dar. Daher haben sich eine Reihe von Studien in den letzten Jahrzehnten auf Proteine konzentriert, die an diesem Prozess beteiligt sind. Allerdings ist die Forschungsarbeit hauptsächlich auf den Modelorganismus *Escherichia coli* beschränkt, sodass tiefere Erkenntnisse in anderen Modelorganismen wie dem α-Proteobakterium *Caulobacter crescentus* fehlen. Im Rahmen dieser Arbeit wurde daher die funktionelle Dynamik von bifunktionellen Penicillinbindeproteinen (bPBPs) in *C. crescentus* untersucht und der Fokus auf ihre Rolle während der Zellteilung gelegt. Die Ergebnisse zeigen, dass zwei der fünf bPBPs, PbpX und PbpY, spezifisch an der Peptidoglykansynthese in der Zellteilungsebene mitwirken. Außerdem zeigen die Studien, dass ihre Rekrutierung zur Zellteilungsebene vom späten und essentiellen Zellteilungsprotein FtsN abhängig ist. Dieses Ergebnis stimmt mit der Beobachtung überein, dass PbpX und PbpY erst spät zur Zellteilungsebene rekrutiert werden. Ferner interagieren beide Proteine mit FtsL und der putativen Peptidoglykanhydrolase DipM und sind daher wahrscheinlich Teil eines Multienzymkomplexes, der den Umbau von Peptidoglykan bewirkt. Zusätzlich konnte gezeigt werden, dass im Prinzip jedes bPBP, außer PbpZ, die Aufgaben der anderen übernehmen kann, was bedeutet dass, alle von ihnen ihre Fähigkeit, mit dem Divisom zu interagieren, beibehalten haben. Jedoch wirkt wahrscheinlich jedes bPBP vorzugsweise an spezifischen biosynthetischen Prozessen mit und trägt im Falle von intra- oder extrazellulärem Stress zu einer robusteren Peptidoglykansynthese bei.

Neben der Einschnürung der Zellhülle müssen Bakterien ebenso sicherstellen, dass die replizierten Schwesterchromosomen an die Tochterzelle weitergegeben werden. Für diese Aufgabe benötigen Zellen eine streng kontrollierte räumliche und zeitliche Regulation von DNS-Replikation und Chromosomensegregation, um zu gewährleisten, dass die Zellteilungsebene frei von DNS ist. Daher muss die Zellteilung und folglich der Umbau des Peptidoglykan zeitlich flexibel und in enger Kopplung mit der Chromosomendynamik erfolgen. Jedoch sind solche Kontrollmechanismen selbst in den meisten Modellorganismen noch weitestgehend unerforscht. In dieser Arbeit wird gezeigt, dass ein neuartiges Zellteilungsprotein, CedC, spät zur Zellteilungsebene rekrutiert wird und möglicher-

weise die Zellteilung zeitlich in Bezug zum Status von DNS in der Zellteilungsebene reguliert. Es wird vermutet, dass CedC einen Kontrollpunkt darstellen könnte der Chromosomendimere in der Zellteilungsebene durch direkte oder indirekte Interaktion mit der Tyrosinrekombinase XerC erkennt und im Zuge dessen die Peptidoglykansynthese mit Hilfe von FtsA verlangsamt. Dadurch würden die Zellen mehr Zeit gewinnen um die Chromosomendimere aufzulösen, was zu einer erfolgreichen Aufteilung der Schwesterchromosomen und somit zur Teilung führt.

Contents

Abstract ix

Zusammenfassung xi

1 Introduction 1

1.1 Biology of the bacterial cell wall . . . 1

1.1.1 Peptidoglycan - a robust and highly flexible mesh all at once . . . 1

1.1.2 Building a wall - synthesis of peptidoglycan . . . 3

1.2 Bacterial cell proliferation . . . 5

1.2.1 Diversity of bacterial growth . . . 5

1.2.2 The organism of interest - *Caulobacter crescentus* . . . 6

1.2.3 Getting larger - cell elongation in bacteria . . . 7

1.2.4 Building a contractile ring - assembly of the divisome . . . 10

1.2.5 Spatiotemporal hustle - coordination of final chromosome segregation with late stage of cell division . . . 14

1.3 Scope . . . 16

2 Results 19

2.1 Dynamics of bifunctional penicillin-binding proteins in *C. crescentus* . . . 19

2.1.1 The bifunctional penicillin-binding proteins of *C. crescentus* . . . 19

2.1.2 Localization dynamics of bPBPs in *C. crescentus* . . . 21

2.1.3 PbpX and PbpY are late cell division proteins . . . 21

2.1.4 Divisome localization is dependent on the late-stage actor FtsN . . . 24

2.1.5 bPBPs are functionally redundant . . . 27

2.1.6 bPBPs as part of the divisome . . . 31

2.2 New cell division proteins in *C. crescentus* . . . 33

2.2.1 Identification of CedC and CedD . . . 33

2.2.2 Characterization of CedC and CedD . . . 35

2.2.3 CedC is a late acting cell division protein . . . 36

2.2.4 CedC is required for proper cell division under fast growing conditions . . . 39

2.2.5 CedC acts independent of XerCD . . . 42

2.2.6 Searching for interaction partners of CedC . . . 43
2.2.7 Functional analysis of CedC . . . 47

3 Discussion 53

3.1 Bifunctional penicillin-binding proteins involved in the late stage of cell division . . . 53
3.1.1 PbpX and PbpY are divisome-specific bPBPs . . . 53
3.1.2 The role of Pbp1A, PbpC, and PbpZ regarding cell division . . . 56
3.1.3 Regulation of bPBP activity . . . 57
3.2 CedC - a potential regulator of cell division . . . 59
3.2.1 CedC domain architecture and conservation . . . 59
3.2.2 CedC is a late actor during cytokinesis . . . 60
3.2.3 CedC function is linked to growth . . . 61
3.2.4 Potential cellular role of CedC . . . 63

4 Material and Methods 67

4.1 Material . . . 67
4.1.1 Sources of used reagents and enzymes . . . 67
4.1.2 Buffers and solutions . . . 67
4.1.3 Media and supplements . . . 67
4.1.4 Oligonucleotides . . . 69
4.1.5 Strains . . . 70
4.2 Microbiological methods . . . 70
4.2.1 Bacterial growth conditions . . . 70
4.2.2 Storage of bacteria . . . 71
4.2.3 Measurement of cell density . . . 71
4.2.4 Synchronization of *Caulobacter crescentus* . . . 71
4.2.5 Bacterial adenylate cyclase two-hybrid (BACTH) system . . . 72
4.3 Molecular biological methods . . . 73
4.3.1 Isolation and purity of DNA . . . 73
4.3.2 Polymerase chain reaction (PCR) . . . 73
4.3.3 Restriction digestion and ligation of DNA fragments . . . 73
4.3.4 Agarose gel electrophoresis . . . 75
4.3.5 DNA sequencing . . . 75
4.3.6 Plasmid construction . . . 75

4.3.7 Transformation of *Escherichia coli* . . . 77
4.3.8 Transformation of *C. crescentus* . . . 77
4.3.9 UV mutagenesis of *C. crescentus* . . . 78
4.3.10 Gene replacements in *Caulobacter crescentus* . . . 78
4.4 Microscopic methods . . . 78
4.4.1 Light microscopy and fluorescence microscopy . . . 78
4.4.2 Time-lapse microscopy . . . 79
4.4.3 Cryo-electron microscopy . . . 79
4.4.4 Nucleoid staining . . . 80
4.4.5 Image processing . . . 80
4.5 Biochemical methods . . . 80
4.5.1 SDS-Polyacrylamide gel electrophoresis (SDS-PAGE) . . . 80
4.5.2 Immunoblot analysis . . . 81
4.5.3 Heterologous overproduction in *Escherichia coli* . . . 82
4.5.4 Protein purification . . . 82
4.5.5 Antibody synthesis . . . 83
4.5.6 Crystallization of CedC . . . 83
4.5.7 Coimmunoprecipitation and mass-spectrometry . . . 84
4.5.8 Gel shift assay . . . 85
4.6 Bioinformatic analyses . . . 85
4.6.1 DNA sequence analyses . . . 85
4.6.2 Protein analyses . . . 85
4.6.3 Genomic tree . . . 85
References 87
Appendix 111

1 Introduction

Bacteria belong to the first living beings in earth's history and have evolved sophisticated mechanisms to adjust to hostile living conditions. An essential event in proliferation is cell division. Although a seemingly simple process, the molecular machineries are highly elaborated and coordinated with other events, such as chromosome duplication and cell growth. Failure of one of the systems is tantamount to cell death. Thus, cells have developed spatial and temporal regulation and developmental checkpoints to ensure proper function of these systems and coordinate their activities. This thesis is shedding light on a blink of an eye in terms of bacterial evolution - with a focus on late cell division proteins.

1.1 Biology of the bacterial cell wall

1.1.1 Peptidoglycan - a robust and highly flexible mesh all at once

Peptidoglycan (PG), also known as murein, has evolved as an essential component of all bacteria, except planctomycetes and mollicutes [1, 2], and it is the main component of the bacterial cell wall. Based on the architecture of PG, bacteria can be divided into two groups: in Gram-negative bacteria, such as *Escherichia coli*, the cell wall is made of a thin layer (1-3) of PG with a thickness of 3-6 nm, whereas Gram-positive bacteria, such as *Bacillus subtilis*, have a multi-layered (20-40) PG with a thickness of 10-20 nm and with cross-linked cell wall polymers such as teichuronic acids, surface and capsule proteins [3]. PG forms a mesh-like structure around the cytoplasmic membrane and is composed of numerous glycan (sugar-based) polymers that are covalently cross-linked to one another by short peptide side-chains, creating a single bag-like macromolecule, called the sacculus [4]. The glycan chains consist of alternating *N*-acetylmuramic acid (Mur*N*Ac) and *N*-acetylglucosamine (Glc*N*Ac) sugar units, which are linked via β-1,4 glycosidic bonds and are orientated perpendicular to the longitudinal axis of the cell [5]. The degree of oligomerization of the glycan strands can vary dependent on the species, but is in average about 25 to 40 disaccharide units [6, 7]. In general, the stem peptides are composed of *L*- and *D*-amino acids and are attached by an amide linkage to the lactyl group of Mur*N*Ac. Similar to the glycan chains, the stem peptides differ in the number and nature composition of the amino acids, dependent on the species as well as growth

conditions [8]. *E. coli* and most other Gram-negative species possess a DAP-type PG containing the dibasic *meso*-diaminopimelic acid (*m*DAP), and the sequence of the pentapeptide is *L*-Ala - *D*-Glu - *m*DAP - *D*-Ala - *D*-Ala (Fig. 1.1 A). In many Gram-positive Firmicutes, the *m*DAP is replaced by a *L*-lysine in position three (Fig 1.1 A) [9]. The stem peptides are most often connected between the carboxyl group of *D*-Ala at position four of one peptide to the amino group at the *D*-center of the *m*DAP residue at position three of another peptide. Although the fourth and fifth position of the peptide chain normally comprises *D*-alanine, it can also be replaced by two glycines, *D*-methionines, *D*-tryptophanes or *D*-phenylalanines, dependent on the growth conditions and species [8, 10, 11]. In particular, these alterations can inhibit the activity of and, hence, regulate PG biosynthetic enzymes [12]. The murein sacculus undergoes permanent modifications and is composed of more than 50 different subunits, called muropeptides (disaccharide peptide units). They can differ with regard to the length of the peptide chain (di-, tri-, tetra- or pentapeptide), the presence of either *D*-Ala or glycine at positions four or five, the state of cross-linkage (monomer, dimer, trimer or tetramer), the type of cross-linkage (*DD* or *LD*) or the presence of 1,6-anhydroMur*N*Ac residues (from the glycan strand termini). The most prominent muropeptides in *E. coli* are the disaccharide tetrapeptide monomer (∼30 %) and the *DD*-cross-linked disaccharide tetra-tetrapeptide dimer (∼20 %) [6].

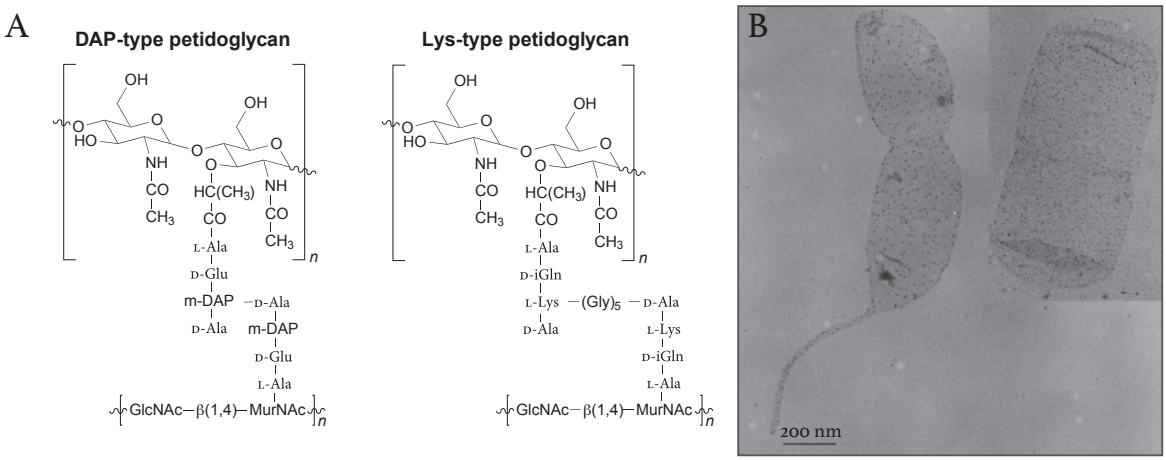

FIGURE 1.1: Peptidoglycan as micro- and macromolecular structure. (A) The structure of the polysaccharide backbone is conserved among bacteria, in contrast to the stem peptide composition. Gram-negative bacteria and some Gram-positive bacilli use *m*DAP as the third amino acid (DAP-type PG), whereas Gram-positive cocci use a *L*-lysine bridge (Lys-type PG) to crosslink the peptide side chains **(B)** Electron microscopy image of isolated sacculi from *Caulobacter crescentus* (left) and a dividing *Escherichia coli* cell (right). An important function of PG is the maintenance of the cell shape, which is still retained after sacculus isolation. Images taken and modified from [13] and [14].

As mentioned in the beginning, the murein sacculus is an essential component of nearly all bacteria. It protects the cell from bursting by its internal turgor pressure, maintains the cell shape (Fig 1.1 B) and is the anchoring point for proteins and other polymers [4]. Although the murein has protective functions, it is not a rigid structure. In contrast, murein forms an elastic net, which is highly flexible and can reversibly expand and shrink three-fold without rupture to adapt to the turgor pressure of the cell [15]. In the direction of the long axis of the cell, isolated sacculi were two- to threefold more deformable than in the direction perpendicular to the long axis [16]. The elasticity of the PG is based on the flexibility of the peptides rather than the glycan strands, which are rigid structures. Under stretched conditions, the peptides change their spatial confirmation, allowing the murein net to become expanded [17, 18].

Concomitant with cell growth, the murein sacculus has to expand to increase the cell size. This process requires incorporation of new material. About half of the existing muropeptides will be released and recycled in each generation. The biosynthesis of PG is a quite complex and highly controlled process. An overview of the biosynthetic steps and PG processing is given in the following section.

1.1.2 Building a wall - synthesis of peptidoglycan

During growth, a bacterial cell must add new material into the pre-existing murein sacculus in order to accommodate the increase in cell size. However, not only during growth but also during cell division, the PG must be remodeled, allowing the cell to synthesize a septum that spatially separates both cells. The biogenesis of PG is a highly complex process and includes about twenty reactions that take place in the cytoplasm and at the inner as well as the outer face of the cytoplasmic membrane. In principle, the synthesis of PG occurs in three steps: (1) synthesis of the precursor molecule lipid II in the cytoplasm by the linear activity of ligase and transferase reactions [19–23], (2) translocation of lipid II across the inner membrane to the periplasm by the action of a flippase, and (3) incorporation into the sacculus by two specific reactions, transglycosylation and transpeptidation. The transglycosylation reaction links the sugar backbones, whereas the transpeptidation reaction connects peptides between newly polymerized glycan strands as well as between nascent and present peptides of the sacculus (Fig 1.2). An important class of enzymes that catalyze these reactions are the so-called “penicillin-binding proteins” (PBPs). They are named after their ability to bind β-lactam antibiotics such as penicillin, which are structurally similar to the common substrate of transpeptidases (TPases), *D*-alanyl-*D*-alanine. Originally, PBPs were identified by SDS-PAGE and radiolabeled with benzylpenicillin. In agreement to these studies, they were numbered according to their molecular mass [24, 25]. As a consequence, their names are not con-

sistent between different species or related to their structure and function, respectively. According to their domain composition, they are classified into several groups. PBPs with both a transglycosylase and transpeptidase domain are bifunctional (bPBPs) and called “class A PBPs" or “high molecular weight PBPs”, whereas enzymes with only a transpeptidase domain fall into the group “class B PBPs” or “low molecular weight PBPs” [26, 27]. The class of PG synthesizing proteins is completed with monofunctional transglycosylases (MTGs), enzymes with only transglycosylase activity. Before new material can be inserted, the murein sacculus needs to be “opened”, which is achieved by hydrolytic enzymes. The group of "class C PBPs" comprises endopeptidases (EPases) and *DD*-carboxypeptidases (CPases) [28], which are, in principle, “reverse TPases”. EPases cleave peptide cross-links, whereas CPases cut the terminal amino acid residue of the peptide side chain (Fig 1.2).

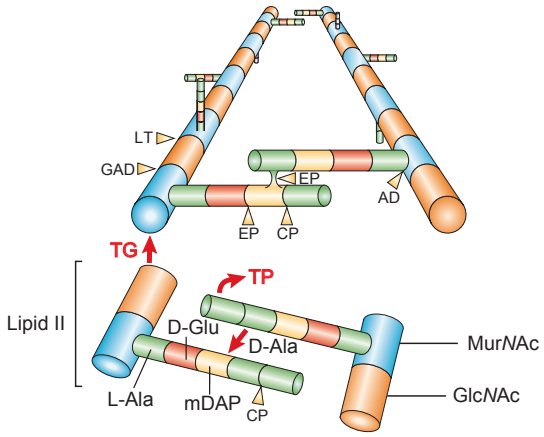

FIGURE 1.2: Overview of PG processing by synthases and hydrolases. The polysaccharide backbone, consisting of *N*-acetylmuramic acid (Mur*N*Ac) and *N*-acetylglucosamine (Glc*N*Ac), is extended by the action of transglycosylases that catalyze a β-1,4-glycosidic bond between the terminal Mur*N*Ac residue of a nascent glycan strand and the Glc*N*Ac residue of the lipid II precursor [29]. Transpeptidases form a peptide cross-link between peptide side chains with a concomitant release of *D*-alanine. This reaction requires a pentapeptide as a donor that loses the terminal *D*-alanine, resulting in a tetrapeptide as an intermediate, which is bound to the active center (serine) of the transpeptidase domain. The intermediate is then resolved by nucleophilic attack of the amino group of the acceptor peptide, generating the new peptide bond. The acceptor peptide can be a tri-, tetra- or pentapeptide and can be either a monomer or a peptide which is already cross-linked. Red arrows indicate synthetic reactions: TP = transpeptidation activity, TG = transglycosylation activity. Yellow arrows depict hydrolytic reactions: LT = lytic transglycosylase activity, EP = endopeptidase activity, CP = carboxypeptidase activity, AD = amidase activity, GAD = *N*-acetylglucosaminidase activity. Image taken and modified from [30].

A tight balance between PG synthetic and hydrolytic enzymes is crucial for viability of the cell. The detailed mechanism for insertion of new material is still poorly understood, but a favored model is the “3 for 1” model [31]. It postulates that during insertion of three new chains, one old chain is

removed simultaneously and recycled by a dynamic multi-enzyme complex that involves both PG synthesizing and hydrolyzing enzymes. Thereby, these dynamic multi-enzyme complexes whose activities are tightly regulated in time and space, facilitate PG synthesis and hydrolysis [5, 31]. This process allows the controlled expansion of the cell envelope and coordinates PG biosynthesis with cell growth.

1.2 Bacterial cell proliferation

1.2.1 Diversity of bacterial growth

Bacteria exist in a broad variety of morphologies. Two of the most common types of bacteria are rods, or variations of rods, and cocci. Rod-shaped bacteria themselves can be vibroid or helical, form hyphae or branches, and generate extensions of the cell envelope, such as stalks. As a consequence of this, distinct growth modes and life cycles have evolved. The underlying determinant, which maintains the bacterial cell shape, is the PG sacculus [9] (see also subsection 1.1.1). Strictly speaking, the determinant of bacterial cell shape is not PG itself, but rather the tightly regulated protein machinery that builds up the sacculus. The composition and spatial distribution of these machineries define the growth mode of species. Bacteria have adapted their growth modes to changing environmental conditions and can, for example, alter their PG metabolism in response to nutrient availability or cell envelope stress [32]. In general, bacteria undergo two different phases of growth: elongation of the cell body and formation of a septum prior to cell division. Among rod-shaped bacteria, there is a high diversity of mechanisms by which cells increase in size. Actinobacteria, such as *Streptomyces coelicolor*, or α-proteobacteria, such as *Agrobacterium tumefaciens*, elongate by tip extension, where cell elongation strictly occurs at both poles or just one pole [33, 34]. In contrast, PG turnover at the poles of the well-studied model organisms *E. coli* and *B. subtilis* is low, leaving the poles inert. These organisms grow by inserting new PG material along the sidewall and switch to septal PG synthesis during cell division. In addition to polar and lateral cell elongation, some α-proteobacteria have developed a greater variety of modes of PG insertion, such as zonal growth to form buds and/or stalks. One example is the crescent-shaped bacterium *C. crescentus*, which adapted zonal growth to build up a stalk.

The following subsection will focus on *C. crescentus*, the model system of this work to study cell cycle events, such as cell division. This process requires the coordinated assembly of a large protein machinery to drive chromosome segregation, membrane invagination and PG remodeling and, thus, facilitate successful cell division.

1.2.2 The organism of interest - *Caulobacter crescentus*

C. crescentus is a Gram-negative, oligotrophic α-proteobacterium and ubiquitously present in freshwater habitats. It belongs to the family of Caulobacteraceae and was first isolated from a surface freshwater site and described in 1964 [35]. The commonly used laboratory strain CB15N (NA1000) has lost its ability to form a holdfast for adhesion to surfaces [36] and is a derivative of *C. crescentus* CB15. Since the genome of *C. crescentus* is fully annotated [37–39] and a variety of genetic tools, including plasmids for overproduction, depletion and production of fluorescent hybrid proteins, have been established [40], it is a commonly used model organism nowadays. The possibility to synchronize populations by density gradient centrifugation to follow cell cycle progression, makes *C. crescentus* an ideal candidate to study the spatiotemporal mechanisms like the assembly of the cell division machinery, cell differentiation and cell polarity.

A very particular characteristic of *C. crescentus* is its asymmetric cell division, which gives rise to two morphologically and physiologically distinct cell types: a “swarmer cell” and a “stalked cell” (Fig. 1.3). The swarmer cell possesses a flagellum and several type IV-pili at one pole, providing motility and allowing to colonize new, nutrient-rich environments. In contrast, the stalked cell is sessile and sticks to surfaces by a holdfast, located at the tip of an elongated extension, the “stalk” [41]. Different to many other bacteria, but in analogy to eukaryotes, *C. crescentus* replicates its chromosome only once per cell cycle [42]. Due to this fact, the cell cycle can be divided into distinct phases, similar to eukaryotes (Fig. 1.3). It starts with the G_1 phase, in which a motile swarmer cell grows to the size of a stalked cell ($\sim$ 1.5 μm), while chromosome replication is blocked. After transition to a chromosome replication-competent state (S phase) mediated by an intracellular signaling cascade, chromosome replication is initiated. Concomitantly, the cell undergoes a morphological transition by shedding the flagellum and building a stalk at the same pole instead (Fig. 1.3). Once the stalked cell has elongated to almost twice the length of a swarmer cell, it synthesizes a new flagellum at the pole opposite the stalk. In parallel, the replicated chromosome segregates and the asymmetric predivisional cell starts to constrict its outer and inner membrane (G_2 phase). The completion of constriction in the division phase (M phase) leads to the release of a swarmer cell that starts the cell cycle all over again, whereas the stalked cell immediately progresses into another S phase (Fig. 1.3) [43].

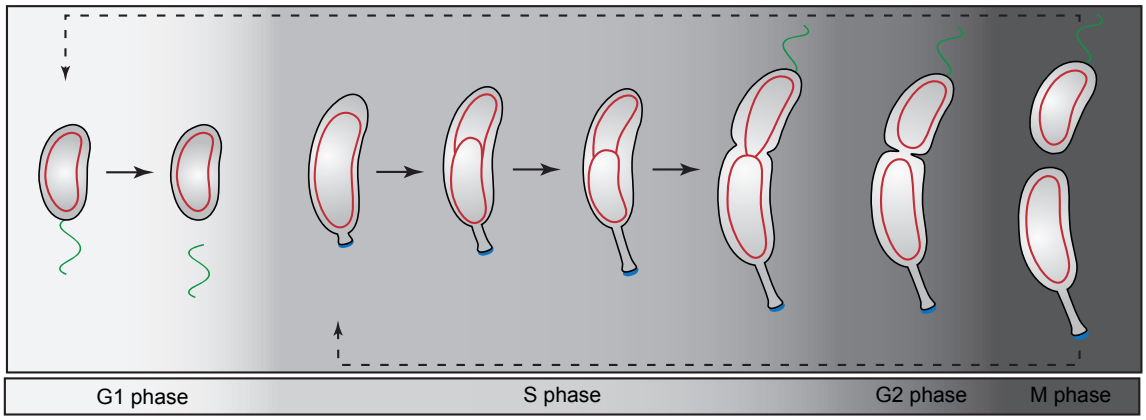

FIGURE 1.3: Life cycle of *C. crescentus*. The development of *C. crescentus* starts with a motile swarmer cell, which carries a polar flagellum (G_1 phase). After cell growth and during differentiation from the swarmer to a stalked cell, the flagellum is shed and the cell starts to grow a stalk at the same pole. Simultaneously, chromosome replication is initiated (S phase). Additionally, the cell division machinery assembles at midcell and the replicated *origin of replication* (*oriC*) is segregated towards the other pole. During S phase, the cell starts to constrict both the outer and inner membrane and synthesizes a flagellum at the pole opposite the stalk. Once the chromosome is fully replicated and segregated (G_2 phase), the mother cell divides into a stalked cell and a swarmer cell (M phase). Whereas the sessile (stalked) cell immediately enters S phase and initiates a new round of chromosome replication, the swarmer cell starts the cell cycle from the beginning. Structures are depicted in different colors: blue: holdfast, red: chromosome(s), green: flagellum.

1.2.3 Getting larger - cell elongation in bacteria

Generally, rod-shaped bacteria extend their cell envelope by employing the activity of two multi-enzyme complexes, called the “elongasome” and the “divisome”. Both consist of several specific enzymes, including cytoplasmic and membrane integral scaffold proteins as well as periplasmic PG synthases and hydrolases [5, 44, 45]. While the elongasome inserts new PG material along the longitudinal axis of the rod [46, 47], the divisome leads to constriction of the cell envelope and remodeling of the PG to complete cytokinesis [48].

Pulse-chase experiments using *D*-cysteine have revealed, how *E. coli* and *C. crescentus* cells grow during cell cycle progression [49, 50]. In young *E. coli* cells as well as in *C. crescentus* swarmer cells, the cell body is elongated by insertion of PG material at multiple sites along the lateral sides of the cell body (Fig. 1.4). The complex responsible for this dispersed mode of growth is the elongasome, which is thought to be directed by MreB [51–53]. MreB is an essential actin-like protein and highly conserved among rod-shaped and non-spherical bacteria, which possess at least one homolog of MreB. In contrast, spherical bacteria tend to lack *mreB* [34, 54–58]. MreB

polymerizes into membrane-associated filaments and forms distinct patches that move around the cell circumference roughly perpendicular to the longitudinal axis of *E. coli*, *C. crescentus* and also *B. subtilis*, [59–61]. The movement of the patches does not depend on MreB polymerization but rather on both the presence and activity of PG synthases [59–61]. As the major scaffold, MreB coordinates and directs the location of the elongasome, including membrane-spanning and PG-modifying proteins [34, 54]. The elongasome comprises MreB-interacting proteins such as the membrane-bound MreC, MreD, RodZ, and RodA [58, 62–64], as well as the lipid II synthetic enzymes MraY and MurG [65]. Additionally, MreB interacts with the essential elongasome-specific transpeptidase PBP2 and the bifunctional PBP1A in *E. coli* to direct lateral PG synthesis [66]. How the elongasome and MreB, respectively, are regulated is not clear yet. Presumably, other unidentified factors regulate the localization and dynamics of MreB, which in turn directs the elongasome to distinct places. Notably, a recent study in *E. coli* has provided some insight into the mechanism of MreB localization. It was shown that MreB maintains the rod-shape by directing the elongasome to regions with excessive negative cell wall curvature, leading to an enrichment of MreB at those regions, and thus, elevated PG synthesis [67]. Consistent with this finding, another study in *E. coli* has shown that the MreB rotation is not essential for rod-like growth but rather promotes robust rod-like growth under adverse growth conditions by preventing amplification of local defects in the PG mesh [68]. It was additionally shown that the linker protein coupling the cytoplasmic MreB protein with the cell wall synthesis machinery in the periplasm is RodZ, which directly modulates the activity of the elongasome-specific transpeptidase PBP2 [68].

Although the core components of the cell wall biosynthetic machinery are conserved among rod-shaped bacteria, their spatiotemporal regulation is distinct and adapted to the life style of each organism [69], exemplified by members of the Caulobacterales, which have modified the elongasome to synthesize a stalk. In *C. crescentus*, stalk elongation is facilitated by another class of cytoskeletal elements, bactofilins. It was shown that BacA and BacB specifically recruit the bifunctional PG synthase PbpC to the stalked pole during the swarmer-to-stalked-cell differentiation [70] (Fig. 1.4). Another example of how bacteria use cytoskeletal elements as landmarks to achieve different cell morphologies, is the intermediate filament-like protein crescentin (CreS) from *C. crescentus*. CreS forms a lateral scaffold along the inner cell curvature and is attached to the membrane by MreB [71, 72]. The scaffold acts as a mechanical force, altering cell wall elongation rates to produce the typical curved morphology of *C. crescentus* [71].

Concomitant with stalk synthesis at the former flagellated pole of *C. crescentus*, the laterally active elongasome is re-directed to midcell for preseptal growth (Fig. 1.4). In *E. coli*, the expansion of the sacculus by dispersed insertion of new PG material is also followed by zonal PG synthesis at

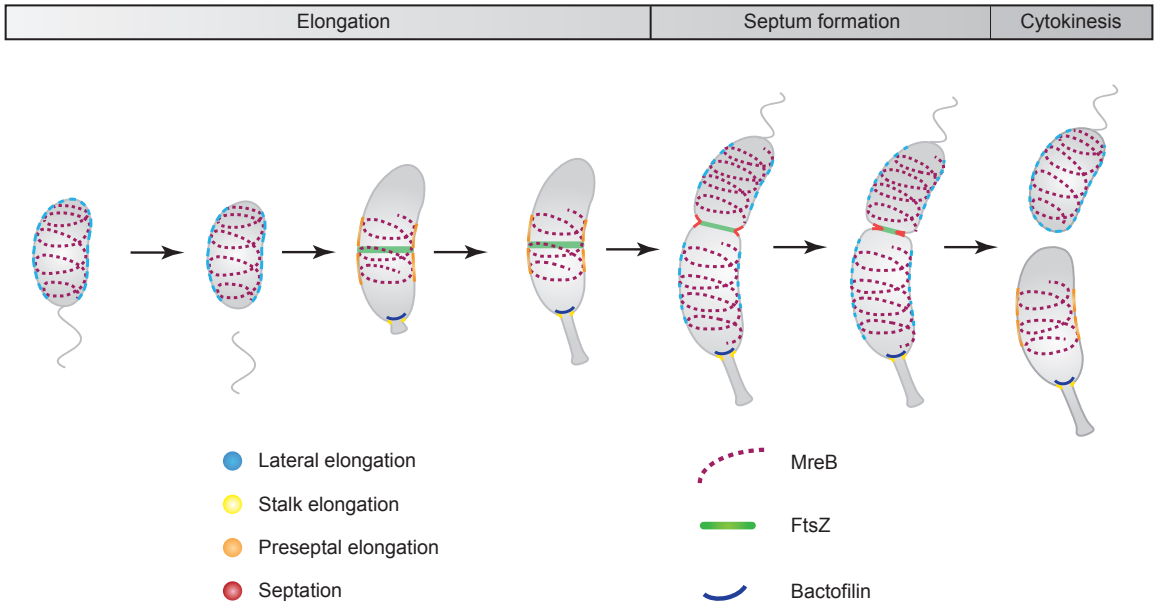

FIGURE 1.4: Growth modes in *C. crescentus* and their cytoskeletal landmarks. The activity and dynamics of the PG synthesis machineries are regulated by the localization of different scaffold proteins. In swarmer cells, complexes of MreB are distributed along the longitudinal axis of the cell and mediate lateral elongation. During the swarmer-to-stalked-cell transition, the flagellated pole is elongated by the stalk synthesis machinery, including PbpC, which is recruited by bactofilins. Concomitant with this transition, FtsZ is placed at midcell and interacts with MreB, leading to a zonal (preseptal) elongation. The zonal elongasome is then replaced by the divisome and its specific PG remodeling machinery, leading to formation of the septum and a dispersed MreB localization again. After septation, the swarmer cell undergoes the same growth phases again, whereas FtsZ in stalked cells is quickly re-assembled at midcell, facilitating preseptal elongation.

midcell [49]. However, in contrast to *C. crescentus*, in which the dispersed elongation is rapidly followed by preseptal growth after transition into a stalked cell (Fig. 1.4) [50, 73], the zonal growth in *E. coli* is temporally short [49, 74, 75]. A known spatiotemporal signal for the change of the growth mode is the midcell positioning of FtsZ and its interaction with MreB. Over the past decades, extensive studies on the positioning of FtsZ have uncovered several regulatory mechanisms. The best-studied examples are the negative FtsZ regulators found in *E. coli* and *B. subtilis*: the Min system and nucleoid occlusion (NO) [76]. The Min system of *E. coli* is an oscillating complex (non-oscillating in *B. subtilis* [77]), moving from one pole to the other. Thus, it negatively controls the positioning of FtsZ, more precisely restricting FtsZ ring formation to midcell by inhibition of its polymerization [78–82]. Additionally, the NO-specific proteins SlmA in *E. coli* and Noc in *B. subtilis* are bound non-specifically to DNA, inhibit Z-ring formation and, thus, divisome assembly over segregating chromosomes [83, 84]. Another well-studied negative regulator is the Walker ATPase

MipZ of *C. crescentus* [85]. It is conserved among α-proteobacteria without Min system orthologs, even though exceptions harboring both systems, such as *Phenylobacterium zucineum*, do exist. MipZ directly interacts with FtsZ and inhibits its polymerization into a ring-like structure [85]. Additionally, MipZ coordinates Z-ring positioning with chromosome segregation by associating with ParB. ParB belongs to the ParABS partitioning system and binds to the *parS* sites, located in proximity of the *oriC*. MipZ forms a subcellular gradient with the lowest concentration at midcell, preventing polymerization of FtsZ at both poles and, thus, positioning FtsZ at the cell center [85, 86]. Once located there, the interaction between FtsZ and MreB leads to a change from the dynamic patch-like pattern in swarmer cells of *C. crescentus*, to an intense band at the midcell region, which facilitates the re-direction of elongasome components [50, 87–89]. Similar to *C. crescentus*, the change from dispersed to zonal growth in *E. coli* occurs also after positioning of FtsZ at midcell by the Min-system [90, 91]. After that and during progression of divisome assembly (see subsection 1.2.4), elongasome components are exchanged by PG synthases and hydrolases, which are specific for cell division. Thus, the elongation complex and the divisome seem to collaborate during this stage. After the onset of divisome assembly, a transverse septum (new cell pole) is formed in *E. coli*, which eventually results in septation and the release of two identical cells. In *C. crescentus*, the cell body is elongated to the size of a predivisional cell with simultaneous maturation of the divisome, which leads to gradual constriction of the cell envelope by PG remodeling. At the same time, the stalked cell of *C. crescentus* grows slightly longer by dispersed elongation, until it is completely separated by constriction (Fig. 1.4). While the swarmer cell restarts the cell cycle and gains size by dispersed elongation, the stalked cell immediately grows by preseptal elongation (see Fig. 1.4) [43].

1.2.4 Building a contractile ring - assembly of the divisome

Bacterial cell division is a fundamental biological process and carried out by a macromolecular machinery, called the divisome (Fig. 1.5). Septation is tightly regulated in space and time and can be separated into three steps: (1) arrival of FtsZ and the stabilization of FtsZ protofilaments, (2) maturation of the divisome, and (3) PG remodeling and constriction to complete cytokinesis. The core cell division proteins are highly conserved among proteobacteria [92], although differences in the timing of divisome assembly and composition of the divisome do exist. A control player in divisome assembly is the tubulin-like GTPase FtsZ [93–96]. FtsZ monomers polymerize in a GTP-dependent manner into linear protofilaments that assemble into a ring-like structure, the so-called Z-ring. The Z-ring is the structural basis for the assembly of other cell division proteins to drive cell division.

Beside FtsZ, the first components recruited to the *E. coli* divisome are the bitopic membrane protein ZipA and the amphitropic protein FtsA to stabilize the FtsZ protofilaments that form the Z-ring. The essential transmembrane protein ZipA is only conserved in γ-proteobacteria, specifically interacts with the C-terminal region of FtsZ to tether it to the cytoplasmic membrane [97–99], and possibly also recruits downstream cell division proteins [100]. FtsA, on the other hand, is a widespread essential actin-like protein. Like other actin-like proteins, FtsA has two domains, subdivided in domain 1A, 1C and 2A and 2B [101]. All domains, except 1C, contribute to the ATP-binding site, whereas domain 2B specifically binds to the same C-terminal peptide of FtsZ (CTC) as ZipA [101–104]. The orientation of subdomain 1C is unique to FtsA and not conserved in other actin homologs. This subdomain plays an important role in self-assembly [105, 106] and recruitment of other cell division proteins [107, 108]. FtsA facilitates FtsZ protofilament assembly and serves as a membrane anchor to stabilize the so-called proto-ring. On the other side, FtsA might also regulate the dynamic assembly of FtsZ. It has recently been shown in *E. coli* that FtsA provides a negative unidirectional regulatory effect on the FtsZ filament network, causing fragmentation of FtsZ polymers [109], thus it inherits antagonistic functions during cell division. Recent studies demonstrated that FtsA also acts as a control regulator of PG synthesis and hydrolysis, which will be discussed later in this section. In contrast to *E. coli*, the ZipA protein is absent and the FtsA homolog of *C. crescentus* arrives significantly later at the divisome [110, 111], suggesting that other Z-ring stabilization factors probably exist. Recent studies indicate that the FtsZ-associated proteins FzlA and FzlC as promising candidates. Both are only conserved among α-proteobacteria. FzlA is an essential glutathione S-transferase-like protein, which does not bind to glutathione and has been functionally adapted for cytoskeletal purposes, facilitating negative curvature of the FtsZ protofilaments [112]. FzlC, on the other hand, is a non-essential cytoplasmic protein and recruited to midcell early upon FtsZ polymerization at midcell. It directly binds to the C-terminal conserved peptide of FtsZ and is able to recruit FtsZ to the membrane [113]. Further players that promote the stability of the Z-ring are the non-essential regulatory Zap proteins (Z-ring Associated Proteins) ZapA [114], ZapB [115], ZapC [116, 117] and ZapD [118] that exhibit functionally redundant roles. Whereas ZapA is widely conserved among bacteria with apparent orthologs in many species, the other three are mainly restricted to γ-proteobacteria. All proteins do not have much in common, although ZapA and ZapB seem to function together [119]. ZapA, ZapC and ZapD were shown to bind directly to FtsZ and affect FtsZ polymerization and bundling *in vitro* [114, 116–118]. In contrast, ZapB interacts with the chromosome-structuring factor MatP (see subsection 1.2.5) at the division site of *E. coli*, suggesting that it has a putative role in spatiotemporal regulation of chromosome segregation with cytokinesis [120]. A recent study identified another Zap protein, ZapE, which is conserved among γ-proteobacteria. In *E. coli* it was shown to be required for growth under conditions of low

oxygen, acting as a Z-ring destabilizer at late stage of cell division in an ATP-dependent manner [121]. Another potential candidate for FtsZ membrane tethering is the ATP-binding cassette (ABC) transporter-like complex FtsEX. Beside its role in activating PG hydrolases in *E. coli* [122], the ATPase FtsE was shown to interact with FtsZ, whereas FtsX acts as a transmembrane anchor of the complex, suggesting role in FtsZ-recruitment and tethering [111, 123]. In support of this idea, FtsE is one of the first proteins recruited at the onset of Z-ring assembly in *C. crescentus* [111]. The proposed role of FtsEX suggests a correlation between tethering FtsZ to the membrane and PG hydrolysis exists, since it has been also shown that FzlC interacts with FtsE and the non-essential cell division proteins DipM and AmiC, which are involved in PG hydrolysis [113].

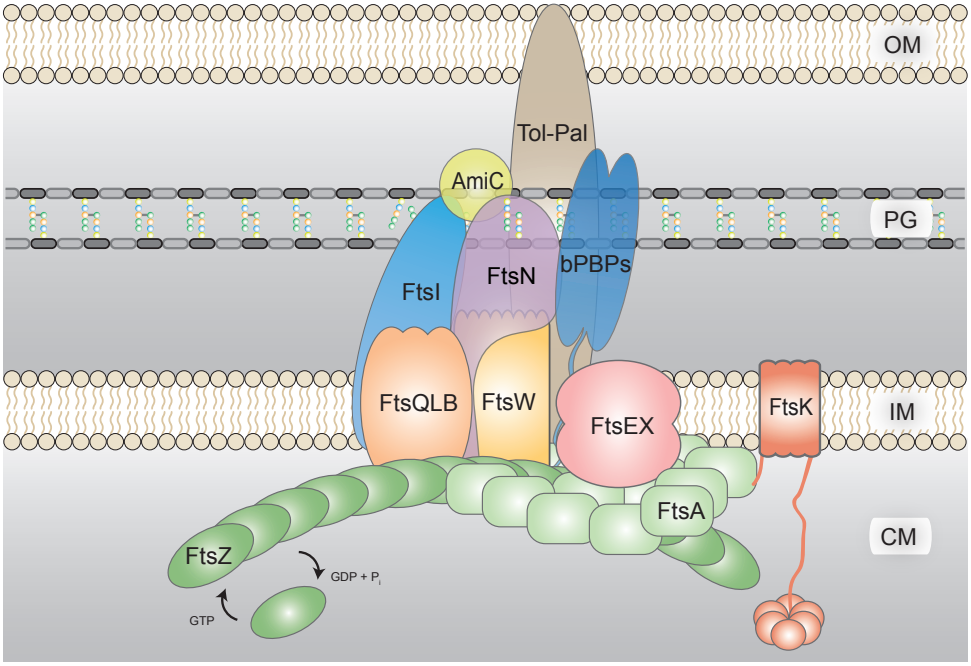

FIGURE 1.5: Conserved components of the divisome. Schematic representation of cell division proteins involved in Z-ring tethering / stabilization, PG remodeling and membrane invagination. For simplicity, only highly conserved cell division proteins are shown. Since the nomenclature of bifunctional PBPs involved in cell division is not consistent, they were depicted as bPBPs. In *E. coli*, the corresponding bPBP is PBP1B. OM = outer membrane, PG = peptidoglycan, IM = inner membrane, CM = cytoplasm.

Upon stabilization of the proto-ring, the divisome matures to become a contractile machinery by the arrival of a core set of other conserved and essential (as well as non-essential) cell division proteins. This set includes proteins that bridge interactions between FtsZ-associated proteins and PBPs (e.g. FtsW), as well as proteins that link cell division and chromosome segregation (e.g. FtsK). Apart from cell elongation, the crucial step in cytokinesis is to form a constriction-competent assembly, where

PG remodeling is the driving force. On doing so, elongasome components (see subsection 1.2.3) are exchanged for cell-division specific PG biosynthetic enzymes during divisome maturation. However, in *E. coli* elongasome and divisome components were shown to be simultaneously present at midcell for ∼40 % of the time of the cell division procedure [124]. In addition, it was shown that the elongasome-specific transpeptidase PBP2 interacts with several cell division proteins [124].

The first proteins to be recruited after proto-ring stabilization are the bifunctional protein FtsK and the highly conserved complex FtsQLB, the latter of which controls PG remodeling at the division site. FtsK links cell division and chromosome organization during cytokinesis, thus becoming more important during the late stage of cell division, which is discussed later (see subsection 1.2.5). Notably, the FtsQLB complex is first assembled prior to localizing to the division site in *E. coli* and *C. crescentus* [111, 125]. Earlier studies report a scaffolding function of the complex [125, 126], but recent studies unveiled a more specific role for FtsQLB in key signaling pathways important for septal PG synthesis (described below). FtsL, another key factor, is also required for the localization of FtsW and FtsI (PBP3) in *C. crescentus* [111]. FtsW is an integral membrane protein and belongs to the SEDS (shape, elongation, division, and sporulation) superfamily. In *E. coli*, it forms a complex with FtsI and is required for its midcell localization [127, 128]. FtsW was proposed to be the flippase that translocates the PG precursor lipid II from the cytoplasm to the periplasm during cytokinesis [129, 130]. However, the identity of the bacterial lipid II flippase is a currently controversially discussed topic. A recent study suggests that rather than FtsW (and RodA during elongation), MurJ is the lipid II flippase [131], although a third flippase, AmJ, has been recently identified in *B. subtilis*, which is specifically transcribed in response to cell envelope stress [132]. Until now, there is no evidence that excludes one or the other as the lipid II flippase. It is unlikely that they have redundant functions, since both proteins are essential on their own in *E. coli* [130, 131]. However, a recent study provides evidence that proteins of the SEDS family, in this case RodA of *B. subtilis*, act as the principal TGase in the elongasome, thereby responsible for its movement [133]. Thus, FtsW may play a similar role as a TGase during cytokinesis. Unlike in *E. coli*, FtsI localizes to midcell prior to FtsW in *C. crescentus*, indicating that FtsW is not required for the recruitment of FtsI [111]. FtsI is the divisome-specific transpeptidase (class B PBP) and highly conserved among bacteria. It interacts with the elongasome-specific transpeptidase PBP2 in *E. coli* and replaces it for septal PG synthesis [124]. The recruitment of late cell division proteins occurs in a strictly sequential manner in *E. coli*, but not in *C. crescentus*. However, there is recent experimental evidence for interactions between proto-ring proteins and later divisome proteins. One example is the interaction between FtsA and FtsN. FtsN is highly conserved among proteobacteria and described as the last known essential cell division protein [110, 134]. Recent studies in *E. coli* have suggested a central role

for FtsN during cytokinesis in triggering and inducing PG synthesis. Despite being a late recruit to the division site, a low number of FtsN molecules is probably already recruited to midcell through interaction with subdomain 1C of FtsA [107, 108, 135, 136]. Once FtsN accumulates at midcell, its N-terminus activates the FtsQLB complex by direct interaction, which, in turn, then senses the FtsA conformation to signal that septal ring assembly is complete [137, 138]. Simultaneously, the interaction of the activated FtsQLB complex with FtsI and FtsW stimulates septal PG synthesis, which, in turn, enhances further recruitment of FtsN by binding of its PG-binding sporulation-related (SPOR) domain to septal glycan strands that lack stem peptides [139–141]. Thus, FtsN displays self-reinforced accumulation at the septum [142, 143]. Its accumulation further facilitates the interaction with other proteins belonging to the septal PG machinery, such as the amidase AmiC, the monofunctional transglycosylase MtgA, and the divisome-specific bifunctional PG synthase PBP1B, which is stimulated by its interaction with FtsN in *E. coli*. In *C. crescentus*, a direct interaction with AmiC and components of the Tol-Pal (PG-associated lipoprotein) complex was reported, although the localization of AmiC is independent of FtsN [144–147]. The Tol-Pal complex physically connects the three envelope layers of Gram-negative bacteria by multiple interactions and coordinates the constriction of the outer membrane and PG synthesis [148, 149]. Unlike in *E. coli*, the Tol-Pal complex of *C. crescentus* is essential and is additionally involved in the proper localization of the polarity factor TipN [148]. In *E. coli*, the invagination of the inner and outer membrane is linked to septal PG remodeling by PBP1B and the interaction with its cognate regulatory lipoprotein LpoB, whereas *C. crescentus* lacks such a regulatory mechanism. Another difference is the presence of the division and polarity-related metallopeptidase DipM in *C. crescentus*. DipM was identified as a further interaction partner of FtsN, which is required for the midcell localization of DipM [150]. It was shown to be involved in the remodeling of the PG layer and in coordinating constriction of the cell envelope during the division process [150–152]. However, it is not known yet whether DipM has a catalytic function or not.
Altogether, these protein-protein interactions at midcell lead to the assembly of a fully functional contractile ring that re-directs PG synthesis and coordinates membrane invagination and septum formation, resulting in cell septation.

1.2.5 Spatiotemporal hustle - coordination of final chromosome segregation with late stage of cell division

Beside its function to mediate constriction and septal PG biosynthesis, resulting in the generation of the new poles and the final septation of the cells, the divisome has an additional important function. A crucial point during septation is that the division site is free of DNA to ensure that

cell division occurs precisely between the newly formed sister nucleoids to generate offspring with equal distributed DNA. Therefore, the divisome additionally has a role in the placement of the chromosome relative to the divisome. The events of chromosome segregation and cytokinesis in bacteria are spatiotemporally coupled. An important, highly conserved component of the divisome is the bifunctional protein FtsK, which acts as a developmental checkpoint and couples cell division with the segregation of the chromosomal terminus (*ter*) regions by active re-arrangement of the chromosome in an ATP-dependent manner. As part of the divisome, its essential, membrane-bound N-terminal region (Fig. 1.6 A), plays an architectural role in localizing several proteins required for cell division progression to the division site [153–156]. FtsK is thought to contribute to divisome stability, since overproduction of FtsZ, FtsA, and FtsQ can partially compensate the loss of *ftsK* in *E. coli*. The large C-terminal region can be divided in three subdomains with the α- and β-domain forming a homohexameric ATP-dependent dsDNA translocase (Fig. 1.6 A) [154, 157, 158]. In contrast, the small γ-domain (Fig. 1.6 A) is involved in both protein-protein interactions activating site-specific recombination by XerCD and orienting the motor domain (Fig. 1.6 A) in the proper direction at the binding step [159–161]. By binding specifically to DNA, it recognizes so-called KOPS (FtsK-orienting polar sequences) (Fig 1.6 B) motifs that are distributed over the chromosome and oriented in opposite directions on the left and right arms of the chromosome and are more frequent in proximity of the *ter* region, where they tend to invert their orientation. Thereby, the directionality of DNA pumping and specific DNA-binding of FtsK is determined [159, 160, 162, 163]. Upon DNA-binding and unidirectional translocation activity, FtsK leads to positioning of the chromosomal *dif* sites toward the divisome during the late stages of cell division [161, 164, 165]. The *dif* site is a 28 bp sequence, located in close proximity to the replication terminus region, and also the locus for site-specific recombination by XerCD [166–168]. These tyrosine-recombinases are required when the cell faces the topological problem of chromosome dimers. Under some circumstances, double-strand breaks occur during chromosome replication, which are repaired by homologous recombination events between the sister chromosomes. As a result, both chromosomes are conjoined if an odd number of homologous recombinations occur, which is the case in about 15 % of an *E. coli* cell population [169]. To prevent chromosome guillotining at the septum [170], the γ-domain directly activates XerD [171], which cuts and swaps the first pair of strands, resulting in the formation of a Holliday junction at the *dif* site that is subsequently resolved by the stimulation and action of XerC to eliminate chromosome dimers (Fig. 1.6 C) [158, 172]. Additionally, the γ-domain activates the topoisomerase IV complex to resolve possible chromosome catenanes (topologically interlinked chromosomes)[173, 174], which are formed due to the two bidirectional replication forks, and facilitate final *ter* segregation.

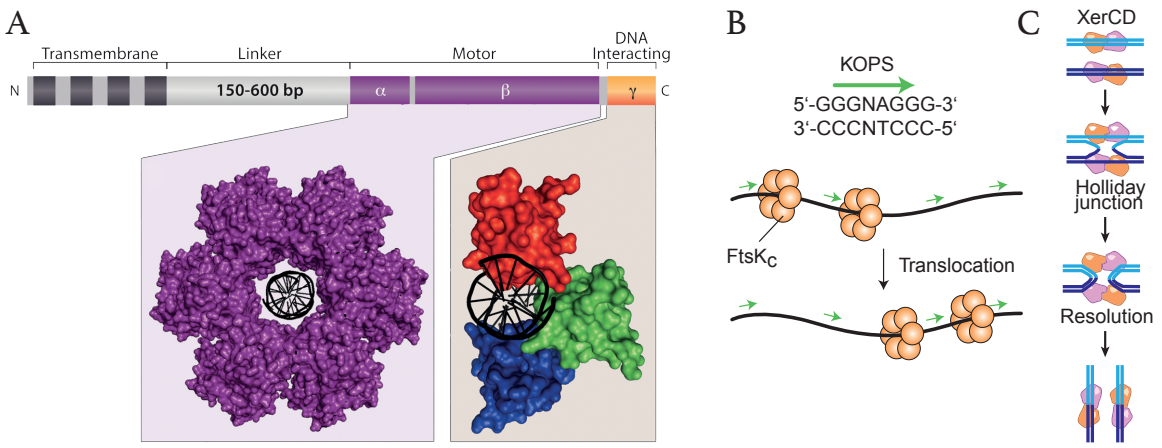

FIGURE 1.6: FtsK and its subcellular function. (A) The domain structure of FtsK. The α- and β-subdomain assemble into a homo-hexamer to act as an ATP-dependent DNA translocase, whereas the γ-subdomain interacts with sequence-specific motifs on the DNA (KOPS) and, furthermore, with XerCD. From [175]. **(B)** The polarity of the KOPS (FtsK-orienting polar sequences. Shown is the consensus sequence of *E. coli*) elements determines the direction of DNA translocation by FtsK (green arrows). Modified from [176]. **(C)** XerCD-mediated monomerization of chromosome dimers acting at the *dif* site in the *ter* region. XerD is directly activated by the γ-subdomain of FtsK to catalyze a site-specific recombination, forming a transient Holliday junction, which is resolved by XerC stimulation. Modified from [177].

In *E. coli*, the spatiotemporal organization of the terminus region during cell division is not only mediated by the septum-associated translocase FtsK, but also by an additional mechanism. A recent study revealed that the *ter* region is linked to the Z-ring [120]. The chromosomal terminus region of *E. coli* forms a compact structure, termed the "*ter* macrodomain", which is organized by a specific protein, MatP [178, 179]. MatP binds to specific binding sites (*matS*), which can be found only around the *dif* sequence, and interacts indirectly via its C-terminal coiled-coil region with FtsZ through the Z-ring associated proteins ZapAB [119, 120]. The formation of this complex guarantees that the positioning of the *ter* region relative to the divisome does not change after Z-ring formation. However, this system is only conserved in Enterobacteriacae and Vibrionaceae [179]. Similar positive organization systems in other bacteria are not known yet.

1.3 Scope

Cytokinesis is a highly complex process that requires tight spatiotemporal regulation of several essential cellular processes, including DNA replication, chromosome segregation and cell growth. Over the last decades, fundamental knowledge about bacterial cytokinesis has accumulated. How-

ever, each new finding raises several new questions. Although the core mechanisms are conserved among bacteria, genetic and/or functional differences do exist. Beside the model species *E. coli* and *B. subtilis*, *C. crescentus* with its asymmetric lifestyle is an interesting model organism to elucidate the spatiotemporal organization of proteins involved in cell division, chromosome segregation and PG remodeling. This work aims at the functional characterization of proteins that play important roles during the late stages of cell division in *C. crescentus*.

Although most bacteria share a core set of biosynthetic enzymes to carry out cell elongation and division, alternative growth modes and life styles require specialized enzymes and orchestration of the PG biosynthetic enzymes. Given the unique developmental program of *C. crescentus* and the resulting asymmetric morphology, the question arises how this organism has adjusted the PG biosynthesis specifically the function of bifunctional penicillin-binding proteins (bPBPs). Although bPBPs have been well-studied in *E. coli* and *B. subtilis*, their spatiotemporal dynamics and physiological roles are still poorly understood in *C. crescentus*. The number of PBPs differs from species to species, while *C. crescentus* possesses an unusual high number. In this study, the bPBPs of *C. crescentus* were investigated in more detail, specifically with respect to cell division. Deletion mutants, lacking one or more bPBPs, were generated and used in complementation studies to address the question, of whether bPBPs have redundant functions as known from *E. coli*. Furthermore, fluorescent fusions to each individual bPBP were used to examine their localization dynamics within the cell. Moreover, these studies were expanded to test for localization dependency on other known proteins, in particular cell division components. To confirm the localization and complementation studies and to determine which bPBPs are able to interact with the septal PG biosynthetic complex, *in vivo* studies were performed using a bacterial two-hybrid approach.

A crucial step during cell division is the faithful distribution of the sister chromosomes to the two daughter cells. Studies in the past have revealed various systems involved in this process in bacteria. However, there are presumably a number of yet unknown mechanisms to coordinate and regulate the final steps of cell division. In the second part of this work, light is shed on a so-far uncharacterized, but highly conserved protein, namely CedC. Previous results suggested that CedC is part of the divisome and possesses a cellular function, since its deletion has an influence on cell morphology. In this work, I performed various experiments to characterize the protein in more detail. Localization and timing experiments were performed to confirm that CedC is part of the divisome. In order to get a fundamental idea in which cellular process CedC is involved, a comprehensive deletion study was executed. Moreover, a crystallization approach was used to solve the protein structure and to get a better idea of its role.

2 Results

2.1 Dynamics of bifunctional penicillin-binding proteins in *C. crescentus*

Peptidoglycan remodeling combined with the constriction of the divisome provide the major driving force for cell division and separation. Although a variety of divisome components of *C. crescentus* have been identified and characterized in the past, the bifunctional penicillin-binding proteins involved in septal PG synthesis are still poorly investigated. In this study, we expand the knowledge of bPBPs in *C. crescentus* with respect to their function and localization, especially during cell division.

2.1.1 The bifunctional penicillin-binding proteins of *C. crescentus*

Most Gram-negative bacteria possess several bPBPs with overlapping and redundant cellular functions. One of the best studied example is *E. coli*, whose genome codes for the three bPBPs PBP1A, PBP1B, and PBP1C. However, previous studies only investigated the biological subcellular roles of bPBPs in the the dimorphic model organism *C. crescentus* [70, 144, 180]. Consistent with its complex morphology, it harbors an unusually high number of bPBP paralogs, five in total. They have a modular structure and are anchored to the cytoplasmic membrane via a single transmembrane domain (TM) close to the N-terminus (Fig. 2.1 A). The large periplasmic part consists of a transpeptidase (TP) domain, and, in contrast to mPBPs, additionally of a transglycosylase (TG) domain. As known for other bPBPs, they are variable in the sequence of their amino acid length, even though the catalytic domains are conserved. PbpY with the highest molecular weight is followed by Pbp1A, which features an unusual long cytoplasmic tail, PbpC, PbpZ, and finally PbpX with the lowest molecular weight (Fig. 2.1 A). All bPBPs share the same nine conserved motifs in the TG domain, the junction, and the TP domain as well as the respective active site residues (Fig. 2.1 B), which have been described for *E. coli* [89]. Interestingly, PbpZ of *C. crescentus* lacks highly conserved amino acid residues in the non-penicillin-binding (nPB) domain, comparable to PBP1C of *E. coli*. This finding is in line with the reported similarity between PbpZ and PBP1C, whereas all other bPBPs are most related to *E.coli* PBP1A [183].

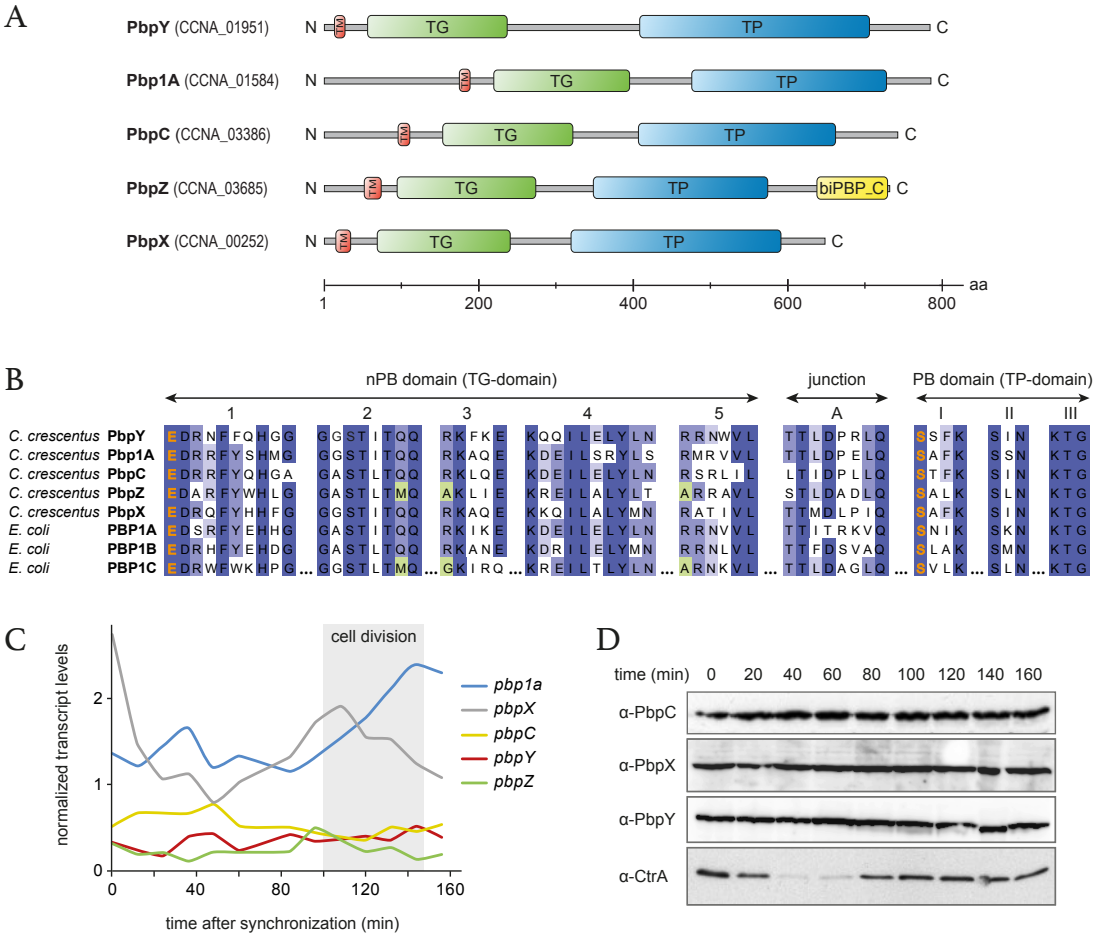

FIGURE 2.1: The bPBPs of *C. crescentus*. **(A)** Schematic structure showing the domain of the five bPBPs of *C. crescentus*. Typically, all bPBPs are composed of a N-terminal cytoplasmic part, followed by a single transmembrane domain (TM), and a large periplasmic region containing the catalytic domains for the transglycosylation (TG) and transpeptidation (TP) reaction. PbpZ harbors an additional domain called biPBP_C, which is conserved in a subgroup of PBPs and predicted to be an all beta fold with no catalytic activity (Source: Pfam, entry PF06832). **(B)** Conserved signature motifs among *E. coli* and *C. crescentus* bPBPs. Residues in the respective active center are highlighted in orange, whereas deviations of *C. crescentus* PbpZ and *E. coli* PBP1C from the consensus are depicted in green; nPB=non penicillin-binding domain. **(C)** Cell cycle transcript levels of *C. crescentus* bPBPs-encoding genes. The data are from a microarray-based transcriptome analysis of synchronized *C. crescentus* cells, followed over the course of one cell cycle [181]. **(D)** Immunoblot analysis of PbpC, PbpX and PbpY over the course of the cell cycle. Swarmer cells were isolated and grown in M2G medium, and samples were withdrawn at the indicated time points. The cell cycle-dependent protein levels of the master regulator CtrA were used to verify the synchrony of the cells. Figure taken from [182].

When microarray-based transcriptome data of a synchronized *C. crescentus* culture from a previous study [181] were analyzed, significant expression level changes of *pbpX* and *pbp1a* were noticeable.

Specifically over the course of the cell cycle, *pbpX* transcripts accumulated at the early cell division event at the onset of cell division, whereas *pbp1a* levels accumulated during the late stage of cell division (Fig. 2.1 C). However, an immunoblot analysis of PbpX did not mirror its transcript levels, since the protein level of PbpX remained constant over the course of the cell cycle (Fig. 2.1 D). The same observations were made for the protein levels of PbpC and PbpY, consistent with their relatively constant mRNA levels. For the other bPBPs, the protein levels during the cell cycle could not be determined, since no functional antibodies were available.

2.1.2 Localization dynamics of bPBPs in *C. crescentus*

The discovery and usage of fluorescent proteins in living cells has revolutionized cellular biology in the past decade [184, 185]. Native proteins can be tagged with a fluorescent label by chromosomal insertions to unravel their subcellular localization, which is often linked to a specific function [186]. *C. crescentus* can be easily followed as it progresses through its life cycle, so that the precise localization of spatiotemporally regulated proteins can be readily traced. To determine which bPBP potentially localizes at the cell division site, each of them was fused N-terminally to the fluorescent protein Venus and expressed ectopically from a xylose-inducible promoter (P_{xyl}). Upon induction, both Venus-PbpX and Venus-PbpY were detectable along the whole cell body, but additionally showed a distinct accumulation at the cell division plane, whereas Pbp1A and PbpZ were evenly distributed over the cell body (Fig 2.2 A). PbpC accumulated at the stalked pole, as reported before [70]. To exclude the possibility that the midcell localization is an effect of overproduction by the xylose-inducible promoter, endogenously expressed *venus-pbpX* and *venus-pbpY* fusions were generated. Apart from a decreased fluorescence intensity, the same localization pattern was observed (Fig 2.2 B). Moreover, all fluorescent fusions were stably expressed (Fig. 2.2 C), and Venus-PbpX and Venus-PbpY accumulated to similar cellular levels (Fig. 2.2 D).

2.1.3 PbpX and PbpY are late cell division proteins

The midcell localization of PbpX and PbpY suggested a possible role of the two proteins in cell division. To further analyze their precise localization dynamics, synchronized *C. crescentus* cells expressing either *venus-pbpX* or *venus-pbpY* from the xylose-inducible promoter, were analyzed by time-lapse microscopy. It was not possible to use the native fusions, because the fluorescence signal bleached too rapidly. Even though, bleaching effects during the experimental procedure resulted in partially loss of the focus of the inducible fluorescence fusion proteins, thus midcell localization

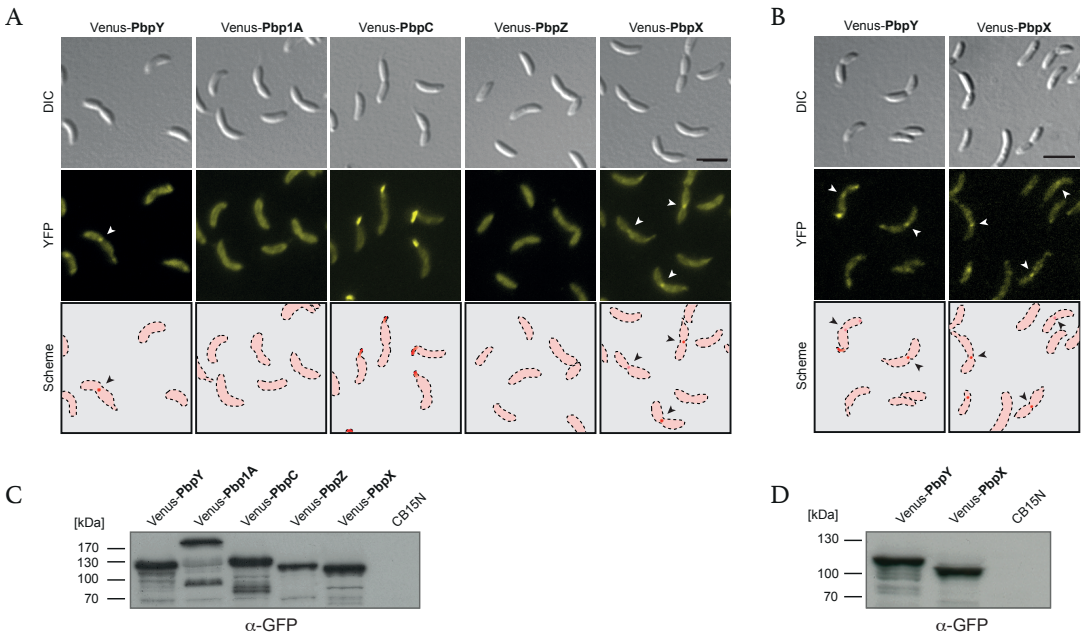

FIGURE 2.2: PbpX and PbpY localize at the site of cell division. **(A)** Subcellular localization of each individual bPBP of *C. crescentus*. Strains expressing *venus-pbpY* (AM457), *venus-pbp1a* (KK33), *venus-pbpC* (MT279), *venus-pbpZ* (AM458) and *venus-pbpX* (MT278), respectively, under the control of the xylose-inducible *xylX* promoter were induced for 3 h with 0.3 % with xylose and imaged by DIC and fluorescence microscopy. Scale bar: 3 µm. **(B)** Localization of PbpY and PbpX when expressed from their endogenous promoter. Derivatives of the wild-type strain expressing the respective hybrid gene in place of native *pbpY* (WS045) and *pbpX* (WS055). Scale bar: 3 µm. **(C)** and **(D)** Immunoblot analysis of the strains shown in (A) and (B), respectively, using α-GFP serum. Wild-type strain CB15N served as a negative control. Figures taken and modified from [182].

could not be observed in every cell. However, early in the cell cycle, both proteins formed patches or foci at one or both poles, but not consistently in all examined cells (Fig. 2.3 A and B), which could be a result of overexpression. During progression through the cell cycle, additional and apparently random accumulations appeared within the cells, before Venus-PbpX and Venus-PbpY condensed at the cell division site. Notably, both PbpX and PbpY only localized at the division plane after a clear constriction of the cell envelope was visible. Hence, they are possibly late recruits to the divisome. In order to reveal their timing of midcell recruitment, the localization dynamics of both bPBPs were quantified in a large number of synchronized cells, and the timing was compared relative to the first and last essential cell division protein, FtsZ and FtsN. For this purpose, fluorescent protein fusions of FtsZ, FtsN, PbpX, and PbpY were used and the fraction of cells exhibiting a midcell focus and a constriction were counted. The data revealed that PbpX localized at midcell slightly before or concomitant with the onset of cell constriction (Fig. 2.3 C). PbpY, in contrast, accumulated to a

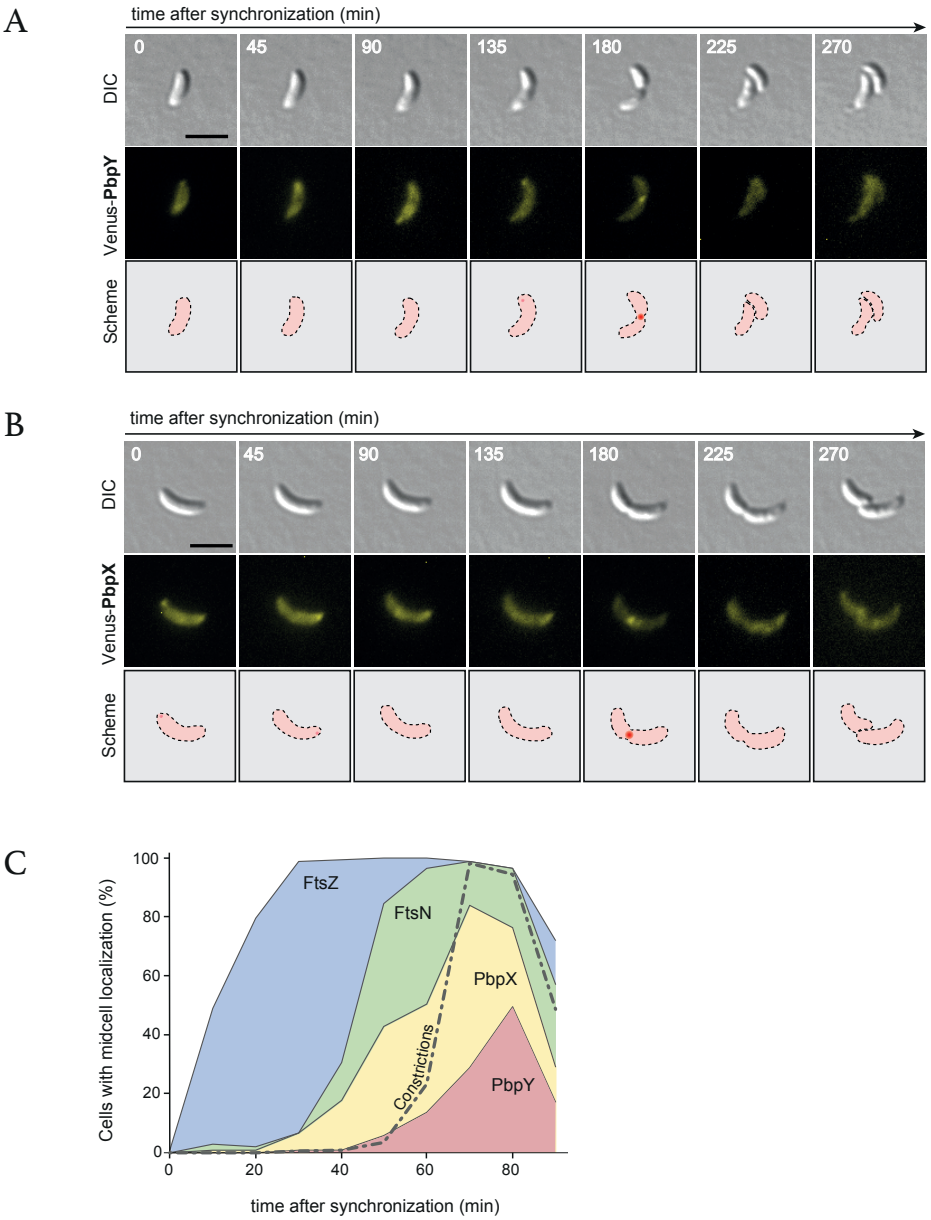

FIGURE 2.3: Localization dynamics of PbpX and PbpY during the cell cycle of *C. crescentus*. (A) Cells carrying *venus-pbpY* (AM457) under the control of the *xylX* promoter were grown to exponential phase in complex medium (PYE) and induced for 3 h with 0.3 % xylose. Isolated swarmer cells were transferred onto M2G agarose pads, supplemented with 0.3 % xylose, and imaged at the indicated time points using DIC and fluorescence microscopy. **(B)** Cells carrying *venus-pbpX* (MT278) were treated and analyzed as described in (A). Scale bar: 3 µm. **(C)** Quantification of PbpX and PbpY midcell localization. Swarmer cells of strains producing fluorescent protein fusions of FtsZ and FtsN (AM160), PbpX (MT278) or PbpY (AM457) were transferred into PYE medium and grown for the duration of one cell cycle. Samples were taken at regular intervals and analyzed for the fraction of cells showing a noticeable focus of the indicated protein at midcell (n>100 for each time point and strain). The quantification of constricted cells is shown for AM160. Note: the time scale used in panels A/B and C differ, since different media and growth conditions (PYE liquid/M2G agarose pads) were used. Figure taken and modified from [182].

less extent at midcell and significantly later than PbpX, suggesting that it may be involved mainly in the late steps of cell division. Notably, the percentage of cells showing midcell foci of both PbpX and PbpY was lower than that of cells with FtsZ and FtsN foci. Thus, it is conceivable that their midcell localization is relatively short, which was also observed in a time-lapse experiment (Fig 2.3 A and B). Interestingly, both proteins accumulated after the late cell division protein FtsN became visible at midcell. Based on this, I addressed the question which divisome factors are required for the recruitment of PbpX and PbpY.

2.1.4 Divisome localization is dependent on the late-stage actor FtsN

The assembly and polymerization of FtsZ molecules into a ring-like structure at midcell is crucial for the recruitment of all other downstream cell division proteins [111]. In the absence of FtsZ, the cell division machinery fails to assemble, leading to long, smooth filamentous cells that are unable to divide [187]. Since PbpX and PbpY localize to the division plane and are thus likely to interact with the divisome, I tested whether this localization pattern is indeed dependent on FtsZ. For this purpose, the localization dynamics of fluorescently tagged PbpX and PbpY derivatives were examined in a conditional *ftsZ* mutant. In cells depleted of FtsZ, Venus-PbpX and Venus-PbpY were evenly distributed within the long, smooth filaments (Fig. 2.4 A and B). Thirty minutes after re-induction of FtsZ synthesis, cell division resumed, and discrete fluorescent foci were formed at the future division site (Fig 2.4 A and B). Consequently, PbpX and PbpY are recruited to the divisome in an FtsZ-dependent manner.

Since the localization studies indicate that PbpX and PbpY are recruited to midcell after FtsN, I further tested the localization dependency on FtsN. FtsN is the last essential cell division protein, which localizes at the division site and is involved in coordinating cell wall remodeling [110, 150, 188]. Similar to the previous experiment (Fig. 2.5 A and B), a strain was generated that carried an inducible fluorescent fusion to either PbpX or PbpY in a conditional mutant of *ftsN*. As observed for the FtsZ depletion strains, Venus-PbpX and Venus-PbpY were evenly distributed within the cell body under restrictive conditions (Fig. 2.5 C and D). A switch to permissive conditions and, consequently, FtsN synthesis, led to the formation of distinct foci of the PbpX and PbpY derivatives at the future division site, as observed for the FtsZ depletion strain.

I also tested the possibility that the localization of both bPBPs may be dependent on the nonessential cell division protein DipM. DipM is a putative PG hydrolase that interacts with FtsN and is involved in cell wall invagination [150–152]. Fluorescence microscopic analysis revealed a DipM-

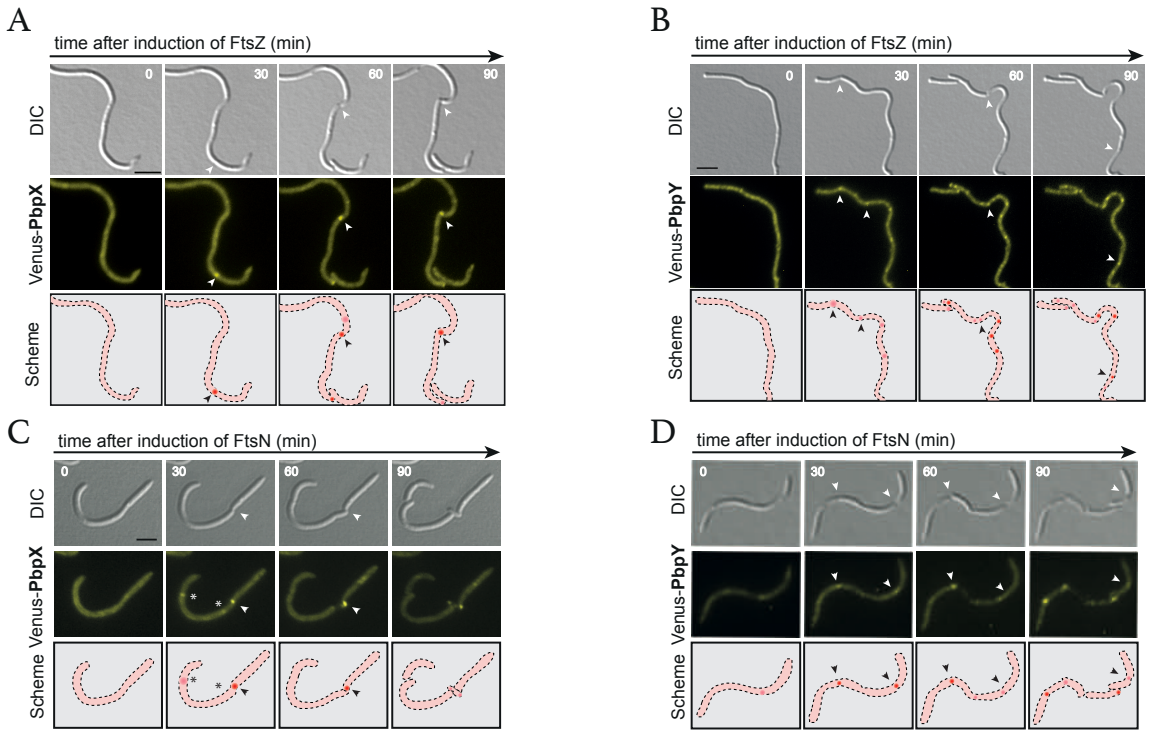

FIGURE 2.4: Time-lapse-imaging of the FtsZ- and FtsN-dependent localization of PbpX and PbpY. **(A)** A conditional *ftsZ* mutant (*ftsZ*::P_{iol}-*ftsZ*) carrying *venus-pbpX* under the control of the *xylX* promoter (WS063), was grown in M2G medium lacking myo-inositol to deplete FtsZ. Three hours prior to microscopic analysis, expression of the fluorescent protein fusion was induced by addition of 0.3 % xylose. Subsequently, cells were transferred onto M2G-agarose pads supplemented with 0.3 % xylose and 0.3 % myo-inositol to replete FtsZ. At the indicated time intervals, cells were analyzed by DIC and fluorescence microscopy. **(B)** Cells of strain WS062 (*ftsZ*::P_{iol}-*ftsZ* P_{xyl}::P_{xyl}-*venus-pbpY*) were treated and analyzed as described in (A). **(C)** Effect of FtsN depletion on Venus-PbpX localization. A conditional *ftsN* mutant (AM473) carrying *venus-pbpX* under the control of the *xylX* promoter (Δ*vanA* Δ*ftsN* P_{van}::P_{van}-*ftsN* P_{xyl}-*venus-pbpX*) was cultivated for 12 h in PYE to deplete FtsN. The expression of *venus-pbpX* was induced by addition of 0.3 % xylose 3 h before time-lapse microscopy was started. To re-induce *ftsN* expression, cells were transferred onto a M2G-agarose pad supplemented with 0.3 % xylose and 0.5 mM vanillate. The cells were imaged at the indicated time points. Arrowheads point to constriction sites. Asterisks indicate Venus-PbpX foci at incipient division sites that faded during the course of the experiment, possibly by photobleaching. **(D)** Localization dependency of Venus-PbpY on FtsN. Cells of strain AM472 (Δ*vanA* Δ*ftsN* P_{van}::P_{van}-*ftsN* P_{xyl}-*venus-pbpY*) were handled and analyzed as described in (C). Scale bar: 3 µm. Figures taken and modified from [182].

independent localization of Venus-PbpX and Venus-PbpY, since both derivatives localize to the division sites in DipM-depleted cells (Fig. 2.5 A).

A recent study reported that the midcell localization of the cell division-specific bPBP of *E. coli*, PBP1B, is dependent on the interaction between FtsZ and the cytoskeletal element MreB [189].

In *C. crescentus*, the MreB homolog also condenses to an intense band at midcell, dependent on divisome formation [87, 88]. To test the role of the MreB and FtsZ interaction in the localization dynamics of the fluorescently tagged derivatives of PbpX and PbpY, a mutant form of MreB that no longer accumulates at midcell ($MreB_{Q26P}$) [50] was used. However, distinct foci of both fusion proteins still formed at the cell division site, suggesting that their midcell recruitment to midcell occurs independently of MreB (Fig. 2.5 B).

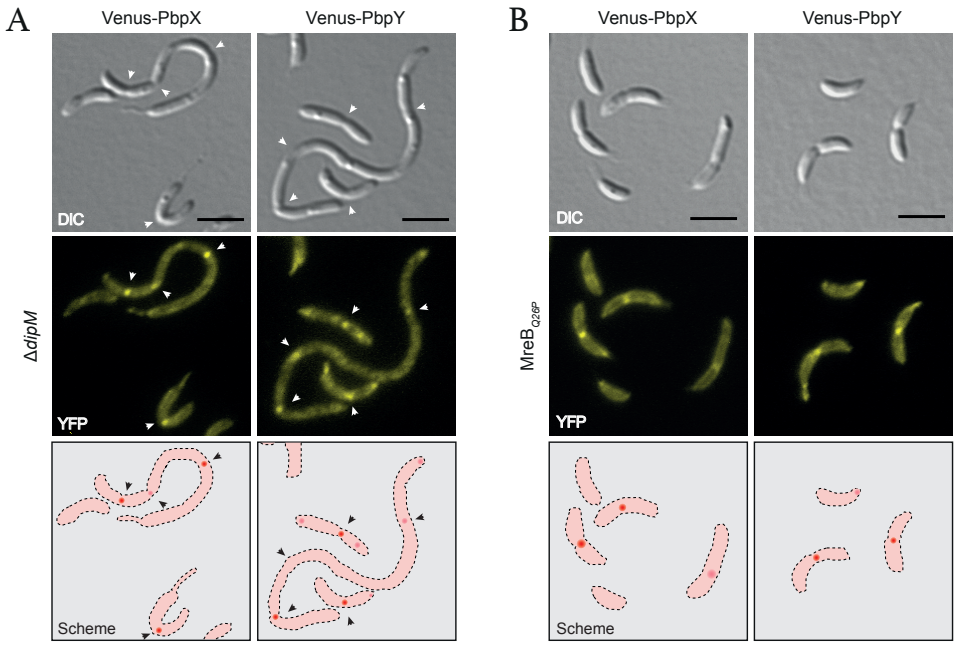

FIGURE 2.5: PbpX and PbpY midcell localization is independent of DipM and the cytoskeleton element MreB. (A) Localization of Venus-PbpX and Venus-PbpY in the absence of DipM. Cells of a Δ*dipM* mutant expressing *venus-pbpX* (WS057) and *venus-pbpY* (WS058) from the xylose-inducible *xylX* promoter were grown to exponential phase and cultivated for 3 h by addition of 0.3 % xylose with subsequent imaging by DIC and fluorescence microscopy. Arrowheads indicate constriction sites. **(B)** MreB-independent localization of PbpX and PbpY to the cell division site. Cells of the $mreB_{Q26P}$ mutant, which is unable to interact with FtsZ, expressing *venus-pbpX* (WS084) and *venus-pbpY* (WS085) from the xylose-inducible *xylX* promoter for 3 h by addition of 0.3 % xylose, were grown to exponential phase and imaged by DIC and fluorescence microscopy. Scale bar: 3 μm. Figure taken and modified from [182].

The localization studies performed strongly suggest that PbpX and PbpY are associated with the divisome and their midcell recruitment relies on the presence of the late cell division protein FtsN. Thus, they might be implicated in PG remodeling at the late stage of cell division.

2.1.5 bPBPs are functionally redundant

E. coli possesses three bifunctional PBPs, of which PBP1A is the elongasome-specific and PBP1B the cell division-specific PG synthase [66, 188, 190]. Nevertheless, the two proteins can functionally replace each other, and only the double deletion is lethal [191]. Putting this into the context of *C. crescentus*, I addressed the question of whether the five bPBPs are also redundant and have overlapping functions. To determine the degree of functional redundancy, a set of mutants lacking one or several bPBPs was generated, and the morphological changes were analyzed using cell length as a read-out. Neither in complex PYE nor in minimal M2G medium, any morphological differences could be detected between the mutant strains and the wild-type (WT), suggesting a high functional redundancy (Fig. 2.6 A). Next, I attempted to generate a quintuple bPBP mutant, which I was not able to obtain. Consistent with this finding, cell lysis was observed upon depletion of PbpX in a conditional *pbpX* mutant strain lacking all native bPBP-encoding genes (Fig. 2.6 B and C). Interestingly, the conditional mutant grew normally with regard to its doubling time and cell morphology upon induction of *pbpX*, indicating that PbpX alone is sufficient for cell viability under normal growth conditions. This result shows that the function of PbpX is not limited to septal PG remodeling but also contributes to a thus-far unknown degree to dispersed and preseptal elongation.

Both the functional redundancy of the bPBPs and the requirement of PbpX raised the question of whether any of the other bPBP paralogs is sufficient to ensure normal growth and cell shape. To address this question, I performed complementation studies in the conditional *pbpX* mutant lacking all chromosomally encoded bPBPs, in which ectopically integrated copies of each paralogous gene were expressed under the control of an inositol-inducible promoter (Fig. 2.7 A).

To induce expression of the respective bPBP and to assess its ability to complement the loss of PbpX activity, cells grown in xylose-containing medium to express *pbpX* were washed and induced with myo-inositol to test for complementation of the loss of PbpX expression. Next, the growth of each strain was followed in batch cultures and the cell lengths and growth rates were determined upon full depletion of PbpX (Fig. 2.7 B to E). These studies demonstrated that complementation with PbpC, PbpX, or PbpY resulted in very similar growth properties, with slightly longer doubling times than the wild-type but similar optical densities after 24 h of growth (Fig. 2.7 B). Cells only synthesizing Pbp1A as the sole bPBP, were viable and had a comparable doubling time in the beginning but reached a significantly lower cell density in the stationary phase. In constrast, PbpZ could not complement the absence of PbpX, since cells producing only PbpZ could not reach

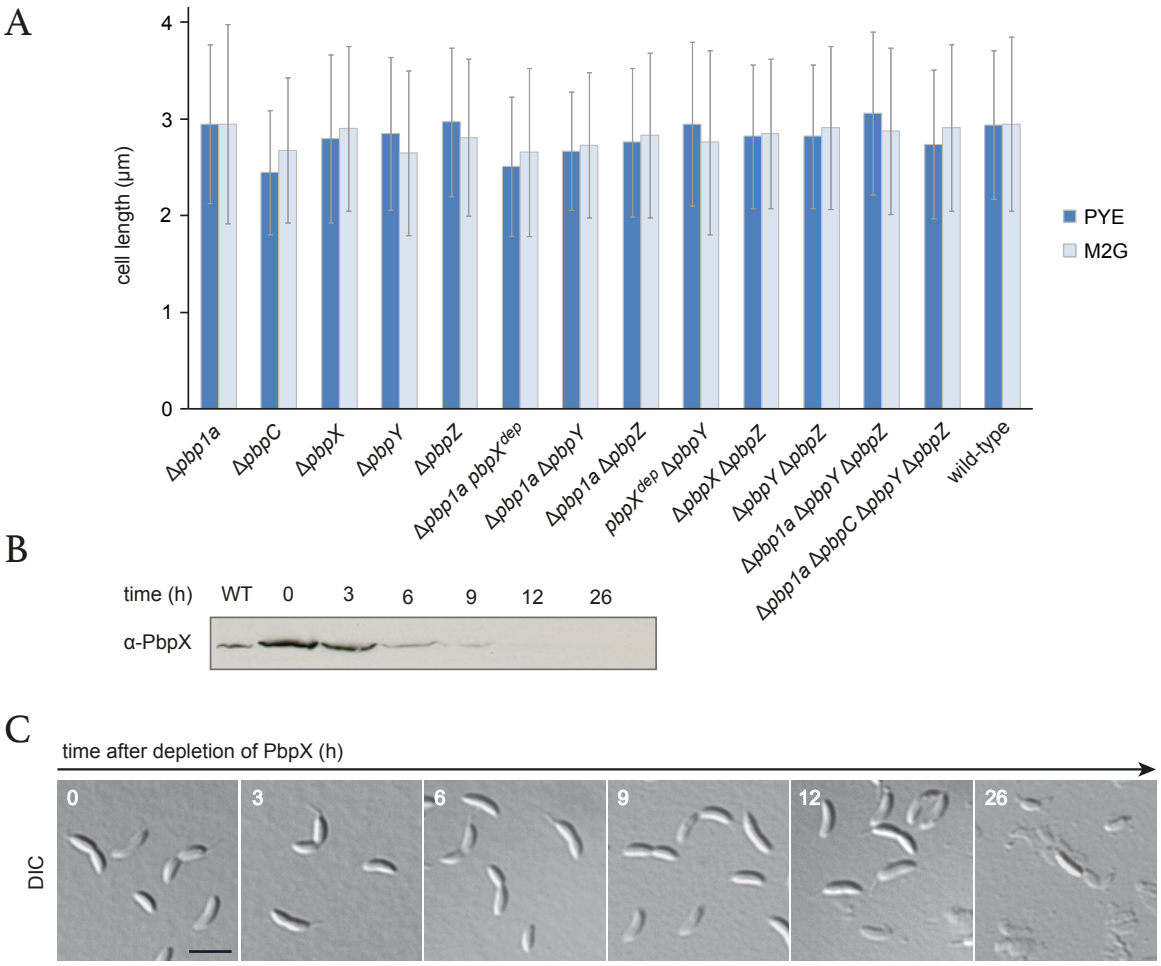

FIGURE 2.6: The bPBPs of *C. crescentus* are highly redundant but required for viability. (A) Quantification of cell length in the wild-type and mutant strains lacking one or more bPBPs. All strains were grown to exponential phase in complex medium (PYE) and minimal medium (M2G), and the average cell length was determined (>300 per strain, error bars depict standard deviations). The genes labeled with "dep" in the respective strain were inactivated by growing the cells in the absence of the inducer xylose. **(B)** Immunoblot analysis of PbpX levels upon depletion in strain WS056 (Δ*pbp1a* Δ*pbpC* Δ*pbpX* Δ*pbpY* Δ*pbpZ* P_{xyl}::P_{xyl}-*pbpX*). The cells were grown in PYE medium supplemented with 0.3 % xylose, washed, and transferred into fresh PYE medium lacking the inducer (t=0). Samples were taken at the indicated time intervals and subjected to immunoblot analysis using PbpX antiserum. **(C)** Time-lapse-imaging of cells depleted of bPBPs. Cells from the samples described in (B) were visualized by DIC microscopy. Scale bar: 3 µm. Figure taken from [182].

high cell densities, similar to the control cells lacking any inositol-inducible bPBP gene (empty vector). The cell lengths of the respective bPBP mutant strains were assessed after depletion of PbpX for 30 h (Fig. 2.7 C to E). The control strain not producing of any bPBPs exhibited 30 % of

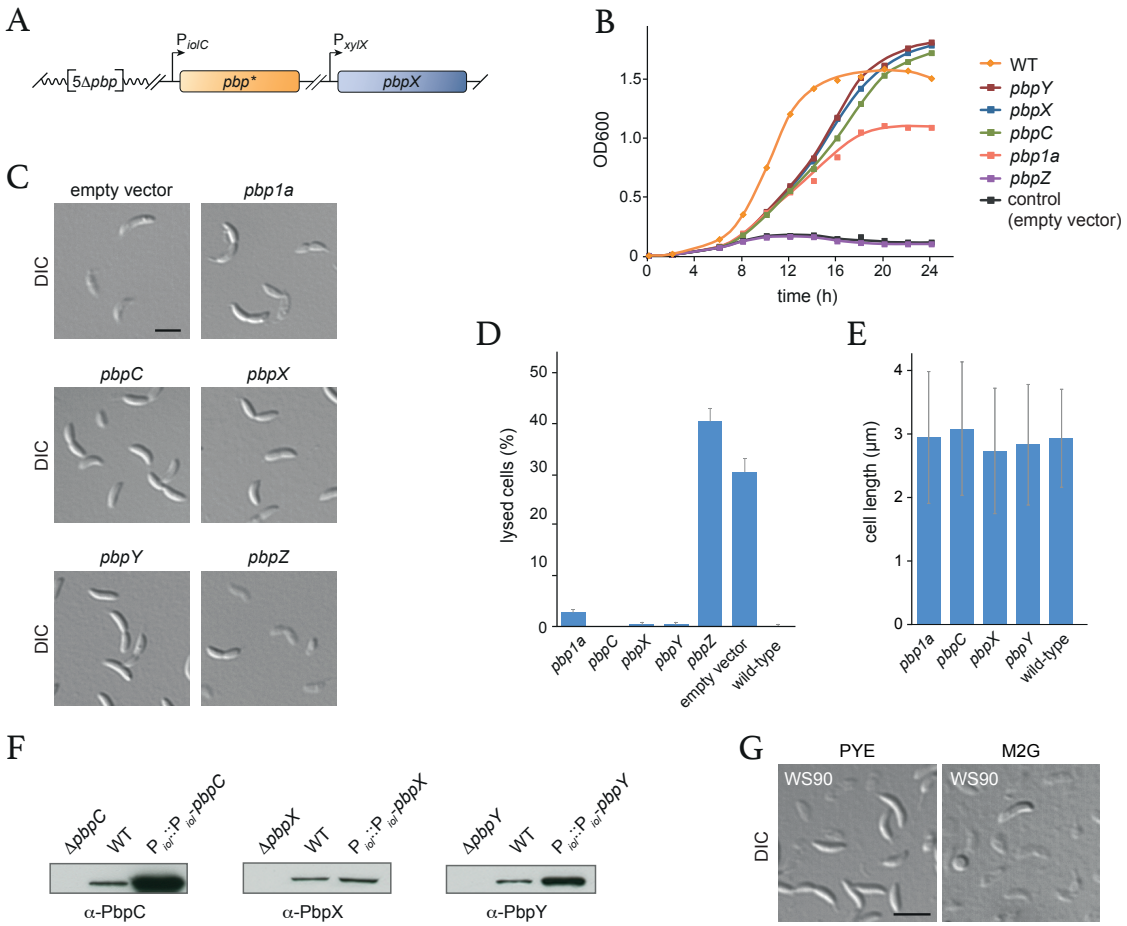

FIGURE 2.7: All bPBPs except PbpZ are able to support cell growth. (A) Genetic complementation system for analyzing the functionality of individual bPBP-encoding genes. A copy of *pbpX* was placed under the control of the xylose-inducible *xylX* promoter in a strain lacking all bPBPs (Δ*pbp*). In addition, a second copy of the bPBP of interest (*pbp**) was placed downstream of the myo-inositol-inducible *iolC* promoter. Depletion of PbpX and induction of a bPBP paralog will unveil the ability of individual bPBPs to support growth in an otherwise bPBP-free background. **(B)** Growth properties of cells synthesizing only a single bPBP. Strains were constructed as described in (A), carrying a myo-inositol-inducible copy of *pbp1a* (WS072), *pbpC* (WS073), *pbpX* (WS070), *pbpY* (WS071) or *pbpZ* (WS074). Each strain was grown in PYE supplemented with 0.3 % xylose, washed, and transferred into PYE medium containing 0.3 % myo-inositol (t=0). Their growth was followed by monitoring the optical density (OD_{600}). **(C)** Morphological analysis of the strains described in (B) by DIC microscopy. Each strain was grown and handled as described in (B) and imaged after 30 h of growth in the presence of 0.3 % myo-inositol. Scale bar: 3 µm **(D)** Quantification of cell lysis observed for the strains described in (B). The fraction of lysed (ghost) cells was counted (n>300) for each individual strain after 30 h of growth in PYE supplemented with 0.3 % myo-inositol. Error bars depict standard deviations. **(E)** Quantification of cell lengths in the cultures described in (B). Measurements were made at t=30 h (n=100 cells per strain; error bars show standard deviations). **(F)** Expression levels of PbpC, PbpX and PbpY upon expression from the native or inositol-inducible promoter. The wild-type and strains WS070, WS071, and WS073 were grown and treated as described in (B). Samples were withdrawn after 30 h of growth in the presence of 0.3 % myo-inositol and used for immunoblot analysis with the indicated antisera. Strain MT282 (Δ*pbpC*), KK1 (Δ*pbpX*) and KK16 (Δ*pbpY*) were used to control for the specificity of the respective antibody. **(G)** Complementation with native levels of PbpC. Cells of strain WS090 (Δ*pbp1a* Δ*pbpX* Δ*pbpY* Δ*pbpZ* P_{xyl}::P_{xyl}-*pbpX*) were grown in PYE and M2G, respectively, supplemented with 0.3 % xylose, washed, and transferred into the same medium lacking inducer. After 45 h of growth, the cells were imaged by DIC microscopy in the exponential growth phase. Scale bar: 3 µm. Figure taken and modified from [182].

lysed cells. Comparable to the cell growth in batch culture, complementation with PbpC, PbpX and PbpY yielded in fully viable cells, displaying a wild-type-like growth rate and cell morphology. Expression of only *pbp1a* resulted in normal cell morphology, but cells showed an increased frequency of cell lysis, which may account for the lower final cell density. Cells producing only PbpZ were not able to survive, because they exhibited extensive cell lysis with 40 % of the cell population lysed after 30 h of growth (Fig. 2.7 B to D). Similar complementation studies were also performed with fluorescently-tagged bPBPs. Identical results were obtained, with efficient complementation with Venus-PbpC, Venus-PbpX, and Venus-PbpY, respectively, partial complementation with Venus-Pbp1A, and extensive lysis of cells, in which Venus-PbpZ was the only expressed bPBP [182], confirming the results obtained with the native proteins. Immunoblot analysis revealed that the Pbp1A fusion accumulated to a significantly lower extent than the PbpC, PbpX and PbpY fusions [182], which may explain its impaired ability to support growth compared to the others. Furthermore, a strong signal was detected for Venus-PbpZ in the immunoblot assay [182], excluding the possibility that a weak gene expression is the reason for the failed complementation (data not shown). Moreover, the functionality of the fusion constructs could be confirmed, since efficient complementation for particular bPBPs was obtained, suggesting that the midcell localization of PbpX and PbpY (Fig. 2.3, page 23) is not an artifact. Since an artificial expression system was used for the complementation studies resulting in overproduction of the respective bPBP, I addressed the question of whether native expression levels were sufficient to support efficient growth, as observed for PbpX (see Fig. 2.6 A). I compared the native and induced protein levels of PbpX, PbpY, and PbpC, using specific antibodies. The results indicate that PbpY and, in particular, PbpC were significantly overproduced in the respective native complementation strains, whereas the levels of PbpX were only slightly elevated (Fig. 2.7 F), opening the possibility that the tested bPBPs may only complement at elevated levels. Based on these results, a more detailed study was performed with PbpC to clarify the requirement of elevated expression levels for complementation. It was not possible to generate a mutant strain that contained only *pbpC* at the native locus as the sole bPBP-coding gene, suggesting that native levels of PbpC are not sufficient to compensate for the loss of all other paralogs. To further verify this result, a conditional mutant of *pbpX* lacking all native bPBP genes except for PbpC was generated, and its growth was followed under restrictive conditions. As expected, cells were prone to lyse, in particular when grown in M2G minimal medium (Fig. 2.7 G). The more pronounced lysis in M2G could be explained by osmotic effects, since the osmolality (measure of osmoles of solute per kilogram of solvent) of M2G is ∼2.4x higher than that of PYE.

In summary, the mutational analyses indicate that Pbp1A, PbpC, PbpX and PbpY are, in principle, functionally redundant and are able to contribute to different growth modes, including elongation,

preseptal elongation, and septal PG synthesis during cell division. Moreover, PbpX may be the most effective bPBP, since no significant changes in morphology and growth properties could be observed under standard conditions, when expressed at native levels and as the sole bPBP in *C. crescentus*.

2.1.6 bPBPs as part of the divisome

Previous experiments have shown that Pbp1A and PbpC could, in principle, also contribute to septal PG synthesis (see Fig. 2.7 B to E). Thus, it is conceivable that the latter two are also able to interact with the divisome. In order to identify divisome components, which interact with PbpX and PbpY, respectively, and potentially also with Pbp1A and PbpC, a protein-protein interaction screen was conducted. I tested all five bPBP paralogs for interaction with a set of cell division proteins (data not shown), using a bacterial two-hybrid assay [192]. With the exception of PbpZ, all bPBPs showed an interaction with FtsN, FtsL, and DipM, albeit some interactions were only clearly visible in one configuration (Fig. 2.8 A). The observed *in vivo* interaction with FtsN underscores the localization dependency of PbpX and PbpY, suggesting that the dependency is probably based on direct interaction. The inability of PbpZ to interact with divisome components may explain its inability to complement the loss of all other bPBP paralogs in previous experiments (see subsection 2.1.5). In immunoblot analyses, a clear accumulation of the PbpZ hybrids was detected, which was comparable to that of the PbpX hybrids, excluding the possibility that weak, inefficient expression or reduced stability of the PbpZ fusion protein (Fig. 2.8 C) prevented an interaction. I also tested the homo- and heterodimerization potential of all bPBPs, since *E. coli* PBP1A and PBP1B were reported to form homodimers but to be unable to associate with each other [193]. Thus, the *C. crescentus* bPBPs were screened in all pairwise combinations to test for potential dimerization. Surprisingly, Pbp1A, PbpC, PbpX and PbpY were able to form homo- as well as heterodimers (Fig. 2.8 B). PbpZ showed no dimerization, supporting the notion that its role is distinct from that of its bPBP paralogs.

Altogether, the two-hybrid interaction studies support the previous findings that, in principle, every bPBP except for PbpZ is able to associate with the divisome, although the abundance of the interaction partners was not considered. PbpZ may have a yet unknown biological role and a catalytically inactive transglycosylase or transpeptidase domain. However, the results of the bacterial two-hybrid assay need to be regarded with care because components of the *E. coli* divisome may in some cases affect the interactions *in vivo*.

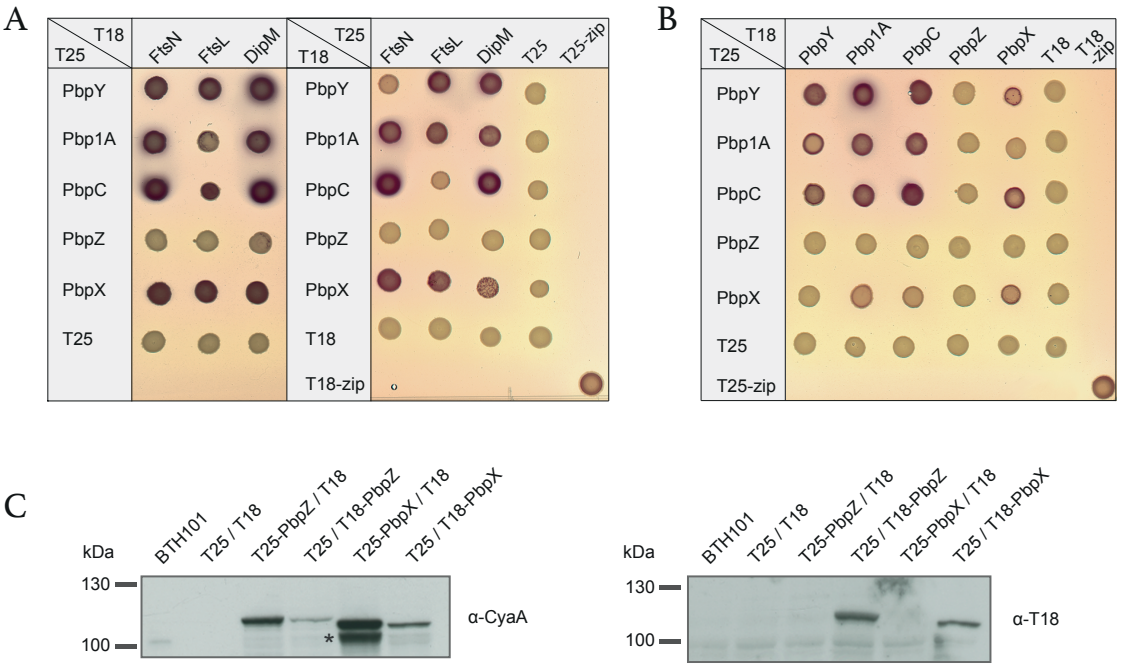

FIGURE 2.8: The bPBPs of *C. crescentus* form homo- and heterodimers and interact with divisome components *in vivo*. (A) Bacterial two-hybrid analysis testing the interaction between *C. crescentus* bPBPs and selected divisome components. For the assay, the *E. coli* reporter strain BTH101 was co-transformed with plasmids encoding fusions of the T25 and T18 fragments of *Bordetella pertussis* adenylate cyclase to the N-termini of the listed bPBPs and divisome components or to the yeast GCN4 leucin-zipper region (zip) as a positive control. Transformants were grown in LB media and spotted on MacConkey agar. Interactions between the two adenylate cyclase fragments are indicated by the formation of red colonies. In case of the periplasmic soluble DipM protein, a transmembrane linker ($MalG_{1\text{-}77}$) was inserted between DipM and the T18/T25 fusion partner. **(B)** Bacterial two-hybrid study of the interaction between *C. crescentus* bPBPs. The respective strains were generated and analyzed as described in panel (A). **(C)** Expression levels of the bacterial two-hybrid fusion proteins. *E.coli* BTH101 strain harboring pWS48 (pKT25-*pbpZ*), pWS49 (pUT18C-*pbpZ*), pWS30 (pKT25-*pbpX*) or the empty pKT25 and pUT18 plasmids respectively, were grown in LB supplemented with the respective antibiotics until they reached the early exponential phase. Expression was induced with 0.5 mM IPTG for 3 h, with subsequent sample withdrawal. The samples were analyzed by immunoblotting with an α-CyaA antibody [194], which primarily recognizes the T25 fragment, but to some extent also the T18 subunit. For the T18 fragment, a commercial monoclonal antibody directed at its C-terminus (α-T18) was used. The asterisk indicate a degradation product of T25-PbpX. Figures taken from [182].

2.2 New cell division proteins in *C. crescentus*

Once FtsZ has assembled into a ring-like scaffold, multiple protein-protein interactions lead to the formation of the divisome and the start of cell constriction by PG remodeling, membrane invagination and eventually cell-cell separation. The first chapter described the proteins involved in PG synthesis and in particular two proteins that are implicated in PG remodeling at the late stage of cell division. The following chapter will describe the identification and characterization of two new cell division proteins which are, similar to the respective bPBPs, involved in late cell division processes.

2.2.1 Identification of CedC and CedD

In an attempt to identify new factors involved in cell division, Susan Schlimpert, a former PhD student in the group, has identified two novel divisome components. In an interaction partner search approach, she identified CC3007 and investigated its subcellular localization. The analysis revealed that CC3007 localized to midcell in predivisional cells, suggesting a role in cell division (Fig. 2.9 A). According to this, it was termed with the preliminary name CedD (**Ce**ll **d**ivision protein D). Interestingly, *cedD* is co-conserved with *xerD* in proteobacteria, and typically located immediately upstream of the *xerD* gene. In *C. crescentus*, the two genes overlap by 4 bp, suggesting transcriptional co-regulation. XerD is a site-specific tyrosine recombinase, and binds with its cognate partner XerC to a 28 bp long intergenic region (*dif* site) [166, 167] in the terminus region of the chromosome where it mediates a site-specific recombination event leading to chromosome dimer resolution during final chromosome segregation [166, 167]. Based on this information, S. Schlimpert investigated the chromosomal context gene encoding the other tyrosine-recombinase, XerC. She indeed found a gene, which overlaps by 4 bp with *xerC* and is co-conserved in proteobacteria as well, namely *cc0345*, in the following referred as *cedC*. Similar to CedD, a xylose-inducible fusion of CedC to Venus localized at the division plane in constricted cells but also at the stalked pole (Fig. 2.9 A). To exclude any overexpression effect, a strain carrying *venus-cedC* in place of the native *cedC* was generated. Notably, the stalked pole localization of Venus-CedC could not be observed in this background (Fig. 2.9 A), suggesting that it may be an overexpression artifact.

In order to determine the physiological role of both proteins, S. Schlimpert generated mutant strains with a deletion of either *cedC* or *cedD*. In case of CedD, $aa_{68\text{-}508}$ were removed to prevent polar effects on *xerD*, since the two genes presumably lie in an operon. When the effect of the deletion was examined microscopically, no obvious morphological alterations could be observed

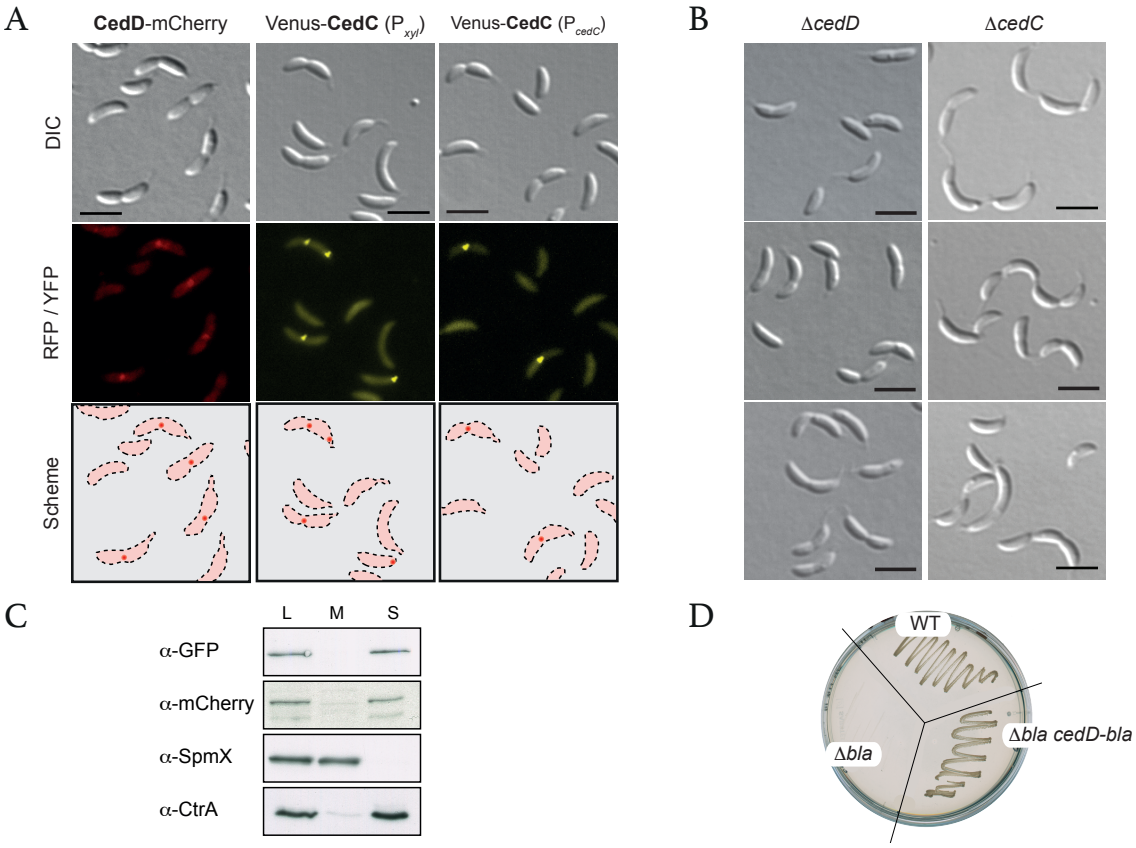

FIGURE 2.9: Protein localization and effect upon deletion of the new cell division proteins CedD and CedC. (A) Derivatives of the wild-type strain expressing *cedD-mCherry* (SS310) or *venus-cedC* (SS330) under the control of the xylose-inducible *xylX* promoter or cells carrying *venus-cedC* in place of the native *cedC* (SS348) were cultivated in PYE supplemented with 0.3 % xylose for 3 h (inducible fusions) and subsequently imaged by DIC and fluorescence microscopy. Scale bar: 3 µm. **(B)** Phenotypic analysis of cells lacking *cedD* or *cedC*. Strains with an *in-frame* deletion of *cedD* (SS426) or *cedC* (SS347) were grown to exponential phase in PYE medium and imaged using DIC microscopy. **(C)** CedC and CedD are soluble proteins. Fractionation experiments were performed by S. Schlimpert. Strains expressing *venus-cedC* (SS330) or *cedD-mCherry* (SS310) were grown in PYE to exponential phase and induced with 0.3 % xylose for 2 h with subsequent sample withdrawal. Samples were used for immunblotting, using the indicated antiserums. To determine the fractionation efficiency, α-SpmX was used as a control for a integral membrane protein [195], whereas α-CtrA was used as a control for the soluble response-regulator [196]. L = lysate, M = membrane, S = supernatant. **(D)** Membrane topology of CedD. The wild-type (CB15N), the TEM1 lactamase-deficient (Δ*bla*) *C. crescentus* strain CS606 [197], and a CS606-based strain carrying a xylose-inducible C-terminal fusion of CedD to the TEM1 lactamase (SS313) were grown on PYE medium supplemented with 0.3 % xylose and ampicillin. WT = wild-type (CB15N)

in complex (PYE) medium (Fig. 2.9 B). For *cedC*, all but the first twelve and last nine amino acids of the originally annotated coding sequence were deleted. When the mutant strain was grown in

standard PYE medium, a clear cell division defect with chained cells was observed (Fig. 2.9 B). Additionally, Δ*cedC* cells grew significantly slower than the wild-type (data not shown), suggesting an important cellular function.

Bioinformatic analyses predict both proteins to be soluble, with CedC possibly being located in the cytoplasm and CedD in the periplasm. Using fractionation experiments, S. Schlimpert confirmed the solubility of both CedC and CedD (Fig. 2.9 C). Furthermore, she obtained evidence for the periplasmic localization of CedD by generating a C-terminal fusion of the TEM1 lactamase to CedD and introducing it into a β-lactamase-deficient *C. crescentus* strain (SS310, Δ*bla* P_{xyl}::P_{xyl}-*cedD-bla*) [197]. Expression of the hybrid protein led to resistance against ampicillin (Fig. 2.9 D), which is only possible if the fusion protein is transported to the periplasm, where the target of β-lactams is localized. Thus, the predicted periplasmic localization of CedD was experimentally confirmed.

In summary, two new potential cell division proteins were identified, which are chromosomally co-conserved with XerC and XerD, respectively, among proteobacteria. Thus, their function may be related to that of the tyrosine-recombinases XerCD, although CedD localizes to another subcellular compartment, the periplasm. The absence of CedC resulted in a chaining phenotype as observed for *xerCD*-deficient cells [167, 198], whereas the deletion of *cedD* had no phenotypic consequences. Based on these results, I aimed at the functional characterization of particularly CedC, since this protein seems to play a more important physiological role than CedD. My work described in the following sections includes a detailed characterization of the Δ*cedC* phenotype and a comprehensive mutational analysis. Furthermore, it contains the elucidation of a functional link to XerCD, localization timing and verification of CedC as a divisome component. Moreover, I searched for CedC-interaction partners.

2.2.2 Characterization of CedC and CedD

In order to gain more information about CedCD, bioinformatical analyses were performed. These revealed that neither CedC nor CedD contains known protein domains (Fig. 2.10 A). CedC is relatively small (226 aa) and a single-domain protein entirely composed of a DUF484 domain, whereas CedD (550 aa) does not show any conserved domain. DUF484-containing proteins are found in 386 genomes of α-, β-, and γ-proteobacteria (Fig. A1, page 122). As mentioned before (see subsection 2.2.1), both proteins are highly conserved: *cedC* and *cedD* are located upstream of *xerC* and *xerD*, respectively, and overlap in case each by 4 bp, suggesting a transcriptional co-regulation with *xerC* and *xerD* (Fig. 2.10 B). Notably, almost 95 % of the *cedC* homologs are

encoded next to a *xerC* homolog (Fig. A1, page 122), suggesting a functional link between XerC and CedC. To determine whether *cedC* and *cedD* are developmentally regulated, their cell-cycle dependent transcriptional profiles were analyzed using existing microarray data [181]. Because of their potential functional link, the *ftsK* and *xerCD* genes were used as a reference. The data revealed that *xerCD* as well as *cedD* transcript levels remain relatively constant over the course of one cell cycle (Fig. 2.10 C). In contrast, the *cedC* transcript level correlates with the one of *ftsK*, showing an upregulation during the late stage of cell division (Fig. 2.10 C). However, despite these temporal variations in mRNA abundance, the protein levels of CedC remained constant throughout the cell cycle (Fig. 2.10 D). The abundance of CedD over the *C. crescentus* cell-cycle could not be determined due to the lack of a functional antibody.

2.2.3 CedC is a late acting cell division protein

The initial localization studies (see Fig. 2.9 A) suggested that CedC and CedD localize to midcell in cells that show a clear constriction of the cell envelope. To obtain more detailed information on the localization pattern of CedC, fluorescence time-lapse microscopy of synchronized cells expressing *venus-cedC* at native levels was performed. In agreement with the previous observations, no polar foci were detected in swarmer or stalked cells, but a clear focus formed at the division plane in predivisional cells (Fig. 2.11 A). This midcell localization was observed in every cell that was followed, but only at the very end of cytokinesis (starting from t=240 min), shortly before separation. This observation suggests that CedC is a very late recruit to the division plane and acts within a very short time frame.

To test whether CedC is part of the divisome and thus requires FtsZ for midcell localization, the effect of FtsZ depletion and repletion on CedC localization was investigated. For this purpose, the localization pattern of a xylose-inducible copy of Venus-CedC was monitored in a conditional *ftsZ* mutant. When cells were depleted of FtsZ, Venus-CedC was either evenly distributed throughout the filamentous cell or it accumulated into a focus at the stalked pole, probably due to slightly overproduction of the fusion protein (see Fig. 2.11 B). In cells showing a polar focus, repletion of FtsZ initiated the re-localization of Venus-CedC to the incipient cell division site (Fig. 2.11 B), otherwise the fusion protein condensed into a discrete focus at the division plane shortly before separation.

I further quantified the timing of the recruitment of Venus-CedC relative to that of FtsZ, FtsK, and FtsN. FtsZ was chosen as the first and FtsN as the last essential cell division protein, whereas FtsK was included because of its potential mechanistic link (via XerCD) to CedC (see subsection 2.2.2). A fluorescent protein fusion to XerC or XerD could not be included in this analysis, given the low

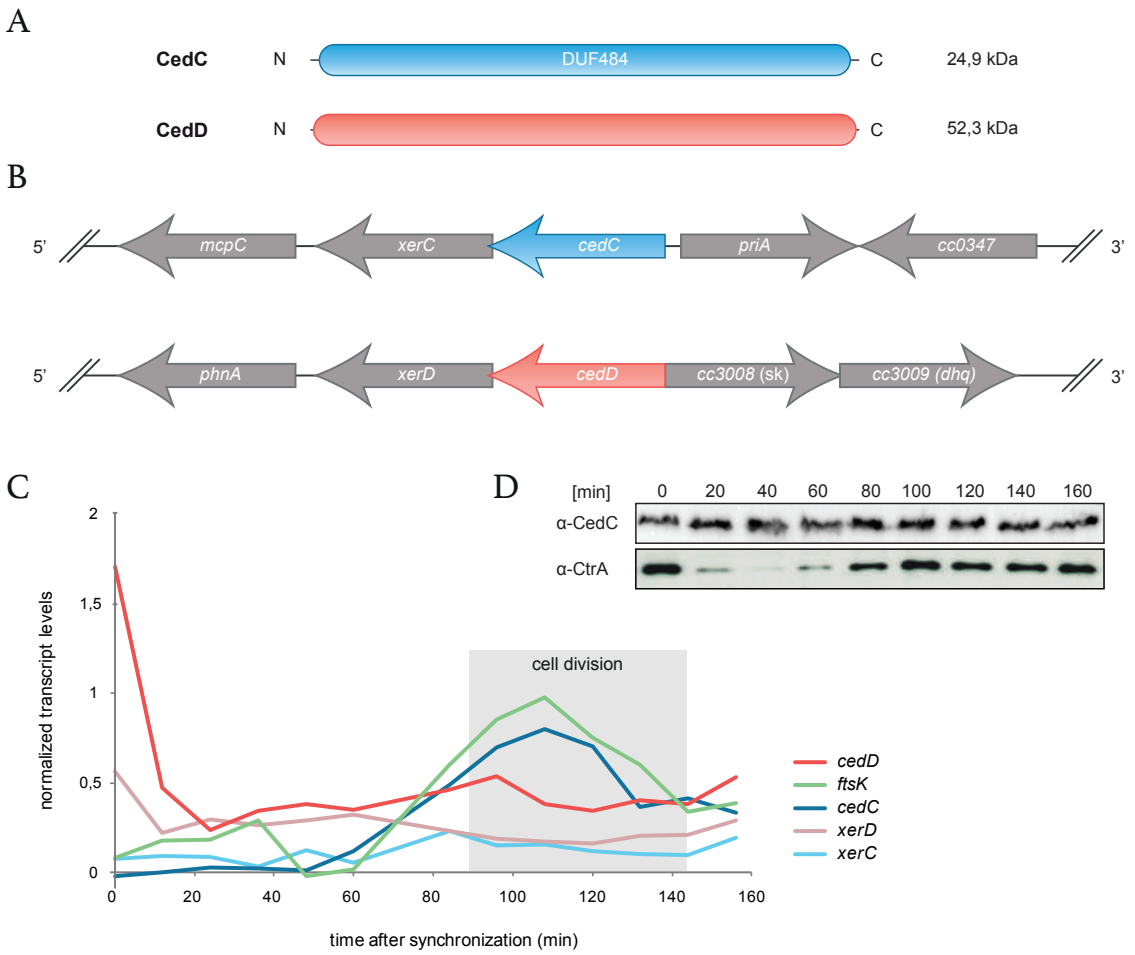

FIGURE 2.10: Bioinformatic analysis of CedC and CedD. (A) Schematic representation of the two putative cell division proteins of *C. crescentus*. CedC (226 aa) largely consists of a domain of unknown function (DUF484), whereas CedD (550 aa) has no predicted domains or structures. **(B)** Genomic context of *cedCD*. Both proteins are located upstream of *xerC* and *xerD*, respectively. **(C)** Transcript levels of *cedCD*, *xerCD* and *ftsK*. The graph is based on microarray data of synchronized *C. crescentus* wild-type cells [181]. **(D)** Immunoblot analysis of a synchronized *C. crescentus* culture using purified α-CedC serum. The protein level of CtrA is shown as a control for the synchronicity of the culture.

number of molecules per cell. Validating previous observations, Venus-CedC localized very late to the cell division site in the quantified cells, remarkably later than FtsN (Fig. 2.11 C), raising the possibility that it might be involved in the final steps of cell division. However, the peak value of the amount of cells in which midcell localization was observed was relatively low (approximately 30 %), which may be explained by the very short time-frame during which CedC shows localization at midcell.

In summary, the recruitment of CedC to the cell division site could be validated, in particular at a very late stage of cell division. Thus, the observed localization dependency on FtsZ is most likely indirect.

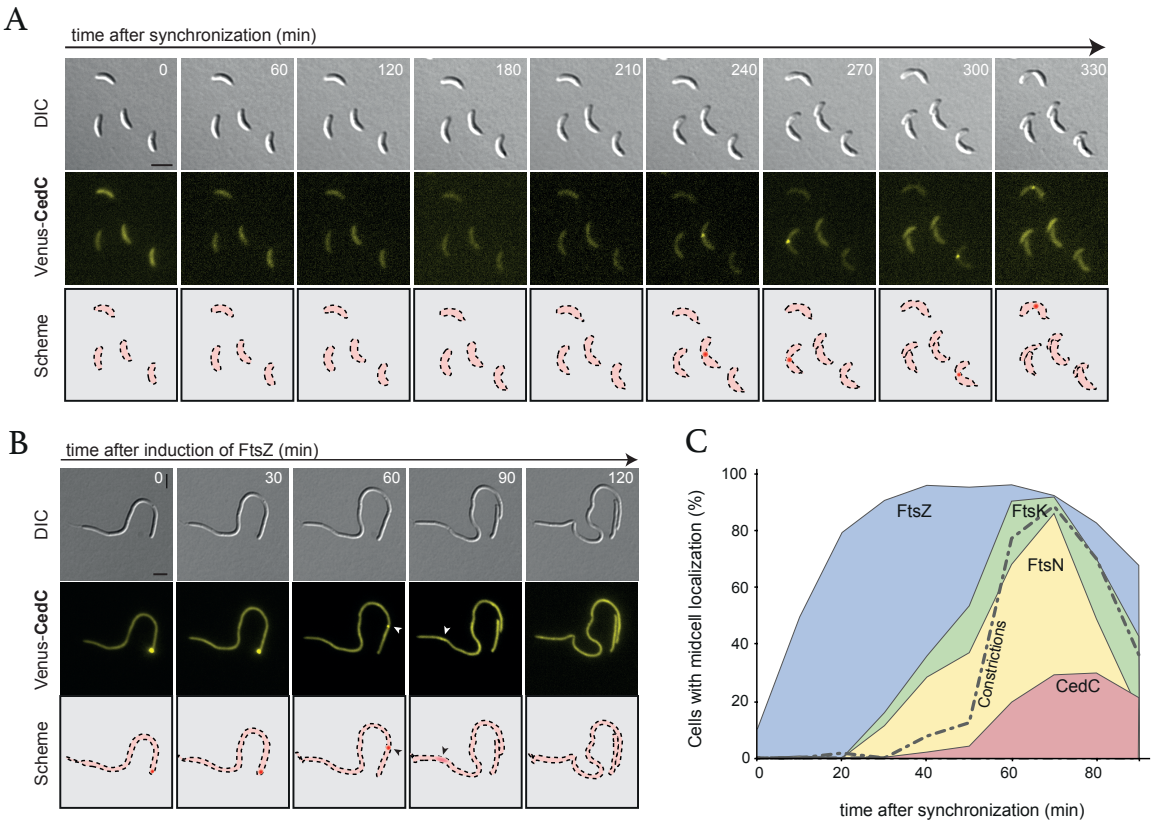

FIGURE 2.11: Cell-cycle dependent localization dynamics of the divisome component Venus-CedC. **(A)** A strain carrying the fluorescent fusion protein in place of native *cedC* (SS348) was grown to exponential phase in M2G medium and synchronized. Isolated swarmer cells were transferred onto M2G-agarose pads and imaged at the indicated time intervals by DIC and fluorescence microscopy. Scale bar: 3 μm **(B)** Localization of Venus-CedC is dependent on FtsZ. Cells of strain WS093 (*ftsZ*::P_{iol}-*ftsZ* P_{xyl}::P_{xyl}-*venus-cedC*) were grown in M2G supplemented with 0.3 % myo-inositol, washed, transferred into fresh M2G medium without myo-inositol, and cultivated for 7 h. Three hours prior to microscopic analysis, the expression of *venus-cedC* was induced by addition of 0.3 % xylose. The cells were then transferred onto M2G-agarose pads containing 0.3 % xylose and 0.3 % myo-inositol to re-induce *ftsZ* expression and imaged at the indicated time intervals. Scale bar: 3 μm. **(C)** Timing of the recruitment of Venus-CedC relative to that of FtsK and FtsZ. Isolated swarmer cells carrying *venus-cedC* in place of the native *cedC* and additionally expressing *ftsZ-ecfp* (WS103), *ftsK-ecfp* (WS104), and *mCherry-ftsN* (WS123) under the control of the xylose- or vanillate-inducible promoter were grown in PYE medium for the duration of one cell cycle. Samples were withdrawn at the indicated time points and analyzed for the fraction of cells showing a visible focus of the indicated protein at midcell (n>100 for each time point and strain). In addition, the percentage of constricted cells of strain WS104 is shown for each time point.

2.2.4 CedC is required for proper cell division under fast growing conditions

Previous experiments have shown that the Δ*cedC* strain is characterized by cell chaining (see Fig. 2.9 B), a growth defect, and smaller colonies on plates (data not shown). Importantly, complementation of the loss of native *cedC* with an ectopically expressed copy (Fig. 2.12 A) resulted in wild-type-like cell morphology and growth, excluding the possibility that the phenotype is caused by a polar effect. I wondered if the observed phenotype is linked to the growth rate, and thus, cultivated cells in different media. Interestingly, when cells lacking CedC were grown in minimal medium, in which the doubling time is increased from ∼90 min in PYE to 120 min, their phenotype (Fig. 2.12 B) and growth rate (data not shown) was comparable to that of wild-type cells. In order to explore whether the phenotype is more pronounced under fast-growing conditions, the doubling time of *C. crescentus* was reduced to ∼75 min by cultivating the cells in two-fold concentrated PYE. In accordance with the hypothesis, Δ*cedC* cells showed an even more pronounced phenotype with (as compared to 17 % in PYE) ∼60 % of the cells displaying a chaining phenotype, characterized by chained cells with deep constrictions (Fig. 2.12 B).

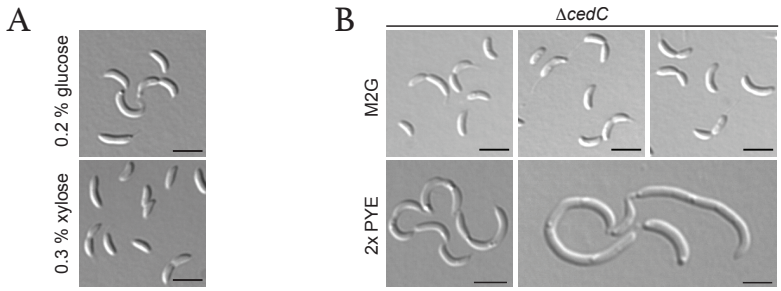

FIGURE 2.12: CedC deletion leads to morphological alterations under fast growing conditions. **(A)** The complementation strain (SS376), carrying a native copy of *cedC* expressed under the xylose-inducible promoter, was grown in PYE under permissive (0.3 % xylose) and non-permissive (0.2 % glucose) conditions and imaged in the exponential phase bye DIC microscopy. **(B)** Phenotypic analyses upon deletion of *cedC*. A strain with an *in-frame* deletion of *cedC* (SS347) was grown to exponential phase in different media as depicted, and imaged using DIC microscopy. Scale bar: 3 μm

In order to explore the reason for the failure to complete cell division in the absence of CedC in more detail, the chromosome content of the Δ*cedC* mutant was determined by flow cytometry to investigate whether chromosome replication is affected. Whereas wild-type cells primarily contained a single chromosome (1N) or partially synthesized sister chromosomes (2N), Δ*cedC* cells contained two or more chromosome equivalents (Fig. 2.13 A). This observation indicated that chromosome replication is not affected. Possibly, the problem could be a defect in DNA segregation, because there still may be DNA in the highly constricted parts that connect chained cells. To investigate this assumption, electron cryo-tomography (cECT) was performed in collaboration with A. Briegel at the Jensen lab (CalTech, USA) to visualize the division site in Δ*cedC* cells that failed to divide.

The tomograms clearly showed that daughter cells had a problem in completing cell division and still shared a common cytoplasm and cell envelope (red arrows, Fig. 2.13 B).

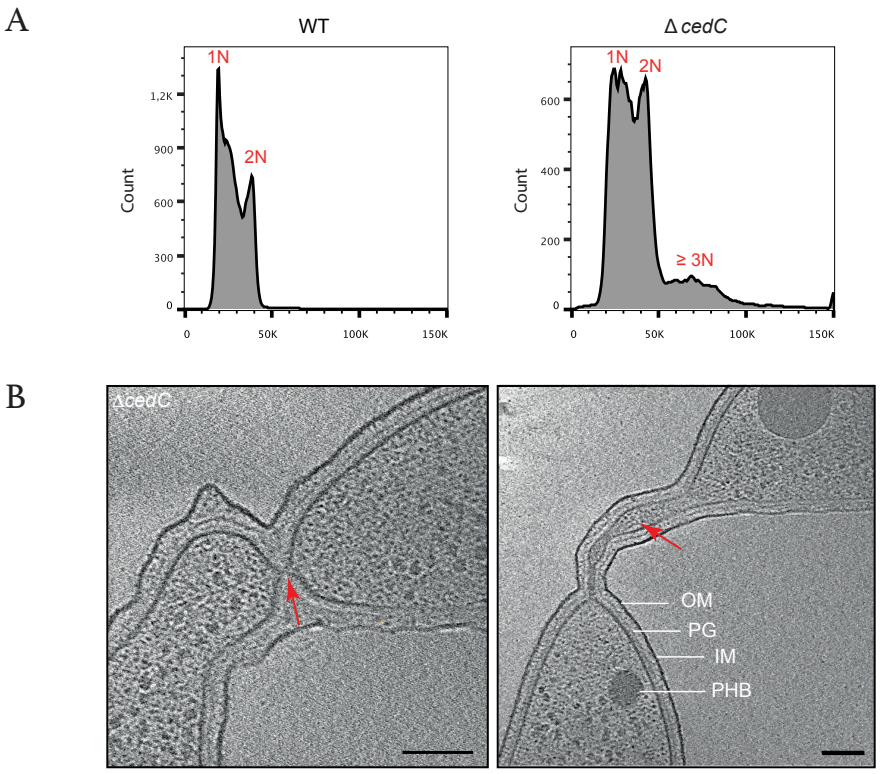

FIGURE 2.13: The chromosome is not fully segregated and trapped at the cell division site in the absence of CedC. (A) Quantification of chromosome content of cells lacking *cedC* compared to wild-type cells using flow cytometry. Strains were grown in PYE to exponential phase and diluted to an equal OD_{600} of 0.3. Subsequently, the chromosome content was determined by flow cytometry. Measurements were performed in collaboration with S. González Sierra (Synmikro, Marburg). The x-axis represents the number of chromosomal copies. **(B)** Slice of cECT tomographs, each showing a cell lacking *cedC* (SS347). Imaging was performed by A. Briegel (CalTech, USA). OM = outer membrane, PG = peptidoglycan, IM = inner membrane, PHB = polyhydroxybutyrat. Scale bar left picture: 90 nm, Scale bar right picture: 200 nm.

A possible DNA segregation defect could be caused by defective chromosome dimer resolution. Interestingly, deletion in *xerC* and/or *xerD* cause *E. coli* cells to grow as septated chains instead of filaments [167, 199, 200], a phenotype similar to that observed for the Δ*cedC* mutant. Based on this phenotypical similarity and the genomic context of *cedC* and *cedD*, a set of mutants with single and multiple *in-frame* deletions in the four relevant genes, *cedCD* and *xerCD*, were generated and analyzed microscopically. As expected, Δ*cedD* cells did not show any morphological changes, whereas Δ*cedC* cells displayed an ∼1.75 fold increase in cell length (Fig. 2.14 A and B), due to delayed cell-cell separation. Intriguingly, the absence of CedD largely suppressed the Δ*cedC* phe-

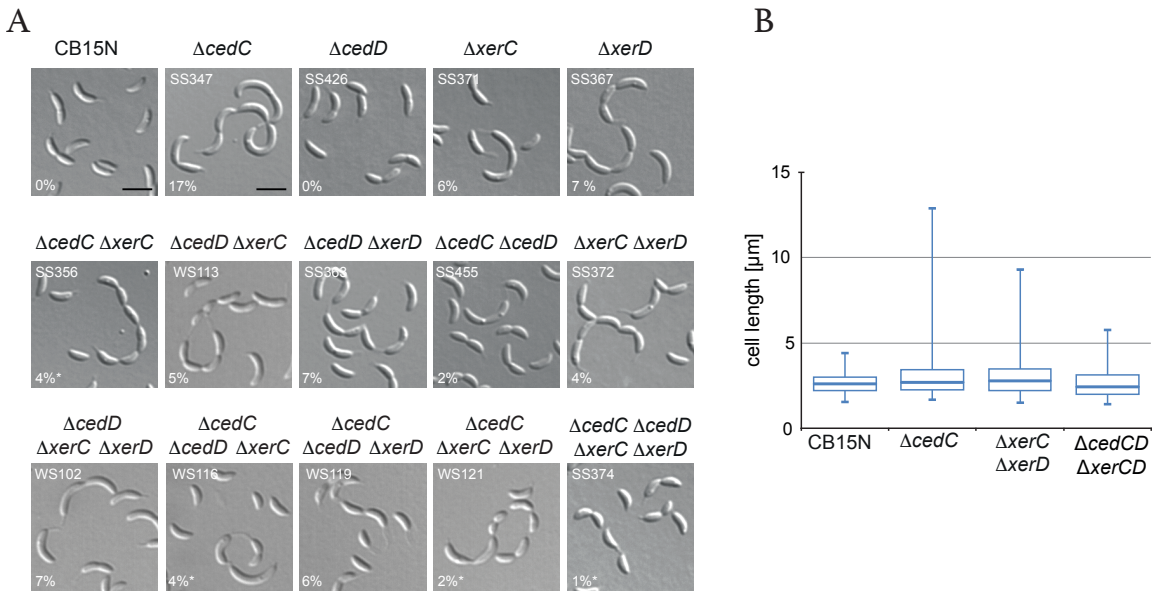

FIGURE 2.14: Impact on cell morphology caused by the deletion of one or more genes of interest. **(A)** Microscopic analysis of mutants with deletions in *cedC*, *cedD*, *xerC*, *xerD* or combinations of those. Strains (white) with the indicated *in-frame* deletions were grown to exponential phase in PYE and imaged using DIC microscopy. The percentages given in the pictures represent the fraction of chained cells for each strain. Scale bar: 3 µm. **(B)** Quantification of the cell length of selected strains shown in (A). The boxplot is based on measurement of the cell lengths of 185 cells per strain, analyzed by DIC microscopy. Data sets are displayed in box-whisker-plots. Shown are the interquartile range (box), the median (thick line), the 5th and 95th percentile (whiskers).

notype, with only 2 % of the double mutant cells displaying a cell separation defect. For the Δ*xerC* and Δ*xerD* single mutants a chaining phenotype was observed in about 6 - 7 % of the cells, which is in agreement with a previous study [198]. The Δ*xerCD* double mutant as well as Δ*cedD* cells carrying additional lesions in a single or both tyrosine recombinases did not show an increased number of chained cells, suggesting that CedD has no impact on the XerCD recombination system under the tested conditions. Interestingly, the combination of lesions in *cedC* and *xerC* or *xerD* had a suppressive effect, resulting in less chained cells. Moreover, the fraction of morphologically altered cells (17 %) and the average cell length of Δ*cedC* cells is higher than that of the Δ*xerCD* mutant (Fig. 2.14 A and B), suggesting that XerCD have an influence on the CedC phenotype. Additionally, when lesions in *xerC* and *cedC* were combined, significantly smaller predivisional cells were observed (Fig. 2.14 A). The effect was more dramatic in the quadruple mutant strain, leading to a decrease in the average cell length of the cell population to about 87 % (Fig. 2.14 B). Surprisingly, also the percentage of chained cells decreased significantly (1 %) and cells grew notably faster (data now shown). Thus, there may be a functional relationship that links chromosome dimer resolution to cell-cell separation.

Taken together, the experiments suggest that in the absence of CedC, cells are not able to complete cytokinesis, possibly due to the entrapment of DNA at the cell division site, in particular under fast-growing conditions. Furthermore, it emerged that CedD and the XerCD recombination system have an effect on the phenotype of Δ*cedC* mutant, since in absence of the tyrosine recombinases XerCD and/or CedD, cells can divide more efficiently.

2.2.5 CedC acts independent of XerCD

Based on the previous experiments, the potential correlation between XerCD-mediated chromosome resolution and the function of CedC was examined. To this end, I determined whether the Δ*cedC* phenotype is caused by chromosome dimers resulting from a failure of chromosome dimer resolution (CDR). Chromosome dimers only occur if an uneven number of crossover events happen between sister chromosomes. Their formation depends on the central player in homologous recombination, the DNA-dependent ATPase RecA [201–203]. It was shown that in *E. coli* site-specific recombination by XerCD depends on RecA [204]. Building on this finding, I further tested for a potential functional relationship between XerCD and CedC by generating a Δ*recA* mutation in the Δ*cedC* genetic background. It was reported before that the deletion of *recA* does not affect the morphology and growth of *C. crescentus* [205]. However, the resulting mutant strain displayed a pleiotropic phenotype, complicating the phenotypic analysis of the cells. To circumvent this problem, a conditional *cedC* mutant was generated, in which the expression of *cedC* is controlled by the xylose-inducible *xylX* promoter, with subsequent deletion of *recA* by homologous recombination. The conditional *cedC* mutant showed the same phenotype and decreased growth speed upon depletion of CedC for 10 h (Fig. 2.15) as the deletion strain. Moreover, the deletion of *recA* did not affect the wild-type morphology of *C. crescentus* (Fig. 2.15 bottom t=0), which is in line with previous observations [205]. When phenotypes of both the conditional mutant and the strain in which *recA* was additionally deleted were compared, no obvious difference in growth rate or cell length was detected (Fig. 2.15), suggesting that the phenotype of the Δ*cedC* mutant is not based on a failure to undergo CDR. This raised the question of whether CedC is involved in cell division rather than CDR or final chromosome segregation.

In order to determine whether the chaining phenotype in the absence of CedC is a result of impaired chromosome segregation, I intended to delete *cedC* in a strain in which the chromosomal terminus region is fluorescently labeled using the fluorescent repressor operator system (FROS) [206, 207]. The *ter*-region is the last part of the chromosome that is replicated and segregated. Thus, in case the duplicated *ter*-region cannot be segregated in the absence of CedC, this would implicate that

chromosome segregation is affected by the loss of CedC. Repeatedly, it was not possible to obtain any colonies of *C. crescentus* carrying a deletion of *cedC* in a FROS strain. The growth and morphology of cells carrying the FROS is usually not affected. However, a possible explanation for the unsuccessful generation of the mutant could be that the deletion of *cedC* negatively affects *ter* segregation, which is tagged with a ∼450kbp large *tetO* array. In further consequence, this could cause strong grow defects or possibly even lethality.

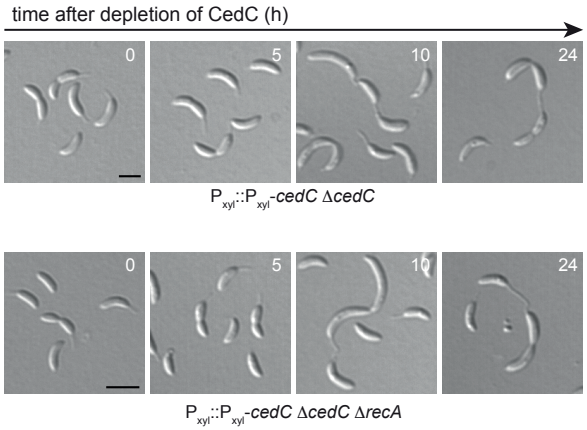

FIGURE 2.15: The phenotype caused by the deletion of *cedC* is still detectable in the absence of chromosome dimers. The conditional *cedC* mutant (WS120, P_{xyl}::P_{xyl}-*cedC* Δ*cedC*) and a strain carrying additionally a deletion in *recA* (WS125, P_{xyl}::P_{xyl}-*cedC* Δ*cedC* Δ*recA*) were grown in PYE medium supplemented with 0.3 % xylose, washed, and transferred into fresh PYE medium (t=0). At the indicated time intervals, the cells were imaged by DIC microscopy. Scale bar: 3 μm.

In summary, the cell division phenotype observed in cells that lack CedC is not caused by chromosome dimers that have been trapped in the closing septum. These results are further supported by previous findings that showed that CedC can localize independently of XerCD to midcell (S. Schlimpert, unpublished).

2.2.6 Searching for interaction partners of CedC

To gain more insight into the function of CedC in *Caulobacter* and to identify potential interaction partners, interaction studies were performed. As a first approach, a bacterial two-hybrid assay (see also subsection 2.1.6, page 31) was used to test for self-interaction of CedC and for interaction with candidate interaction partners. No interaction of CedC with the C-terminus of FtsK or XerCD could be observed (Fig. 2.16 A), suggesting that CedC acts independently of XerCD. Similarly, no interaction was observed between XerC and XerD and for $FtsK_C$ with itself and with XerD, which

was not consistent with their proposed mechanistic function [158, 172]. This might be due to the conserved function of the native FtsK protein in *E. coli* which competes with the used hybrid fusion protein, and in case of XerCD, due to the need of binding to the *dif* sites in order to see XerCD interaction. However, a strong self-interaction signal of CedC was observed, suggesting that CedC forms homomeric complexes *in vivo*.

Next, co-immunoprecipitation (Co-IP) was performed to isolate possible CedC interaction partners. For this purpose, a *C. crescentus* strain was used that produced a Venus-tagged derivative of CedC, expressed from the native promoter (SS348). Transient protein-protein interactions were stabilized by crosslinking with paraformaldehyde prior to immunoprecipitation with α-GFP affinity beads. In parallel, the same analysis was carried out with cell extract of wild-type *C. crescentus* to control for unspecific binding to the affinity beads. The identification of proteins was performed by mass spectrometric (MS) analysis in collaboration with U. Linne (Department of Chemistry, Marburg). The binding reaction was highly specific and the bait protein Venus-CedC could be clearly detected by immunoblot analysis (Fig. 2.16 B). Analysis of the whole elution fraction by MS confirmed that the signal obtained in the immunoblot analysis reflected the presence of Venus-CedC. However, the overall peptide count was too low to detect any potential interaction partner (a list with the complete results of the Co-IP is given in the appendix, Table A5, page 120). A possible reason for this could be that the covalently bound protein complexes caused by paraformaldehyde were not stable enough.

To test of whether CedC is able to bind non-specifically to DNA and possibly senses DNA at midcell during cytokinesis, an electrophoretic mobility shift assay (EMSA) was performed. Incubation of purified CedC with a linearized plasmid did not lead to a shift in the mobility of the plasmid, neither with low (1 µM) nor high (10 µM) protein concentrations (Fig. 2.16 C). In contrast, a significant band shift was observed for an ATPase-deficient MipZ variant, which was used as a positive control (Fig. 2.16 C). In conclusion, CedC did not bind to DNA, suggesting that it probably does not directly interact with the chromosome *in vivo*.

In order to identify proteins that are functionally linked to CedC, a genetic screen was performed. For this approach, the CedC homolog in *E. coli*, YigA, was used. Like *cedC*, *yigA* is co-conserved with *xerC* and is localized to midcell in *C. crescentus* when fluorescently tagged. (Fig. 2.17 A). Slight overproduction of YigA-Venus resulted in decreased growth (Fig. 2.17 B) and smaller colonies of *C. crescentus* cells. The cell division defect was significantly more pronounced in comparison to overproduction of Venus-CedC, which had only minor filamentation effects on cells (data not shown, S. Schlimpert). Thus, I utilized the pronounced cell division defect of *C. crescentus* cells with elevated

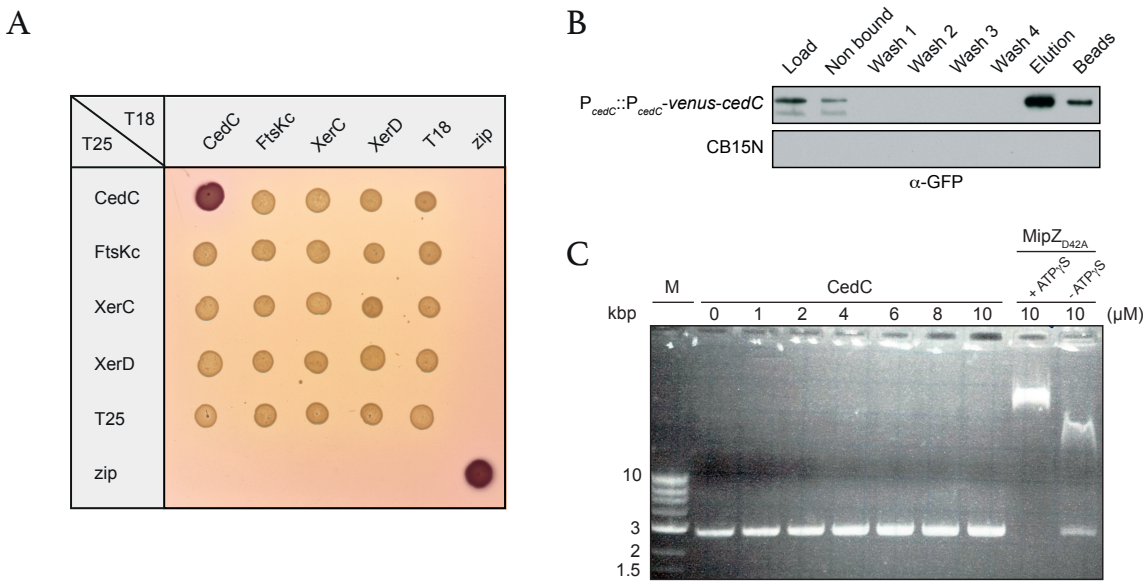

FIGURE 2.16: Interaction studies with CedC. **(A)** Bacterial two-hybrid analysis testing the interaction between CedC and selected proteins. For the assay, the *E. coli* reporter strain BTH101 was co-transformed with plasmids encoding fusions of the T25 and T18 fragments of *Bordetella pertussis* adenylate cyclase to the N-termini of the listed proteins or to the yeast GCN4 leucin-zipper region (zip) as a positive control. Transformants were grown in LB media and spotted on MacConkey agar. Interactions between the two adenylate cyclase fragments is indicated by the formation of red colonies. **(B)** Immunoblot analysis using α-GFP antiserum. Cell lysate of *C. crescentus* wild-type and SS348 (*cedC*::*venus-cedC*) was incubated with α-GFP-coupled agarose beads (Load). After incubation and centrifugation, the supernatant was discarded (Non-bound), while the beads were washed three times (Wash) and proteins eluted from the beads (Elution) by boiling with SDS buffer (Beads = bound proteins after boiling). **(C)** CedC does not interact with DNA. Purified CedC and the ATP-deficient $MipZ_{D42A}$ were incubated at the indicated concentrations for 20 min at room temperature with 10 nM linearized pMCS-2 plasmid in crystallization (CedC) or SPR ($MipZ_{D42A}$) buffer prior to loading of the reactions on an agarose gel. $MipZ_{D42A}$ was used as a positive control and incubated either with or without the slowly hydrolyzable nucleotide analog ATPγS (100 mM) to test for DNA-binding.

YigA-Venus levels and the formation of long, smooth filamentous cells (Fig. 2.17 C). Therefore, cells, synthesizing YigA-Venus, were incubated for a period of four days in the exponential phase via serial dilution. Cells were then spread onto PYE agar containing 0.3 % xylose to maintain constitutive expression of YigA-Venus. The first screen was the isolation of big colonies that were able to grow in the presence of YigA and at a speed comparable to that of the wild-type, since clones with a cell division defect tend to show slower growth on plates. The second screen was a microscopic analysis of (a) the phenotype and (b) YigA-Venus localization in the isolated clones. The aim was to identify clones with wild-type morphology and a midcell signal of YigA-Venus to exclude a frameshift or

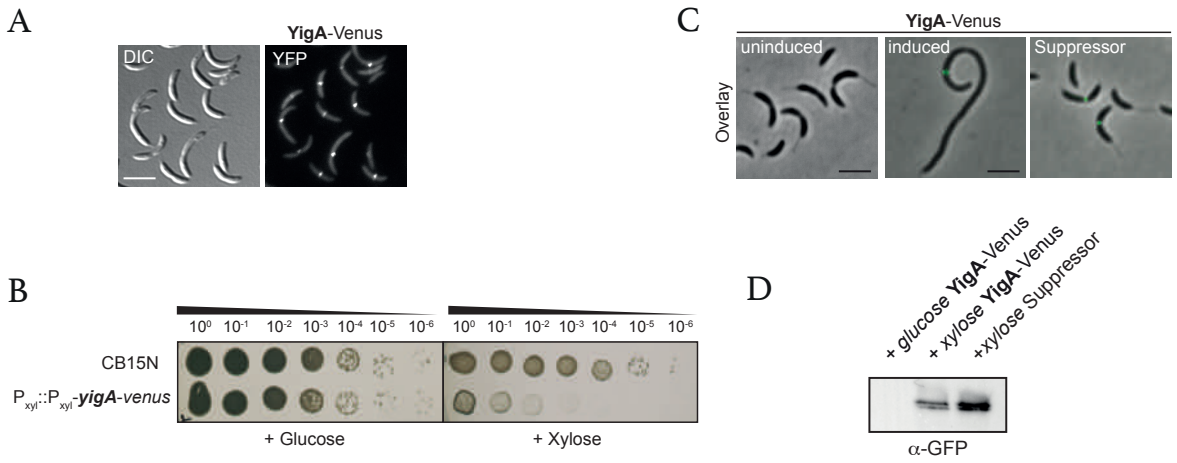

FIGURE 2.17: The CedC homolog YigA from *E. coli* and its use for the search of interaction partners. **(A)** YigA shows the same localization pattern as CedC in *C. crescentus*. Wild-type cells of *C. crescentus* carrying a fluorescently-tagged fusion protein of YigA under the the control of the xylose-inducible promoter (P_{xyl}::P_{xyl}-*yigA-venus*, SS362) were incubated in PYE medium and induced for 2 h by the addition of 0.3 % xylose. Images taken by S. Schlimpert **(B)** Drop assay with the strain described in (A) and its growth behavior under permissive and non-permissive conditions, compared to the wild-type CB15N. Cells of SS362 and CB15N were grown to exponential phase adjusted to an OD_{600} of 0.3, diluted serially as indicated and plated on PYE plates supplemented with either 0.2 % glucose (permissive) or 0.3 % xylose (restrictive). After two days of incubation, the plates were imaged. **(C)** Cells of strain SS362 were grown in PYE supplemented with 0.2 % glucose (uninduced) or 0.3 % xylose (induced) and the respective antibiotic and kept in the exponential phase via serial dilution transfers. After four days of cultivation the cells were plated on PYE agar plates, supplemented with 0.3 % xylose and the respective antibiotic and incubated for three another days until colonies arose. Selected mutants were analyzed using phase contrast and fluorescence microscopy. Shown is a representative suppressor clone (WS112 #3) **(D)** Immunoblot analysis of strains shown in (C) using α-GFP. Scale bars: 3 µm

nonsense mutation that may have abolished YigA synthesis. In the end, seven clones that fulfilled these requirements were isolated (Fig. 2.17 C, on the right). Next, the protein level of YigA-Venus was compared to that in the background strain SS362 using immunoblot analysis to exclude mutations in the promoter region that reduced the level of YigA and, thus, reduced its lethal effect on *C. crescentus* (Fig. 2.17 D). In three out of the seven suppressor mutants the promoter region was not affected (data not shown). Amplification and sequencing of the YigA-Venus fusion showed that in two out of the three clones the suppressor mutation did not lie within the gene itself. Therefore, whole-genome sequencing was performed to map the suppressor mutations in the genome of the strains. The sequencing was performed in collaboration with A. Thürmer at the Genome Center of Göttingen. For identification of the suppressor mutations, the sequence reads were mapped to the genome of the *C. crescentus* wild-type (a list of genes, which were found to have a mutation can be

found in Table A6, page 121). Interestingly, this approach identified a point mutation in the cell division protein FtsA (T17M) (Fig. 2.18 A). FtsA is an actin-like protein and is involved in Z-ring stabilization and interaction with PG synthesis-involved proteins [102, 104, 107, 108, 138, 142]. The mutation was located in the subdomain 1A, one of three domains required for the ATPase activity of FtsA [101, 105]. In order to confirm the suppressive effect of this point mutation on the YigA-Venus overproduction phenotype, the native *ftsA* gene of *C. crescentus* wild-type cells was replaced by a mutated $ftsA_{T17M}$ *allele*. Notably, the synthesis of the $FtsA_{T17M}$ variant had no impact on the cell morphology (Fig. 2.18 B). Next, the *venus*-tagged *yigA* was integrated downstream of the xylose-inducible promoter P_{xyl} in the respective $ftsA_{T17M}$ mutant strain, and the cell morphology of cells with elevated levels of YigA-Venus were examined. Upon induction of the hybrid gene, no filamentous cells were observed (Fig. 2.18 C), confirming that the amino acid substitution in FtsA indeed made the cells insensitive to excessive YigA-Venus levels. It remains to be determined whether the insensitivity of the suppressor strain might be directly dependent on FtsA or not. Obviously, the T17M substitution did not inhibit the recruitment of YigA (see Fig. 2.18 C), thus the mutation likely suppresses a downstream effect on divisome. A potential interaction between YigA (and CedC) and FtsA is suggested by localization dependency experiments in which YigA and CedC derivatives fused to the fluorescent protein Venus were integrated into a conditional *ftsA* mutant. Upon depletion of FtsA, filamentous cells were observed as reported in a previous study [144]. In this state, YigA-Venus and Venus-CedC were evenly distributed within the cell body (Fig. 2.18 D, t=0). After re-induction of the *ftsA* expression, the respective fluorescent fusions were observed at the incipient cell division site (Fig. 2.18 D), suggesting a direct or indirect localization dependency on FtsA.

In summary, a mutation in the ATPase domain of FtsA suppressed the cell division effect caused by the *E.coli* CedC homolog YigA. Dependency studies have shown that the recruitment of both YigA-Venus and Venus-CedC is dependent on FtsA. Whether this is an indirect or direct effect needs to be clarified by future experiments. However, the results on YigA in *C. crescentus* could provide insight into the CedC function, in terms of interaction partners and thus its cellular role.

2.2.7 Functional analysis of CedC

To gain more insight into the function of CedC, I aimed to determine the crystal structure of the protein. To this end, an N-terminally hexahistidine-tagged full-length variant of CedC was overproduced in *E. coli* under standard growth conditions. However, His_6-CedC was exclusively found in the pellet, probably due to the formation of inclusion bodies (data not shown). The

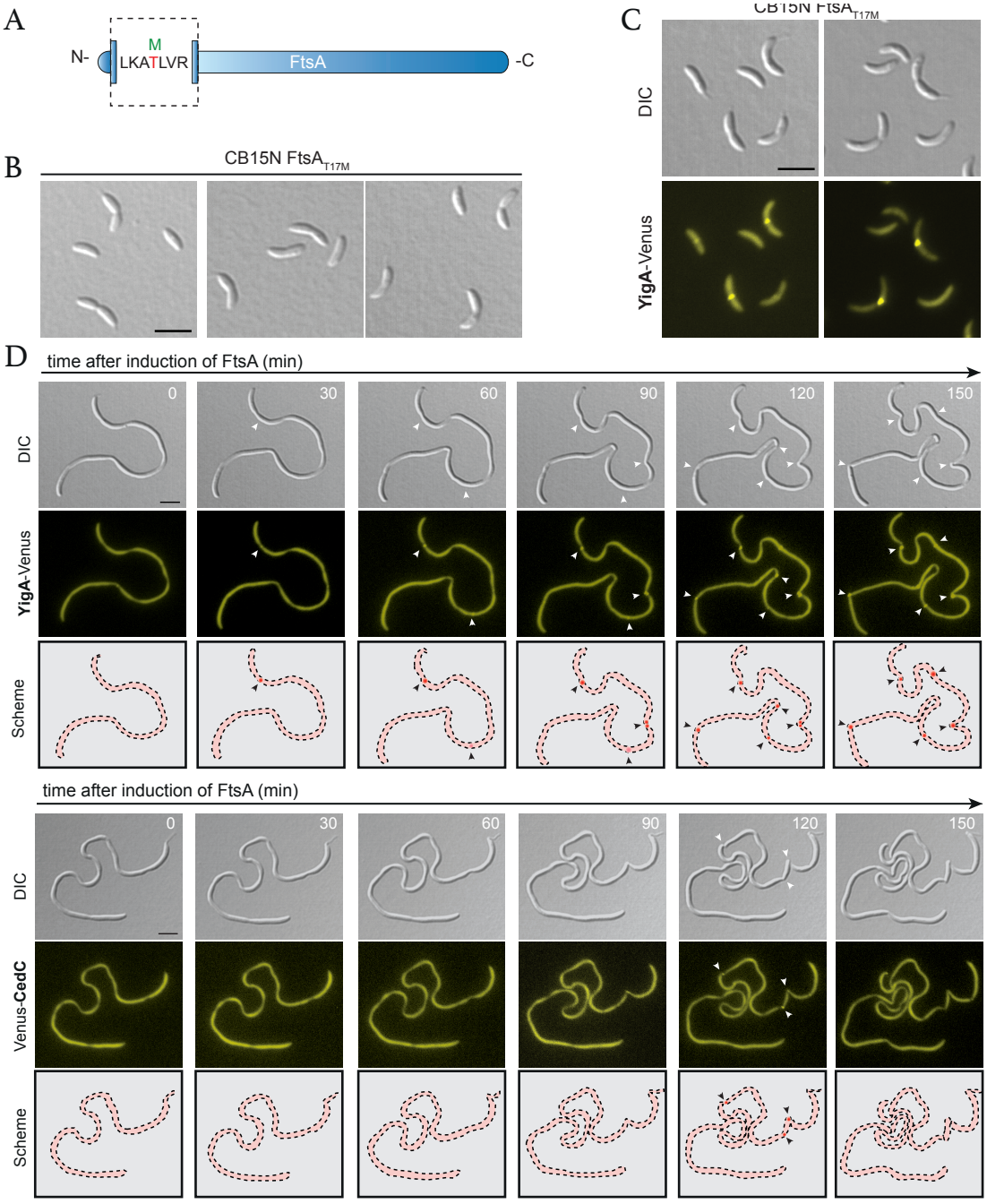

FIGURE 2.18: Phenotypic and localization analysis of YigA-Venus and Venus-CedC in a strain carrying the FtsA$_{T17M}$ variant. (A) Schematic representation of the T17M substitution, revealed by the suppressor screen. **(B)** Morphology of cells synthesizing the FtsA$_{T17M}$ variant (WS134). Cells were grown to exponential phase in PYE medium and imaged by DIC microscopy. **(C)** A xylose-inducible YigA-Venus fusion was introduced in the cells described in (B) and grown in the presence of 0.3 % xylose for three hours. Cells (WS135) were imaged in the exponential phase using DIC and fluorescence microscopy. **(D)** Midcell localization of YigA-Venus and Venus-CedC, respectively, is dependent on FtsA. Cells of strain WS145 (Δ*ftsA* P$_{van}$::P$_{van}$-*ftsA* P$_{xyl}$::P$_{xyl}$-*yigA-venus*) and WS144 (Δ*ftsA* P$_{van}$::P$_{van}$-*ftsA* P$_{xyl}$::P$_{xyl}$-*venus-cedC*) were grown in M2G medium supplemented with 0.5 mM vanillate, washed, and transferred into fresh M2G medium for a cultivation time of 6.5 h. Three hours prior to microscopic analysis, the expression of *venus-cedC* and *yigA-venus*, respectively, was induced by addition of 0.3 % xylose. The cells were then transferred onto M2G-agarose pads containing 0.3 % xylose and 0.5 mM vanillate to re-induce *ftsA* expression and imaged at the indicated time intervals. Scale bars: 3 μm.

problem was solved by using a His_6-SUMO (small ubiquitin-like modifier) tag, which is known to stabilize and increase the solubility of proteins [208]. In collaboration with V. Srinivasan from the Marburg crystallization facility (MarXtal), crystallization screens were performed. The best results were obtained, using 4 % PEG6000, 0.1 M Bicine (pH 9.0) at 18 °C and a protein stock solution with 25 mg/ml protein mixed in a 1:1 ratio (protein:buffer) applied as hanging drops, resulting in the formation crystals within a few days (see Fig. 2.19). We further continued with X-ray diffraction analysis and obtained a maximal resolution of 4.4 Å, which is too low to determine a detailed structure (data not shown). Crystals can be improved by adding substrate analogues, inhibitors, ligands or other additives. Thus, an additional crystallization screen was performed in the presence of various chemicals. Crystals formed significantly faster in the presence of 40 % tert-butyl alcohol (TBA) or hexafluoro-2-propanol. However, this change in conditions did not lead to better diffraction, and thus leaving the resolution of the crystals unchanged. Hence, the crystallization conditions might need to be further optimized.

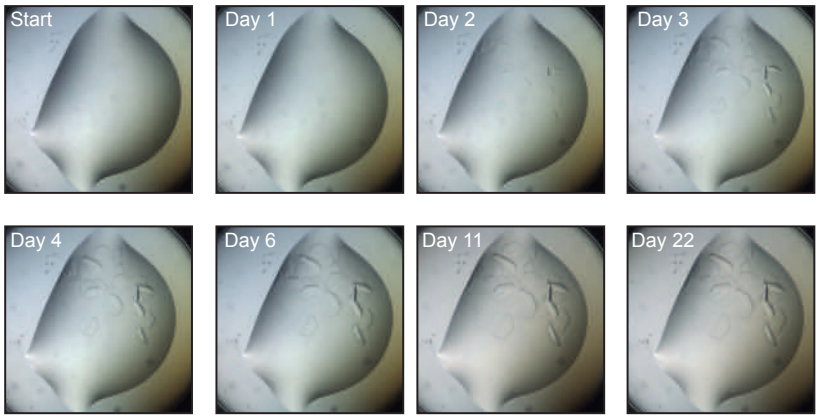

FIGURE 2.19: Crystal formation of purified CedC. Crystallization experiments were performed using the hanging drop vapor diffusion method at a temperature of 18 °C. Drops were prepared by mixing 1 µl of concentrated protein (25 mg/ml) with an equal volume of reservoir solution (4 % PEG6000, 100 mM Bicine pH 9.0) and transferred on a silicon-covered cover slip, which was put upside down on a well filled with 500 µl reservoir solution. The crystallization approach was incubated at 18 °C until proper crystals were formed. Crystallization experiments were performed in collaboration with Dr. V. Srinivasan from the Marburg crystallization facility (MarXtal) using the Digilab Honeybee 963™ crystallization roboter in combination with Formulatrix Rock Imager™ for image documentation.

During the crystallization procedure, the purified protein was subjected to size-exclusion chromatography to determine whether CedC forms oligomerizes that prevent crystallization. Moreover, the knowledge of homooligomerization could be an important prerequisite for its subcellular function. A distinct, single elution peak at a retention volume of 53,6 ml was detected

(Fig. A2, page 123), which corresponded to a size of 148 kDa. This is equivalent to the size of four monomers, suggesting that CedC forms stable tetramers *in vitro*. This result is affirmed by the observation of strong self-interaction of CedC in the bacterial two-hybrid analysis (see Fig. 2.16 A, page 45). Furthermore, the information available in the Protein Data Bank (PDB) indicates that the *Pseudomonas aeruginosa* homolog (PA5279), which shares 14 % sequence similarity with CedC, forms dimers. The subunit interactions are mediated by a coiled-coil motif in its N-terminal region (Fig. 2.20 A), which is known to facilitate protein-protein interactions [209–211]. Additionally, the crystal structure of PA5279 reveals a C-terminal region harboring a GAF (c*G*MP-specific phosphodiesterase, *a*denylyl cyclases and *F*hlA) domain known for a variety of functions (Fig. 2.20 A), which seems to be inactive or closed. Bioinformatic analyses using Phyre2 also strongly suggests the presence of a GAF domain at the C-terminus of CedC (data not shown).

To understand how the different domains of CedC contribute to its function, localization analyses were performed with CedC derivatives lacking one or more protein structures. As a consequence of the unsuccessful crystallization, the structure of CedC was modeled based on PA5279 using I-Tasser [212–214]. The tertiary structure obtained was similar to that of PA5279, but with a significantly longer N-terminal region consisting of α-helices, not homologous to known proteins, a C-terminal GAF domain, both linked by a coiled-coil region (Fig. 2.20 B). For the localization analyses, the CedC mutant proteins were fused to Venus, produced under the control of the xylose-inducible promoter, and analyzed microscopically. *C. crescentus* cells producing full-length CedC displayed the previously observed midcell localization in predivisional cells (Fig. 2.20 C). Fragments comprising the flexible N-terminal region and the coiled-coil region alone, respectively, did not show any distinct localization. Similarly, when a CedC variant without the GAF-domain was fused to Venus and expressed in wild-type cells, only weak fluorescence signal throughout the cells was detected. A variant of CedC comprising the full protein except for the flexible N-terminal region showed the same localization pattern as full-length CedC and localized to midcell. In contrast, the GAF domain and coiled-coil region alone, respectively, were not able to localize to the division plane (Fig. 2.20 C). The integrity of the fusion proteins was determined by immunoblot analysis. In line with the observed localizations for the derivatives, weak bands without degradation bands were detected for those derivatives (Fig. 2.20 D). The fact that the flexible N-terminal region alone is diffusely localized in the cytoplasm suggests that this structure is dispensable for the midcell localization of CedC. This is in agreement with the conservation pattern of CedC, because the N-terminus is highly variable in its sequence and length among proteobacteria. Furthermore, the GAF domain requires the coiled-coil region to be recruited to midcell, which is probably achieved by protein-protein interaction. Another possibility would be that a stable homotetramer complex

is required for the recruitment of CedC. However, the precise functions of the different domains and of whether the GAF domain is active or not, cannot be deduced from this experiment.

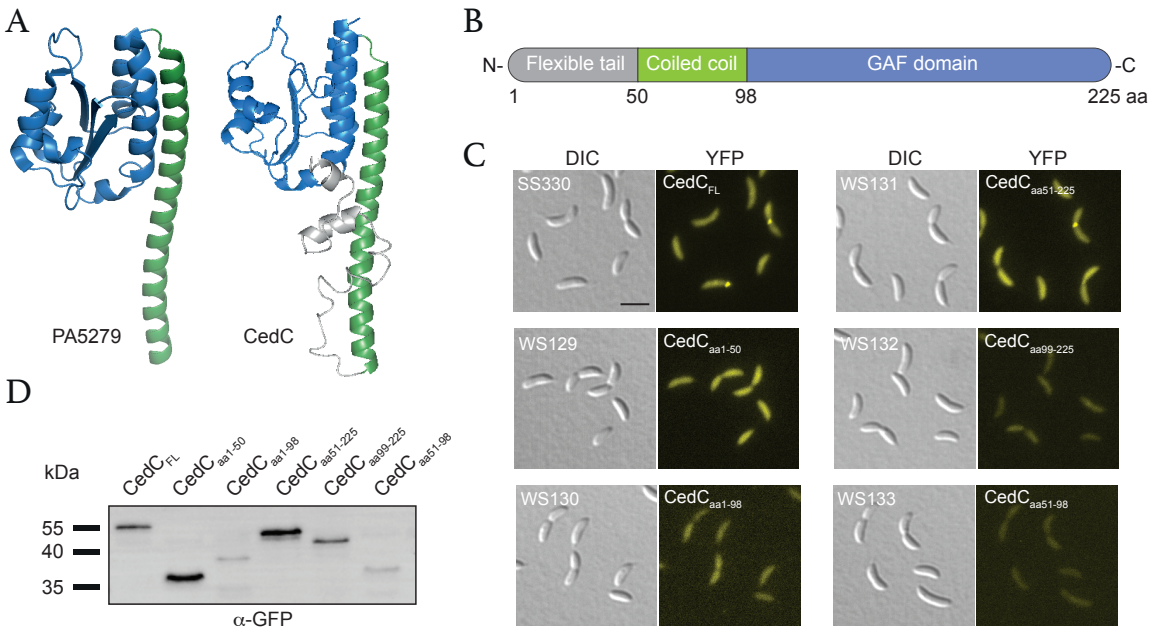

FIGURE 2.20: Localization analysis of CedC mutant derivatives. **(A)** Crystal structure (2.4 Å) of the CedC homolog from *P. aeruginosa* PA5279 and the modeled structure of CedC by I-tasser. The pdb file of PA5279 (3E98) was taken from the European Molecular Biology Laboratory (EMBL) Protein Data Bank. The coiled-coil domain is depicted in green, whereas the GAF domain is shown in blue. In case of CedC, the flexible N-terminal region is shown in gray **(B)** Schematic representation of the domains, based on the modeled structure of CedC shown in (A). Numbers refer to the position of amino acid (aa) residues **(C)** Subcellular localization of CedC derivatives fused to Venus. Strains SS330 (P_{xyl}::P_{xyl}-*venus-cedC*), WS129 (P_{xyl}::P_{xyl}-*venus-cedC*$_{aa1-50}$), WS130 (P_{xyl}::P_{xyl}-*venus-cedC*$_{aa1-98}$), WS131 (P_{xyl}::P_{xyl}-*venus-cedC*$_{aa51-225}$), WS132 (P_{xyl}::P_{xyl}-*venus-cedC*$_{aa99-225}$), and WS133 (P_{xyl}::P_{xyl}-*venus-cedC*$_{aa51-98}$) were grown in PYE medium containing 0.3 % xylose for 2 h and visualized by DIC and fluorescence microscopy. Scale bar: 3 µm. FL=full length **(D)** Stability of Venus-CedC mutant derivatives. The strains described in (B) were grown in PYE medium containing 0.3 % xylose. After 2 h of induction, samples were withdrawn from the culture and subjected to immunoblotting using α-GFP antiserum.

In summary, the initial characterization of CedC has shown that it is part of the divisome and involved in a late step of cell division. Deletion of the protein results in impaired cell division, possibly due to unsuccessful segregation of the chromosome. CedC likely has a regulatory, rather than a catalytic cellular function. However, to fully characterize the role of this proteins, more experimental work is required.

3 Discussion

Fundamental cellular biological properties and mechanisms have evolved over time to ensure permanent life on earth. In almost all bacteria, PG serves as a multifunctional component to determine cell shape and protect the cells from environmental influences and the internal turgor pressure. Apart from that, cell division is a crucial event in every cell to produce offspring. Based on their conserved composition, both the biosynthetic PG machinery and the cell division, are early developments in bacterial evolution. Importantly, the function of both must be strictly coordinated in time and space, in particular at the late stage of cell division prior to cytokinesis, when the replicated chromosomal DNA needs to be equally distributed to the two cells. Thus, mechanisms have evolved to fine-tune the process of PG biosynthesis and cell division. While the core components of the cell division machinery, including PG synthases, are conserved among most bacteria, the systems that spatiotemporally regulate the cell division machinery are diverse and poorly understood.

Here, I report the identification of late-stage cell division proteins that are specifically involved in PG synthesis and the characterization of the new cell division proteins CedC and CedD, which may function in the temporal regulation of the divisome, linking chromosome segregation with PG synthesis. Open questions related to the network of bifunctional penicillin-binding proteins in *C. crescentus*, the possible role of CedCD, and how especially CedC may function with PG remodeling during cell division, will be discussed below.

3.1 Bifunctional penicillin-binding proteins involved in the late stage of cell division in *C. crescentus*

3.1.1 PbpX and PbpY are divisome-specific bPBPs

Bifunctional penicillin-binding proteins are enzymes involved in PG biosynthesis, a highly important and complex process that requires a tight balance between synthetic and also hydrolytic reactions. Bacteria usually possess more than one PG synthase, which can be also present in sets of paralogous proteins with specialized and often overlapping functions to ensure robust cell wall biogenesis [26, 44]. Among the α-proteobacteria, *C. crescentus* possesses a relatively high number

of bPBP genes, five in total. This raised the question of the selective pressure to maintain all of the paralogous enzymes. One potential driving force for the cell may be the need to adapt to different environmental conditions, which leads to high diversification and specialization of each bPBP. Moreover, cells possess different molecular machineries for different growth modes. Studies in *E. coli* have shown that two out of the three bPBPs, PBP1A and PBP1B are largely functionally redundant and conditionally essential, meaning that one becomes strictly essential in the absence of the other [191, 215]. The synthetic lethality of *pbp1a* and *pbp1b* deletions in *E. coli* shows the importance of redundancy of the bPBP network to ensure PG synthesis. Moreover, bPBPs show also functional redundancy in other species. Thus, specialized but also overlapping cellular functions were expected in *C. crescentus*. I focused on bPBPs specifically involved during cell division. Indeed, a specific localization of PbpX and PbpY at the cell division site was detected, which was dependent on the FtsZ scaffold, identifying both proteins as components of the divisome. Moreover, I showed that the divisome recruitment of PbpX and PbpY is also dependent on the essential late cell division protein FtsN. Consistently, both PG synthases were found to arrive in the last third of the cell cycle, classifying them as late cell division proteins. Interestingly, the foci formed by Venus-PbpX were in general more distinct and brighter than those of Venus-PbpY, which may indicate a more prominent role of PbpX during cell division. This notion is in agreement with the reported phenomenon that deletion of PbpX, but not PbpY, results in a strong synthetic growth defect in strains with impaired FtsI activity [183]. Furthermore, it was reported that *C. crescentus* cells showed a decrease in their growth rate in the absence of PbpX, which was more pronounced upon additional lesion in *pbp1a* or *pbpY* [183].

To put the obtained results in context with known studies, with which cell division proteins do both PbpX and PbpY form a multi-enzyme complex to ensure PG remodeling during cell constriction? It was found in the bacterial two-hybrid analysis that PbpX and PbpY interact with FtsN. In addition to FtsN, interactions with FtsL and DipM were found *in vivo*. Localization dependency of PbpX and PbpY were only observed for FtsN, but not on DipM, supporting that FtsN might be the direct localization factor of PbpX and PbpY. In agreement with these results, the role of FtsN to be a central hub for the recruitment of PG synthases and hydrolases to the division site is underscored although FtsN is counted as a late cell division protein. Previous experiments have shown that the midcell localization of DipM, which accumulates after Z-ring stabilization, is dependent on direct interaction with FtsN, suggesting that low concentrations of FtsN are present at early stages of *C. crescentus*, comparable to the situation seen in *E. coli* [111, 150]. Recent studies in *E. coli* have confirmed that FtsN is already active at midcell before accumulating in high concentrations and triggers PG synthesis by two distinct pathways, one that is active in the periplasm and another one that is

active in the cytoplasm. The periplasmic pathway includes the interaction of FtsN with the FtsQLB complex (and PBP1B), which in turn activates the FtsWI complex [137, 154, 188, 216]. In the cytoplasm, FtsN directly interacts with FtsA, thereby leading to a conformational switch of the latter, resulting in the stimulation of PG synthesis by triggering the FtsQLB complex [137, 154, 216]. This mechanism might be also conserved in *C. crescentus* which needs to be determined. The interaction of PbpX and PbpY with FtsL as part of a multi-enzyme complex could be an indication that FtsL in *C. crescentus* might act in a similar manner as it does in *E. coli*, triggering the synthesis of septal PG in concert with FtsN. However, the mechanism of the FtsQLB complex and the interaction between FtsN and FtsA may be different in *C. crescentus*, because the recruitment hierarchy of cell division proteins differs in comparison with *E. coli*. For example, FtsW is required for the localization of FtsI in *E. coli* [127, 128], whereas in *C. crescentus* it is not and localizes at midcell prior to FtsW [111]. In addition and consistent with its late transcription, FtsA in *C. crescentus* accumulates only after the proto-ring is established in the mid-phase of divisome assembly [217], i.e. noticeably later than in *E. coli*.

What could be the advantage of having two divisome-specific bPBPs? One possibility could be the differential adaptation of the two proteins to stress conditions to make PG synthesis robust to changes in environmental parameters, such as temperature, pH value, osmotic pressure, or the presence of PG-targeting antibiotics with different spectra of activity. For example, PbpX could be the result of an antibiotic-induced pressure. A previous study has shown that PbpX has derived from its bPBP paralogs because the deletion of *pbpX* causes hypersensitivity to β-lactam antibiotics and A22 [197, 218]. Thus, PbpX has evolved as a protector against β-lactam antibiotics. However, *C. crescentus* is resistant to β-lactam antibiotics, because it possesses a potent β-lactamase. Thus, the resistance of PbpX to β-lactam antibiotics might be an indirect effect or co-development. Another possibility for the high diversification of bPBPs could be the differences in the constriction process of *C. crescentus*. In contrast to *E. coli*, which synthesizes a relatively thick septum perpendicular to the longitudinal axis, which is then split to release the daughter cells, *C. crescentus* invaginates its inner and outer membrane gradually by simultaneous Z-ring de-polymerization and PG synthesis at the division site. This could require the action of several bPBPs in addition to the division-specific transpeptidase FtsI, particularly because bPBPs are able to act as transglycosylases. The only known monofunctional transglycosylase of *C. crescentus*, MtgA, does not show any divisome-specific localization and no phenotype[144, 183], raising the possibility to require efficient transglycosylation at the division site. Yet another possibility to have two-divisome-specific bPBPs could be the contribution to different steps during the constriction process as there might exist different subcomplexes during PG remodeling.

3.1.2 The role of Pbp1A, PbpC, and PbpZ regarding cell division

Although PbpX and PbpY seem to be the major bPBPs contributing to PG remodeling and the formation of the new cell poles during cytokinesis, the possibility that the remaining bPBPs also contribute to some extent under normal and maybe even more under sub-optimal growth conditions cannot be excluded. Consistent with this idea, our studies have shown that, in principle, every paralog, except for PbpZ, is able to interact with the division machinery and allow WT-like cell division when expressed alone. Under these conditions, their efficiencies of PG synthesis varied and seem to increase with elevated protein levels. However, each bPBP did not change its subcellular localization when expressed alone with a fluorescent tag, although WT-like growth and morphology was maintained [182]. For example, PbpC still formed a distinct focus at the stalked pole in absence of all other bPBP paralogs. In contrast, inactivation of PbpC reduced the stalk length but did not affect the growth of the cell body [70], indicating that PbpC seems to be primarily involved in stalk biogenesis. Despite this fact, I could show that it is additionally able to interact with the elongasome and divisome when it is the only synthesized bPBP. Under these conditions, cells were viable, even though only at elevated levels of PbpC. However, PbpC retained its polar-specific localization at these conditions [182], reflecting binding sites to different PG biosynthetic complexes. The overproduction of PbpC may saturate its binding sites in the polar complex by the interaction with the bactofilin cytoskeleton [70] and, thus, enable its re-direction to and interaction with other PG synthetic complexes with lower binding affinity.

Evidence for a more specific re-direction of a bPBP to the division site is provided by a previous study. It was shown that Pbp1A together with the elongasome-specific transpeptidase PBP2 of *C. crescentus* is recruited to midcell when cells are exposed to salt stress [219]. In our localization studies, Pbp1A showed a patchy distribution throughout the cell cycle under normal growth conditions, reflecting its potential participation in MreB-dependent lateral cell wall biosynthesis. On the other hand, PBP2, is normally only found in patches distributed throughout the cell, with no midcell accumulation [88, 220, 221]. Possibly, the re-direction of the elongasome components PBP2 and Pbp1A supports additional biosynthesis at the division site for robust cell wall synthesis under osmotic stress, allowing the fine-tuning of biosynthetic complexes in response to specific environmental conditions.

The role of PbpZ remains unclear, because, in contrast to other bPBPs of *C. crescentus*, it did not show any distinct localization. PbpZ as the sole bBPB present in the cell was insufficient to complement for the loss of the other bPBPs, not even upon overproduction. A phylogenetic comparison using

BLAST has shown that PbpZ is homologous to *E. coli* PBP1C and shares 34 % sequence identity with its homolog [183]. I also found that highly conserved amino acid residues critical for catalysis are absent in the nPB (transglycosylase) motif in *E. coli* PBP1C as well as in PbpZ. However, PbpZ was not able to associate with cell division components and other bPBPs, in contrast to PBP1C of *E. coli*, which is also not able to sustain the loss of PBP1A and PBP1B [27, 222]. This raises the possibility that PbpZ lacks transglycosylase and/or transpeptidase activity, or has a more specialized role, suggesting that it has functionally diverged from its paralogs.

Altogether and consistently with their functional redundancy, each of the bPBPs, except for PbpZ, was able to interact with the divisome components FtsN, FtsL, and DipM in our bacterial two hybrid analysis and supported proper cell division, although only PbpX and PbpY display a discrete accumulation at midcell as visualized by fluorescence microscopy. Surprisingly, and in contrast to their *E. coli* homologs, the bPBPs of *C. crescentus* were able to form heterodimers in addition to homodimers in our bacterial two hybrid study. PBP1A and PBP1B of *E. coli* form homodimers, but are not able to associate with each other [193], suggesting that bPBPs of *C. crescentus* are less specific in their ability to physically interact with another bPBP. Under normal growth conditions, Pbp1a, PbpC, and PbpZ may be dispensable for cytokinesis, but their quick re-direction to the division site [219] may render PG synthesis more robust in response to changing conditions. Thus, they may have specialized roles and function in distinct subcomplexes but retained their binding affinities for other subcomplexes (e.g. the divisome), to be able to substitute for one another.

3.1.3 Regulation of bPBP activity

Our findings indicate that the bPBPs of *C. crescentus* share basic features of the paradigmatic PG biosynthesis machinery of *E. coli*, including their redundancy and interaction partners. However, there are functional differences. A relevant question that still remains to be answered is how PG biosynthetic enzymes are regulated so that a tight balance between synthesis and hydrolysis is ensured. An early and still valid model is the formation of multi-enzyme complexes that involve PG synthetic and hydrolytic enzymes as well as regulatory components [5]. The results obtained suggest that such a mechanism also exists in *C. crescentus*. Similar to *E. coli* PBP1B, bPBPs of *C. crescentus* associate with divisome components and PG hydrolytic enzymes. PBP1B interacts with FtsN [188] and the transpeptidase FtsI [190], which itself is proposed to be localized adjacent to FtsL in the divisome [146]. In addition, PBP1B interacts with the PG hydrolytic enzyme MltA, a lytic transglycosylase [223]. In *C. crescentus*, bPBPs interact with the endopeptidase DipM, which belongs to a different class of hydrolytic enzymes than MltA endopeptidases [150]. However,

despite similarities in the interplay with core divisome components, it seems that bacteria have evolved an additional way of regulating their septal PG biosynthesis including the outer membrane as a topological factor. A recent study reported that PBP1A and PBP1B of *E. coli* require a cognate outer membrane lipoprotein (LpoA and LpoB) for their PG synthetic activity *in vivo* [224, 225]. The mechanism of activation and their physiological relevance remaines unclear so far. Some studies hypothesize that the lipoproteins detect gaps in the PG sacculus, thereby activating the TP activity of their cognate PBP partner by direct physical contact at locations where the mesh is thinned [45]. Additionally, it has been suggested that LpoB promotes glycan chain polymerization by inducing a conformational change in PBP1B upon binding, facilitating its transmission to the glycosyl transferase active site [226, 227]. In either case, both lipoproteins are thought to play an essential regulatory, rather than a catalytic role in PG synthesis. However, these proteins are not conserved outside of enteric bacteria and no other regulatory factors of bPBPs are known so far. Thus, it remains unclear how the activity of these enzymes is regulated in *C. crescentus*. Furthermore, there are still many unanswered questions regarding the molecular mechanisms and evolutionary concepts that regulate bPBP functions and contribute to the vast diversity of bPBPs among bacteria.

3.2 CedC - a potential regulator of cell division

The second project comprised the functional characterization of two new, so far uncharacterized cell division proteins in *C. crescentus*, namely CedC and CedD. The common characteristic of both proteins is their co-conservation with the tyrosine-recombinases XerC and XerD. Additionally, previous localization studies have shown that both proteins localize to the cell division site of *C. crescentus*, suggesting a potential role in cell division. Despite these similarities, it was experimentally shown that CedC is localized in the cytoplasm, whereas CedD is located in the periplasm. Furthermore, a single deletion of the *cedC* gene resulted in morphological altered cells and slower growth, whereas a Δ*cedD* mutation had no impact on the cells. Thus, it is reasonable that the two proteins do not share the same cellular roles although they are conserved in a similar genomic context, which may be an indication that both proteins function in the same pathway. These results were the basis and motivation for the work in this study. The main focus was set on CedC, since it apparently has a more crucial cellular role than CedD. The issues to be answered in this study were (1) whether there is a functional link between XerCD and CedC (and CedD), (2) whether CedC is a divisome component and (3) if so, with which known protein(s) it interacts.

3.2.1 CedC domain architecture and conservation

Structural analyses have shown that CedD does not contain any known domain, whereas CedC is a single-domain protein entirely composed of a DUF484 domain. This domain is widespread among bacteria and also occurs in combination with extra domains. Typically, these extra domains are GGDEF domains associated with c-di-GMP regulation, but some have HisKA and HATPase_c domains associated with histidine kinases. Interestingly, the genes encoding these multi-domain proteins are not found near a putative *xerC* homolog in α-, β- and γ-proteobacteria and *Magnetococcus*, whereas single DUF484 proteins are located in 95 % of the cases next to a gene encoding Phage_integr_N and Phage_integrase domains, an indicative of a XerC homolog (Fig. 3.1). Some studies identified DUF484-harboring proteins but did not shed further light on them. For example, a study in *Rhodobacter capsulatus* reported of a DUF484-containing gene (*rcc03209*), which is transcriptionally regulated by direct binding of CtrA, but in absence of CtrA its transcription is not affected [228]. However, CtrA of *R. capsulatus* is different to the one of *C. crescentus* and has diverged during evolution, because it is not essential in *R. capsulatus* and does not regulate cell division proteins [228]. Another study used correlation-based calculations of Pfam protein domain sequences found in metagenome data to provide insight into the functional role of DUFs [229].

The study reports that DUF484 clustered with domains involved in sodium translocation that are linked to amino acid transport as well as a ligase that initiates the glutathione biosynthesis pathway [229]. There is, however, no experimental evidence that suggests that CedC is involved in biosynthetic pathways. Apart from these reports, a recent study identified NstA as a novel cell division protein in *C. crescentus*, which inhibits the decatenation activity of topoisomerase IV during early cell division in response to the intracellular redox state [230]. Might CedC function in a similar way together with the tyrosine-recombinases XerCD to resolve chromosome dimers? Does it have a regulatory function, as the GAF domain might implicate? These and other questions are discussed in the following section.

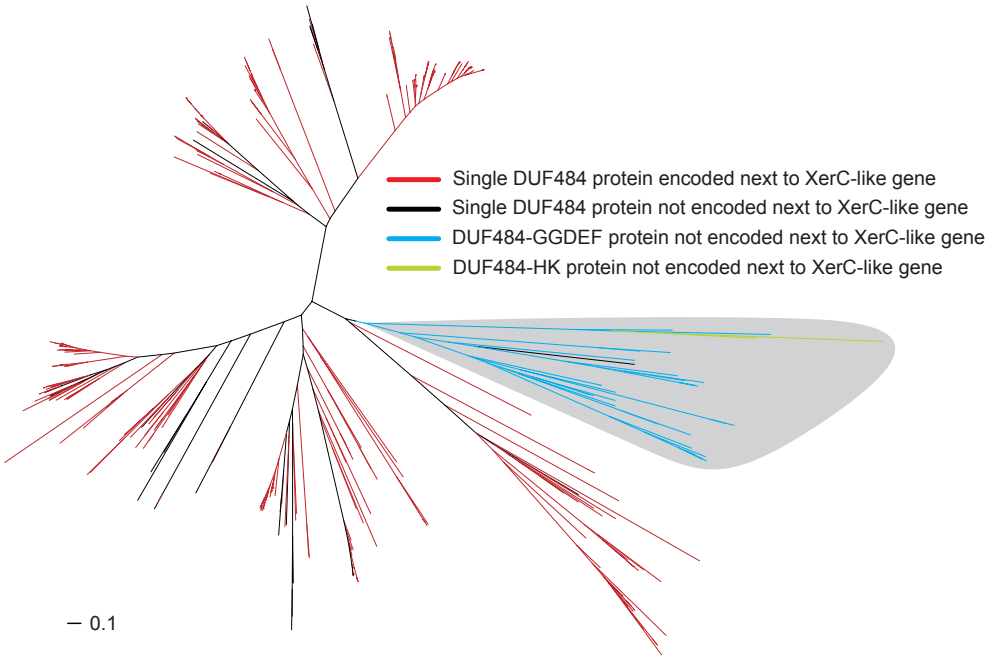

FIGURE 3.1: Identification of CedC orthologs. A phylogenetic tree was constructed from a multiple sequence alignment of 418 putative collected CedC homologs using domain architecture and BLASTP analyses. The clade highlighted in grey identifies divergent sequences that were not considered to be CedC orthologs based on their unusual domain architectures and gene neighborhoods in comparison to CedC and the majority of the other sequences. A XerC-like gene is considered one that encodes a protein containing Phage_integr_N and Phage_integrase domains. The phylogenetic tree was generated by Dr. K. Wuichet, Søgaard-Andersen lab.

3.2.2 CedC is a late actor during cytokinesis

The localization studies performed in this study, including time-course and time-lapse experiments, demonstrated that CedC is recruited to the division plane in a FtsZ-dependent manner

in *C. crescentus* at last stages of cell division. The timing of CedC midcell localization suggests that a potential connection to XerCD does exist, which act at the final stage of cell division, resolving chromosome dimers to monomers thus ensuring the faithful segregation of the sister chromosomes to the daughter cells by FtsK [164, 166–168]. Based on our localization data, it is unlikely that CedC is only required when chromosome dimers have formed. In *C. crescentus*, this is the case in approximately 4 % of the cells in a mixed exponentially growing population [198]. However, CedC was localized to midcell in about 60 % of predivisional cells with a visible constriction in a mixed culture. It is conceivable that the midcell localization of CedC is too short for detection in all cells in single snap-shot images. This hypothesis is consistent with the results of time-lapse experiments, which showed that the midcell localization of Venus-CedC was very short but observed in every cell.

In a screen for interaction partners of CedC, a mutation in FtsA was obtained that suppressed the phenotype caused by overexpression of the CedC homolog in *E. coli*, YigA. However, there is a difference in the timing of FtsA recruitment. In *C. crescentus*, FtsA is recruited at the mid-stage of divisome assembly, whereas in *E. coli* FtsA is recruited at the onset of Z-ring formation [111]. However, the localization dependency on FtsA was tested for both YigA-Venus and Venus-CedC. These experiments revealed that the localization of both fusion proteins is dependent on FtsA, either directly or indirectly. Thus, the FtsA-CedC interaction needs further experiments for evidence. However, how should FtsA be the recruitment factor for the late cell division protein CedC? A possible reason could be that another protein mechanistically links FtsA and CedC, or CedC is already present at midcell during earlier phases of cell division but at concentrations too low to be detectable by fluorescence microscopy, comparable to FtsN [110, 138]. Another possibility could be that FtsN acts as a potential linker for both proteins for reasons which are discussed below. Altogether, our localization experiments qualify CedC as a late cell division protein. Late cell division events include chromosome segregation and resolution (FtsK/XerCD [154, 172, 231]), PG remodeling (FtsN, FtsI, PbpXY, DipM, AmiC [111, 150, 232, 233]) and outer membrane invagination (Tol-Pal complex [148, 149]). Thus, it is likely that CedC is involved in one ore more of these processes.

3.2.3 CedC function is linked to growth

In order to investigate the degree of functional linkage of CedC with CedD and XerCD, a set of deletion mutants lacking one or more of the respective genes was generated. From previous experiments it was already known that the absence of CedD does not affect the cells, whereas CedC

plays a crucial role in normal growth and cell division. Cells lacking CedC displayed a significant fitness disadvantage that led to the formation of chains of cells with extended constrictions. This morphological defect has been described for a number of other cell division proteins in *C. crescentus* ($FtsK_C$ [234], XerCD [198], KidO [235], DipM [150]), involved in FtsZ ring destabilization, chromosome segregation/resolution, and PG remodeling. Based on this phenotype, CedC could be possibly involved in any of these mechanisms. The exact reason for the growth defect observed for *cedC* mutant cells, and why cells partially are not able to complete cell division, is not clear. Magnification of the cell division plane using cECT showed that the cytoplasm (and possibly also the DNA) is still connected between cells that failed to divide in the absence of CedC. It is not clear yet whether this is a direct or indirect result of defective chromosome resolution/segregation or spatiotemporal deficiency of divisome components. Quantification of the cell division defect revealed that 17 % of cells lacking CedC showed cell chaining, which means that CedC is likely not essential for cell division. Interestingly, the chaining phenotype was completely lost at slow-growing conditions, suggesting that an alternative (slower) mechanism may allow to compensate for the loss of CedC. In contrast, when the cells were exposed to fast-growing conditions, the Δ*cedC* phenotype was even more pronounced with 60 % chained cells, suggesting that the malfunction caused by the absence of CedC is linked to growth. A possible reason could be that cells under conditions of slower growth have enough time to clear the division site of the chromosomal *ter* region. This observation would indeed fit to an involvement in chromosome dimer resolution (CDR). Another interesting observation is that the frequency of chained cells is reduced when a lesion in *cedD* or *xerC* is combined with a *cedC* deletion. This effect is even more apparent in a Δ*cedCD* Δ*xerCD* quadruple mutant strain. Notably, a combination of the Δ*cedC* and Δ*xerC* mutation always results in predivisional cells that are noticeably smaller than the wild-type, suggesting that they undergo hyperactive cell division (discussed in subsection 3.2.4). Since this observation was made only in this mutational configuration, a link between XerCD and CedC seems to be obvious. However, the number of cells that have a defect is significantly higher in Δ*cedC* cells than it is in a Δ*xerCD* mutant, in which cell chaining occurs in 4-7 % of the population [169, 198]. Furthermore, the number of cells that are not able to divide properly did not increase when a lesion of *cedC* was combined with a deletion of Δ*xerC* and/or Δ*xerD*. This suggests that CedC is partially involved XerCD-mediated CDR, but also in another mechanism. In support of this result, the characteristic Δ*cedC* chaining phenotype could still be detected in a Δ*recA* background, a condition that should prevent the induction of XerCD-mediated CDR [168, 201–203, 205].

The results described above indicate that the XerCD proteins have an influence on the cell division phenotype caused by the absence of CedC, although it remains unclear to what extent. The level

of sequence conservation indicates that CedC is a highly conserved cell division protein found in a variety of proteobacteria. However, while in *C. crescentus* CedC is clearly important for normal growth and cell division, the *E. coli* homolog YigA is dispensable for growth [236]. A possible explanation may be that in *E. coli* the function of the CedC homolog became unimportant because redundant systems evolved. In support of this, YigA-Venus did not show any defined localization in *E. coli*, whereas it was recruited to the division plane in *C. crescentus*. Thus, it is likely that the interaction sites of YigA with divisome components were maintained and are conserved. However, the requirement of CedC and its homologs may have diverged over time in species in response to different environmental conditions and emergence of redundant mechanisms.

3.2.4 Potential cellular role of CedC

The data obtained give no concrete experimental evidence that helps to clarify the exact function of CedC. The co-conservation of XerC-CedC and XerD-CedD and the described deletion studies suggest a functional relationship of CedC (and possibly CedD) to XerCD-mediated site-specific recombination. However, several lines of evidence indicate that CedC and CedD may fulfill a different function in the cell: (1) CedC is located in the cytoplasm like XerCD, whereas CedD is periplasmic (2) the localization of CedCD is independent of XerCD (S. Schlimpert, unpublished) and (3) the phenotype of CedC is presumably not caused by unresolved chromosome dimers. Thus, it is conceivable that CedC (and CedD) are not direct interaction partners of XerC (and XerD). The potential function of CedC can only be hypothesized. The crystal structure of the CedC homolog in *P. aeruginosa* gives further hints. The N-terminal region forms an extended coiled coil, which is a widespread structure involved in protein-protein interactions and transcriptional control of proteins [209–211]. In contrast, the C-terminal part forms a closed or inactive GAF domain. GAF domains are ubiquitously found in proteins in all three domains of life, archaea, bacteria, and eukarya [237]. Similar to coiled-coil regions, they are diverse in their cellular functions. For example they were shown to be associated with gene regulation and nitrogen fixation in bacteria [237, 238] or with the feedback control of an adenylyl cyclase by cAMP-binding in cyanobacteria [239]. Thus, it is not possible to derive the function of CedC from its predicted domain structure, although it is conceivable that CedC interacts with other proteins and possibly has a regulatory rather than a catalytic activity. The functional analysis of CedC mutant derivatives supports the idea that the coiled-coil region and the GAF domain are crucial for the function of CedC and possibly required for protein-protein interactions, that recruit CedC to the division site. Presumably, they may be also required for the formation of CedC tetramers that were observed in *in vitro* studies.

Altogether, the data obtained suggest that CedC may potentially have a regulatory function during cell division. Although it is not directly involved in CDR because of the RecA-independent phenotype, the activity of CedC seems to be related with this event due to a deletion of XerCD affects the observed phenotype. One possible function of CedC could be the coordination of *ter* region resolution/segregation with cell division (Fig. 3.2 A), similar to FtsK. Cell division must be spatiotemporally coordinated with DNA replication and chromosome segregation during each cell cycle. Additionally, the cell must be able to transiently delay cell division in response to stressful conditions that perturb chromosome replication or affect cell division. In general, the temporal regulation of cell division can be achieved in many ways and at any step of divisome assembly, either by inhibition or activation at a specific time point. Diverse regulatory mechanisms controlling Z-ring assembly have been described over the past decade in several model systems (e.g. MinCDE [76, 240, 241], Noc [83], SlmA [84], or MipZ [85, 86]. Another example of a mechanism that blocks cell division is the SOS-response upon DNA-damage. For most bacteria, the SOS-response is the primary and only mechanism that induces the cleavage of the transcriptional repressor LexA, which leads to induction of a set of genes that includes a cell division inhibitor [242, 243]. In *E. coli*, the corresponding genes that mediate a temporal delay in cytokinesis is SulA, which disrupts FtsZ polymerization [244, 245], whereas in *C. crescentus* SidA targets the late cell division protein FtsW [246]. A recent study further identified a second, SOS-independent damage response pathway, including DidA as a central factor that directly interacts with FtsN, and acts together with SidA to block cell division machinery [247]. This mechanism is in line with another, recently uncovered mechanism to regulate PG synthesis in response to the cell division state. Before the divisome is fully assembled, it must switch from the state of assembly to an active state with septum-synthesizing activity. In *E. coli* and *C. crescentus*, the onset of constriction coincides with the arrival of the late essential cell division protein FtsN [110, 134, 141, 142, 145]. Two recent independent studies provided evidence that FtsN triggers its own accumulation at the septum through a self-reinforcing cycle by interaction with FtsA and FtsQLB [110, 138]. The gradual increase in the FtsN concentration stimulates septal PG synthesis, which in turn recruits more FtsN by interaction with FtsA and FtsQLB [137, 138, 216]. PG synthesis is thought to be the main constrictive force providing directionality for cellular constriction, while the Z-ring itself is primarily required for the correct positioning of the divisome. Possibly, both the Z-ring and PG synthesis act in concert to generate a constrictive force. The recently discovered interplay between FtsA, FtsN, and FtsQLB to stimulate PG synthesis affirms this hypothesis, since FtsA was only thought to be a stabilizer of the proto-ring [101, 105, 109, 142]. CedC may be a potential component of this mechanism, temporally regulating the constrictive force in response to intra- or extracellular conditions. In contrast to *E. coli*, *C. crescentus* constricts gradually over the chromosome, thus no DNA-free gap exists during cytokinesis. Apart from the action of FtsK which links cell division with chromosome

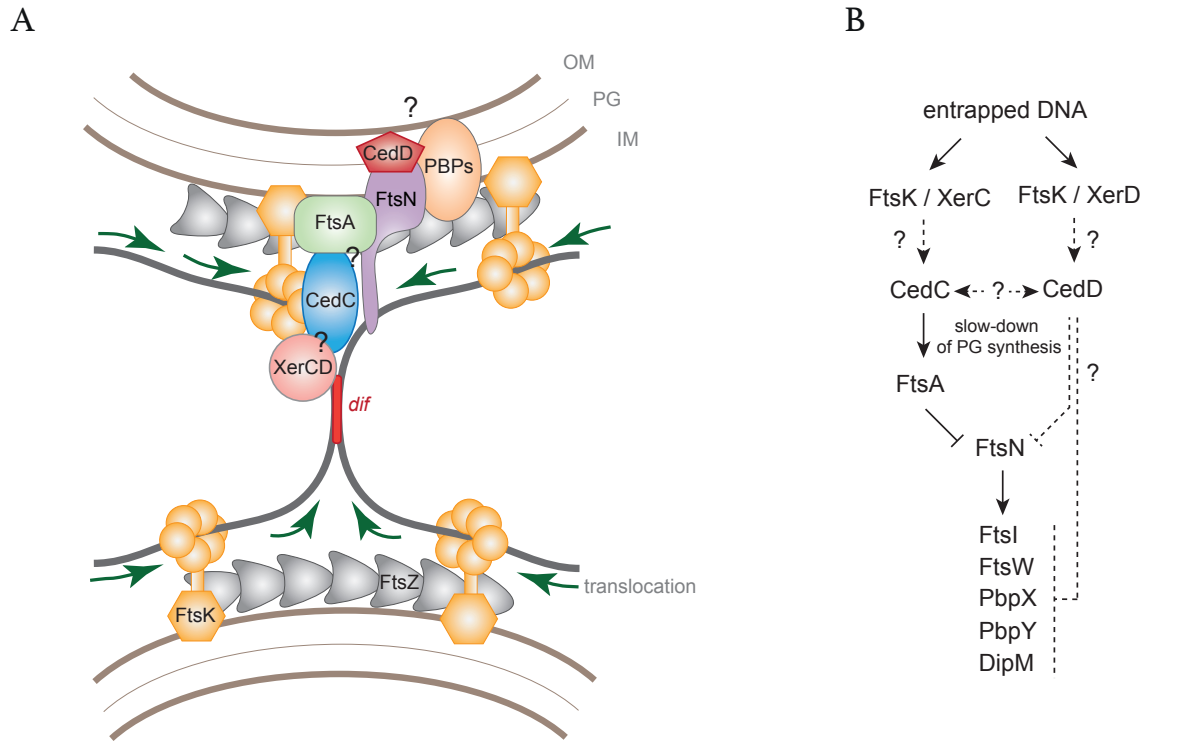

FIGURE 3.2: Model of the function of CedC (A) Schematic representation of the divisome and the action of CedC while the *ter* region of the chromosome is trapped at the cell division site. CedC may act as a regulator and sense DNA at the division plane indirectly through XerCD, FtsK or an unknown factor, thus slowing down PG synthesis by interaction with FtsA or FtsN. The role of the periplasmic protein CedD is not clear yet, but it may possibly act in the same pathway, influencing PG hydrolases. Note that the divisome is simplified and not all essential and non-essential cell division proteins are shown. Question marks indicate potential, but not confirmed (direct or indirect) interactions. **(B)** Schematic of the potential regulatory pathway in which CedC is involved. Dashed lines mark interactions that are not experimentally confirmed.

segregation to ensure that DNA is not dissected during cell constriction, no additional mechanism is known to prevent such a circumstance. I hypothesize that CedC may sense trapped DNA at the division site, which could be the result of unresolved chromosome dimers or a delay in *ter* segregation, e.g. due to DNA repair. In these cases, CedC could slow down cell division to avoid guillotining of the chromosome and, thus, the generation of non-viable offspring. A slow-down of cell division could be realized by a potential protein-protein interaction with FtsA, switching it to an “off” state. However, the data obtained give no evidence for a potential direct interaction with FtsA, FtsN or even a competitive binding between CedC and FtsN to FtsA, to switch FtsA in an “off” mode. Nevertheless, I hypothesize that FtsA is likely involved in the CedC regulatory

pathway (Fig. 3.2 B). Interestingly, a gain of function mutation in *ftsA* led to smaller *E. coli* cells and bypassed the requirement for either ZipA or FtsK, [248], suggesting hyperactive cell division. Consistently, small predivisional cells were also observed in *C. crescentus* cells carrying mutations in FtsW or FtsI that suppressed the cell division inhibitory effect of DidA and SidA in *C. crescentus* [247]. In this work, hyperactive cell division was also observed for cells lacking CedC and XerC. Thus, it is possible that XerC indirectly affects CedC and influences the temporal regulation of cell division. Based on our results, CedC alone is not able to interact with DNA. Consequently, another factor needs to take over this role.

A further idea extends the hypothesis and includes CedD, which is likely involved in the regulatory mechanism to an unknown extent. Given the different subcellular localization of CedC (in the cytoplasm) and CedD (in the periplasm), it appears highly unlikely that both proteins interact directly. However, it may be conceivable that FtsK, as a membrane protein, relays the information (e.g. trapped DNA) to the periplasm and, either directly or indirectly, to CedD, which, in turn, could then affect PG synthesis (Fig. 3.2 B). Altogether, these ideas suggest that CedC, perhaps in association with CedD, regulates cell division in response to the status of chromosome segregation. In general, the *ter* region is the last region that is segregated in bacteria. However, distinguishing between these various hypotheses for the regulatory function of CedC and elucidating the precise mechanisms of action for CedC and CedD will ultimately require more detailed studies. At this point, however, it cannot be excluded that additional, so far unidentified factors are involved for the proposed mechanism.

4 Material and Methods

4.1 Material

4.1.1 Sources of used reagents and enzymes

Common reagents and enzymes used in this study were acquired from Amersham (UK), Applichem (Germany), Becton Dickinson (USA), Bioline (Germany), Carl-Roth (Germany), Difco (Spain), GE Healthcare (UK), Invitrogen (Germany), Kobe (Germany), Merck (Germany), Millipore (Germany), Perkin Elmer (USA), Peqlab (USA), Sigma-Aldrich (USA), and Thermo Fisher Scientific (USA). For certain chemicals and enzymes, the sources are given in the appropriate method section.

4.1.2 Buffers and solutions

Standard buffers und solutions were prepared according to Ausubel [249] and Sambrook [250]. All buffers und solutions were prepared using de-ionized water (Purelab Ultra water purification systems, ELGA, Germany) and autoclaved (20 min at 121 °C, 2 bar) or filter sterilized (pore size 0.22 µm, Sarstedt, Germany) when required. Specific buffers and solutions are listed in the respective method section.

4.1.3 Media and supplements

Complex media were prepared with de-ionized water and sterilized by autoclaving at 121 °C and 2 bar for 20 min. Heat-sensitive minimal medium (M2G) and additives such as antibiotics and carbohydrates were filter sterilized (pore size 0.22 µm, Sarstedt, Germany) and added to the cooled down (~60 °C) medium. For solid media, 1.5 % (w/v) agar was added prior to autoclaving. All antibiotics and media additives were prepared as stock solutions and added to a final concentration as listed in Tables 4.1 and 4.2.

Complex medium for *Escherichia coli*

LB (*Luria Bertani*) **medium**

Tryptone	1.0 % (w/v)
Yeast extract	0.5 % (w/v)
NaCl	1.0 % (w/v)

SB (*Super Broth*) **medium**

Tryptone	3.5 % (w/v)
Yeast extract	2.0 % (w/v)
NaCl	0.5 % (w/v)

Complex medium for *Caulobacter crescentus*

PYE (*peptone yeast extract*) **medium**

Bacto™ peptone	0.2 % (w/v)
Yeast extract	0.1 % (w/v)
$MgSO_4$	1 mM
$CaCl_2$	0.5 mM

Minimal medium for *Caulobacter crescentus*

M2G (*M2 minimal medium with glucose as carbon source*)

Na_2HPO_4	6.1 mM
KH_2PO_4	3.9 mM
NH_4Cl	10 mM
$MgSO_4$	0.5 mM
$CaCl_2$	0.5 mM
Glucose	0.2 % (w/v)
$FeSO_4$/EDTA solution (Sigma, F0518)	0.1 % (v/v)

TABLE 4.1: Antibiotics

Antibiotic [stock concentration]	**Final concentration** [μg/ml]			
	E. coli liquid	*E. coli* solid	*C. crescentus* liquid	*C. crescentus* solid
Ampicillin [100 mg/ml]	200	200	-	50
Chloramphenicol in 70 % EtOH [10 mg/ml]	20	30	1	1
Gentamicin [1 mg/ml]	15	20	0.5	5
Kanamycin [20 mg/ml]	30	50	25	50
Mitomycin C [10 mg/ml]	-	-	1	1
Spectinomycin [20 mg/ml]	50	100	25	50
Streptomycin [10 mg/ml]	30	30	-	5

4.1.4 Oligonucleotides

Oligonucleotides for molecular cloning were designed using Vector NTI Advance™ 11.5. (Invitrogen, Germany) or SnapGene® V3 (GSL Biotech LLC, USA). Oligos were synthesized by either Eurofins MWG Operon (Germany) or Sigma-Aldrich (Germany). A detailed list of oligonucleotides used in this study can be found in the appendix section (Table A3).

TABLE 4.2: Further media additives

Additive	Final concentration			
	E. coli liquid	*E. coli* solid	*C. crescentus* liquid	*C. crescentus* solid
D(+)-glucose [20 %]	0.2 %	0.2 %	0.2 %	0.2 %
D(+)-xylose [30 %]	-	-	0.3 %	0.3 %
D(+)-sucrose [30 %]	-	-	3 %	3 %
IPTG (Isopropyl-β-D-thiogalactopyranosid) [1 M]	0.1 mM	0.1 mM	-	-
myo-inositol [10 %]	-	-	0.3 %	0.3 %
Vanillic acid [50 mM]	-	-	0.5 mM	0.5 mM

4.1.5 Strains

The *E. coli* strains used for cloning, heterologous overproduction of proteins, and bacterial two-hybrid analyses can be found in the appendix section (Table A1).

All strains of *C. crescentus* used in this study are derivatives of the synchronizable strain CB15N (NA1000) [36] and are listed in the appendix section (Table A1).

4.2 Microbiological methods

4.2.1 Bacterial growth conditions

C. crescentus was grown at 28 °C in liquid PYE or M2G with permanent shaking at 220 rpm. On solid media, cells were grown on PYE or M2G agar plates at 28 °C. Antibiotics were added when necessary (Table 4.1). Expression of genes under the control of xylose-, vanillate-, and myo-inositol-inducible promoter was induced with different concentrations (Table 4.2).

E. coli cells were grown at 37 °C in liquid LB or SB broth shaking at 220 rpm or on LB-agar plates. Antibiotics were supplemented to the final concentrations listed in Table 4.1.
E. coli TOP10 and XL-1 blue cells were used for general cloning purposes. For protein overproduction, Rosetta™ (DE3) pLysS cells were used. Expression of genes under control of the T7 promoter was induced with 0.1 mM IPTG. For interaction studies applying bacterial adenylate cyclase two hybrid assay (BACTH), *E. coli* BTH101 was used.

4.2.2 Storage of bacteria

For short-term storage of bacteria grown on solid media, plates were sealed with Parafilm® and stored at 4 °C for a maximum of two weeks.

For long-term storage of bacterial strains, overnight cell cultures were supplemented with 10 % (v/v) DMSO (dimethyl sulfoxide) and stored at -80 °C.

4.2.3 Measurement of cell density

The cell density of liquid cultures was measured spectrophotometrically with an Ultrospec 10 photometer (GE Healthcare BioSciences, USA) at a wavelength of 600 nm. The corresponding medium served as blank value.

4.2.4 Synchronization of *Caulobacter crescentus*

The cell cycle of *C. crescentus* give rise to two distinct cell types that can be easily separated by an adapted density gradient centrifugation [36]. During the synchronization procedure, all equipment and solutions were pre-cooled to 4 °C and cells were constantly kept on ice. For small-scale synchronization, e.g. for time-lapse microscopy, cells were cultured in 25 ml M2G medium and harvested at an OD_{600} between 0.3 and 0.6. The cell pellet was resuspended in 750 µl M2 salts and carefully mixed with an equal volume of Percoll (Sigma-Aldrich, Germany). After centrifugation at 11,000 x g for 20 min, cells were separated into two distinct bands. The upper band corresponds to the stalked cells, while the lower band contains swarmer cells. Swarmer cells were isolated, washed once in 1.5 ml M2 salts at 8,000 x g for 1 min, and then released into 100 to 400 µl pre-warmed M2G medium. For large-scale synchronization, e.g. for time-course experiments, cells were cultured in 1 l M2G medium to an OD_{600} of 0.6. Cells were pelleted at 8,600 x g for 15 min and pellets

were resuspended in 150 ml M2 salts. This cell suspension was then carefully mixed with 50 ml Ludox AS-40 pH 7-8 (Sigma-Aldrich, Germany) and separated by centrifugation at 6,300 x g for 30 min. Swarmer cells were isolated and washed twice with 50 ml M2 salts at 8,000 x g for 10 and 5 min, respectively. Swarmer cells were then resuspended in pre-warmed M2G medium to a final OD_{600} of 0.3 to 0.4 and incubated at 28 °C. Samples were taken at the given intervals.

4.2.5 Bacterial adenylate cyclase two-hybrid (BACTH) system

In vivo interaction between proteins were tested using a bacterial adenylate cyclase two-hybrid system. The assay was performed essentially as described by Karimova *et* al. (1998) and Miller (1972) [192, 251]. It is based on the two complementary T18 and T25 fragments of the catalytic domain of adenylate cyclase of *Bordetella pertussis*. In case the proteins of interest, which are fused to both units, interact, the adenylate cyclase is reconstituted resulting in a functional catalytic enzyme producing cyclic adenosine monophosphate (cAMP). The produced cAMP interacts with the catabolite activator protein (CAP), and the resulting cAMP/CAP complex binds to promoters, thereby activating transcription of several genes, including genes of the lactose and maltose catabolic operons. Their expression can be easily detected by color changes on indication agar plates (e.g. MacConkey).

To test for protein interactions, the adenylate cyclase-deficient strain *E. coli* BTH101 (Euromedex, France) was co-transformed with plasmids expressing the proteins of interest fused to either the T25 or T18 fragment. The transformation mixture was plated on MacConkey agar supplemented with the respective antibiotics and incubated at 28 °C for two days until colonies arose. For spot assays, 10-20 transformants were collected and inoculated in 500 µl LB supplemented with the respective antibiotics and 0.5 mM IPTG with subsequent incubation at 30 °C for 3 h. Afterwards, 4 µl of cell suspension were dropped onto a MacConkey plate (Roth, Germany) supplemented with the respective antibiotics and 0.5 mM IPTG and incubated for one day at 30 °C.

4.3 Molecular biological methods

4.3.1 Isolation and purity of DNA

Plasmid DNA of *E. coli* for cloning purposes was isolated using the GeneElute™ Plasmid Kit (Sigma-Aldrich, Germany). For isolation of chromosomal DNA of *C. crescentus* the illustra™ bacteria genomicPrep Mini Spin Kit (GE Healthcare, Germany) was used. The isolation procedure was followed according to the instruction provided by the manufacturer.

Concentration and purity of nucleic acids was determined spectroscopically using a Nanodrop ND-1000 (Nanodrop, USA) with measurement at wavelengths of 220 - 350 nm. The purity was determined at the ratio of E260 nm/E280 nm. A ratio of 1.5 correlated with a pure protein/DNA mix of 1:1 while a ratio of 2.0 correlated to pure nucleic acid.

4.3.2 Polymerase chain reaction (PCR)

Amplification of specific DNA fragments was carried out using KOD Hot Start DNA polymerase (Merck, Germany) along with the supplied reagents as shown in Table 4.3. Successful amplification of PCR fragments was verified by agarose gel electrophoresis (see subsection 4.3.4) followed by purification of the PCR fragments using either the GeneElute™ PCR Clean-Up Kit (Sigma-Aldrich, Germany) or the GeneElute™ Gel Extraction Kit (Sigma-Aldrich, Germany).

Plasmid uptake in *E. coli* or correct integration of a DNA fragment into the genome of *C. crescentus* cells was confirmed by colony PCR using BioMix™ Red (Bioline, Germany). A standard colony PCR mixture is shown in Table 4.4. As template whole cells (*E. coli* or *C. crescentus*) were used. PCR products were verified by agarose gel electrophoresis (see subsection 4.3.4).

Standard PCR cycling parameters applied for KOD and colony PCRs are given in Table 4.5.

4.3.3 Restriction digestion and ligation of DNA fragments

DNA digestion was performed by incubating 2 µg of DNA with selected restriction endonucleases (NEB, Germany; Fermentas, Canada) for 4-12 h at 37 °C. Digested products were purified directly using the GeneElute™ PCR Clean-Up Kit (Sigma-Aldrich, Germany) or separated on an agarose gel and purified via the GeneElute™ Gel Extraction Kit (Sigma-Aldrich, Germany).

TABLE 4.3: Reaction mix for KOD-PCR (100 µl)

reagent	volume [µl]
10x KOD buffer	10
dNTP mix	10
DMSO (5 %)	5
$MgSO_4$	4
forward primer (100 µM)	0.7
reverse primer (100 µM)	0.7
chromosomal DNA	2
ddH_2O	65.6
KOD polymerase (1U/µl)	2

TABLE 4.4: Reaction mix for colony PCR (8 x 10 µl)

reagent	volume [µl]
BioMix™ Red	40
DMSO (5 %)	4
forward primer (100 µM)	0.4
reverse primer (100 µM)	0.4
ddH_2O	35.2

TABLE 4.5: PCR cycling parameters

step	temperature [°C]	time [min]	
1. initial denaturation	95	2	
2. denaturation	95	0.5	25-35 cycles
3. primer annealing	65	0.5	
4. elongation	72	0.5 pro kb	
5. final elongation	72	4	

DNA ligation was performed using T4 DNA ligase (Fermentas, Canada). In general, a mixture of inserted DNA and recipient vector with a molar ratio of 3 was incubated with 0.5 µl T4 DNA ligase and 3 µl rapid-ligation buffer (Fermentas, Canada) in a total volume of 15 µl for 5-30 min at RT.

4.3.4 Agarose gel electrophoresis

DNA products were mixed with 10 x DNA loading buffer (50 % glycerol, 0.2 % bromophenol blue, 0.2 % xylene cyanol, 0.2 M EDTA) and separated in 1 % agarose gels. The agarose gel was prepared in 0.5 x TAE buffer (20 mM Tris/HCl, pH 8, 0.175 % acetic acid, 0.5 mM EDTA, pH 8.0) and supplemented with 0.005 % ethidium bromide for visualization. An UV-transilluminator (UVP-BioDoc-ITTM Imaging System, UniEquip, Germany) was used to detect DNA exposed to UV light. If necessary, DNA products of interest were excised from the gels for further purification.

4.3.5 DNA sequencing

DNA sequencing was performed by Eurofins MWG Operon (Germany). In general, 50-100 ng of DNA products were provided along with suitable oligonucleotides. Sequencing results were analyzed using Vector NTI Advance™ 11.5 (Invitrogen, Germany) and SnapGene® V3 (GSL Biotech LLC, USA).

Whole genome sequencing of *C. crescentus* was conducted in collaboration with Dr. Andrea Thürmer and the Department of Genomic and Applied Microbiology at the University of Göttingen (Germany). Chromosomal DNA was isolated using the illustra™bacteria genomicPrep Mini Spin Kit (GE Healthcare, USA) of 2 ml of an exponentially grown *C. crescentus* culture and sent for 454 pyrosequencing.

4.3.6 Plasmid construction

Plasmid design and *in silico* construction was accomplished using Vector NTI Advance™ 11.5. (Invitrogen, Germany) or SnapGene® V3 (GSL Biotech LLC, USA). A detailed list of plasmids and vectors used in this study can be found in the appendix section (Table A2).

Plamids for the expression of N- and C-terminal gene fusions in *C. crescentus*
To generate plasmids with the protein of interest tagged N- or C-terminally that integrate into the *C. crescentus* genome at the *vanA*, *xylX* [40] or *iolC* locus [182] by single homologous recombination,

genes of interest were PCR-amplified with specific oligonucleotides that carried restriction enzymes recognition sites. The amplified PCR product and recipient vector were treated with the respective restriction endonuclease and ligated *in frame* as described in section 4.3.3.

High-copy vectors for xylose-inducible gene expression in *C. crescentus*
To achieve high levels of proteins or fusion proteins in cells, the gene of interest or fluorescent gene fusion was inserted into the self-replicating plasmid pBXMCS-2 [40]. For this purpose, the target gene or gene fusion were cut from previously constructed plasmids for the inducible expression of N- or C-terminal protein fusion by restriction digestion followed by ligation into pBXMCS-2. Plasmids for the overproduction of non-fusion proteins were generated by inserting the PCR-amplified gene of interest directly into pBXMCS-2.

Plasmids for the construction of markerless deletions in *C. crescentus*
In frame deletions were generated by double homologous recombination (see subsection 4.3.10), which left 10 to 12 of the terminal codons of the target gene in the genome. To generate knock-out plasmids, two fragments with ~600 bp directly up- and downstream of the target gene were PCR-amplified, purified and fused together in a second PCR by overlap extension (9 bp overlap). The final PCR product was purified, treated with the respective endonucleases and cloned into the suicide vector pNPTS138.

Plasmids for the depletion of proteins in *C. crescentus*
For the depletion of essential proteins, a copy of the native gene of interest was integrated at the *xylX*, *vanA* or *iolC* locus (depending on the used plasmid), while the gene is expressed with the respective inducer in absence of the native gene, which is deleted. To generate depletion plasmids, the gene of interest was PCR-amplified using specific oligonucleotides that carried restriction enzymes recognition sites. The amplified PCR product and recipient vector were treated with the respective restriction endonuclease and ligated *in frame* as described in subsection 4.3.3.

Plasmids for bacterial two-hybrid analysis in *E. coli*
To generate derivatives of the bacterial two-hybrid vectors pKT25, pKNT25, pUT18, and pUT18C [192], genes of interest were PCR-amplified using oligonucleotides that carried a KpnI and a EcoRI cleavage site at their 5' and 3' end, respectively. PCR products were purified by agarose gel electrophoresis and ligated in both orientations into the appropriate bacterial two-hybrid vector that had previously been treated with KpnI and EcoRI.

Plasmids for heterologous overproduction in *E. coli*
To achieve high protein concentrations, the protein of interest was heterologously overproduced in *E. coli* Rosetta™ (DE3) pLysS cells using the T7 promotor, and the SUMO (small ubiquitin like modifier) tag to stabilize the fusion (see subsection 4.5.3 and 4.5.4). To do so, the gene of interest was PCR-amplified with specific oligonuleotides that carried a SapI and BamHI cleavage site at their 5' and 3' end, respectively. PCR products were purified by agarose gel electrophoresis and ligated into the appropriate plasmid pTB146 [63].

4.3.7 Transformation of *Escherichia coli*

The preparation of chemically competent *E. coli* was performed using a modified protocol of Sambrook [250]. In brief, overnight cultures of *E. coli* cells were diluted 1:100 in 500 ml LB medium. Cells were grown to an OD_{600} of 0.6 and incubated on ice for 10 min. Cells were then harvested at 3000 x g and 4 °C, resuspended in ice-cold 0.1 M $CaCl_2$, and incubated on ice for 30 min. After centrifugation, the cells were resuspended in 8 ml of ice-cold 0.1 M $CaCl_2$ supplemented with 15 % (v/v) glycerol. Aliquots of competent cells (100 µl each) were snap-frozen in liquid nitrogen and stored at -80 °C for further use.

The transformation of chemically competent *E. coli* cells was performed as follows: competent cells were mixed with ligation mixtures or ∼10 ng of plasmid DNA and incubated on ice for 30 min. Subsequently, a heat-shock was applied for 90 s at 42 °C. Afterwards, cells were incubated again on ice for 5 min before addition of 500 µl of LB medium. The cell suspension was then incubated at 37 °C for 90 min with shaking and spread on LB agar plates supplemented with appropriate antibiotics. Plates were incubated at 37 °C until single colonies arose.

4.3.8 Transformation of *C. crescentus*

The preparation of electrocompetent *C. crescentus* cells was performed as follows: cells were grown in PYE to an OD_{600} of 1.0 and processed according to [252]. Briefly, cells were harvested by centrifugation at 6,800 x g, 4 °C and 10 min, and washed in ice-cold 10 % (v/v) glycerol, twice in 1 volume and once in 1/10 volume. The final cell pellet was resuspended in 1/50 volume of ice-cold 10 % glycerol. Aliquots of 100 µl were snap-frozen in liquid nitrogen and stored at -80 °C.

To introduce plasmid constructs into electrocompetent *C. crescentus*, cells were thawed on ice and mixed with 0.5 µg (integrating) or 0.25 µg (replicating) purified plasmid. This reaction

mixture was then transferred to a sterile electroporation cuvette, electroporated at 1.5 kV, 400 Ω and 25 µF and immediately mixed with 900 µl ice-cold PYE. The cell suspension was allowed to recover for at least 3 h at 28 °C. To select for recombinant *C. crescentus*, cells were plated and grown on PYE agar supplemented with the appropriate antibiotic for 2 to 3 days at 28 °C. Single colonies were re-streaked onto new PYE agar plates and successful plasmid integration or uptake was confirmed by colony PCR.

4.3.9 UV mutagenesis of *C. crescentus*

UV mutagenesis with *C. crescentus* was performed [235] using an ultraviolet crosslinker (UVP CL1000S) by irradiation of mid-exponential phase cells with 5 J/cm^2. Radiated cells were adjusted to an equal OD_{600} of 0.3 and diluted 1:10 in a serial transfer. 5 µl of each dilution were then dropped on PYE agar and grown for two days at 28 °C.

4.3.10 Gene replacements in *Caulobacter crescentus*

Gene replacement in *C. crescentus* was achieved by double homologous recombination [253]. In general, plasmids for gene replacement were derived from the suicide vector pNPTS138 (M.R. Alley, unpublished). This vector carries a kanamycin resistance cassette and the *sacB* gene for counter-selection. Derivatives of pNPTS138 were introduced in *C. crescentus* by electroporation (see subsection 4.3.8). Recombinant cells were first selected in the presence of kanamycin. The kanamycin-resistant colonies were transferred onto fresh plates with kanamycin and then grown in PYE liquid medium without selection markers to stationary phase to allow for the second recombination to occur. 200 µl of a 1:100 dilution of the culture were then spread onto PYE agar plates supplemented with 3 % (w/v) sucrose for selection of cells that lost the plasmid. Colonies exhibiting sucrose tolerance and high kanamycin sensitivity were further verified by colony PCR.

4.4 Microscopic methods

4.4.1 Light microscopy and fluorescence microscopy

Microscopic analyses were conducted using a Zeiss Axio Imager.M1 microscope (Zeiss, Germany), a Zeiss Plan Apochromat 100x/1.40 Oil DIC objective and a Photometrics Cascade: 1K CCD camera. Alternatively, a Zeiss Axio Imager.Z1 microscope with a 100x/1.46 Oil DIC objective and a pco.edge

sCMOS camera were used. The X-Cite®120PC metal halide light source (EXFO, Canada) and ET-DAPI, ET-CFP, ET-YFP, or ET-TexasRed filter cubes (Chroma, USA) were used for fluorescence detection.

In general, cells were immobilized on pads made of 1.5 % agarose with ddH_2O. Images were processed using MetaMorph® 7.7.5. (Universal Imaging Group, USA). The quantification of imaging data was conducted as described in subsection 4.4.5.

Unless indicated differently, the synthesis of fluorescent protein fusions in *C. crescentus* was induced during early-exponential growth (OD_{600} of ∼0.2) with 0.3 % xylose or 0.5 mM vanillate for 1 h and 2 h, respectively, before imaging.

4.4.2 Time-lapse microscopy

To follow the subcellular localization of fluorescent protein fusion over the cell cycle, synchronized *C. crescentus* cells were immobilized on 1 % M2G agarose pads supplemented with the respective inducer. To protect cells from dehydration, the cover-slide was sealed with VLAP (vaseline, lanolin and paraffin at a 1:1:1 ratio). Images were taken at the given time points.

4.4.3 Cryo-electron microscopy

Electron cryo-tomography was performed by Ariane Briegel in the group of Grant J. Jensen (California Institute of Technology, USA). Briefly, the cells were prepared as follows: strain SS347 was inoculated overnight in PYE with subsequent centrifugation of 1 ml at 1,500 x g for 5 min and suspension of the cell pellet in 30 µl PYE. 20 µl of this concentrated cell suspension were mixed with 100 µl colloidal gold, which was treated with BSA to avoid aggregation of the gold particles. 3 µl of the cell-gold solution were transferred onto a R2/2 Quantifoil copper grid (Quantifoil Micro Tools), manually blotted and plunge frozen in a liquid ethane/propane mix [254]. Tilt series were generated with a FEI Polara G3 (FEI Co., Hillsboro, OR) 300k eV field emission gun microscopy with a gatan energy filter und K2 summit counting electron detector camera (Getan, Pleasanton, CA). Data were captured with the UCSFtomo software [255]. The cumulative dose was ∼ 160e/A2 per tilt series. The data were re-constructed using IMOD software [256].

4.4.4 Nucleoid staining

C. crescentus cells were incubated with 0.5 µg/ml 4',6-diamidino-2-phenylindole (DAPI; Sigma-Aldrich, Germany) for 15 min in the dark with shaking at 28 °C. Stained samples were then processed for further imaging.

4.4.5 Image processing

All images shown in this work were processed using either MetaMorph® 7.7.5. (Universal Imaging Group, USA) or Fiji (Open Source). All pictures were further processed with Adobe Photoshop and Illustrator CS6 (Adobe Systems, USA). The detailed quantification information are given in the respective results section.

4.5 Biochemical methods

4.5.1 SDS-Polyacrylamide gel electrophoresis (SDS-PAGE)

Proteins were separated by their mass using SDS-PAGE according to Lämmli [257]. Protein samples were prepared as follows: mid-exponentially grown cells were collected by centrifugation at 18,000 x g for 2 min and resuspended in 2 x sodium dodecyl sulfate (SDS) sample buffer (300 mM Tris Base, 50 % (v/v) glycerol, 5 % (w/v) SDS, 500 mM dithiothreitol, 0.05 % bromophenol blue, pH 6.8) according to their optical density (100 µl buffer per 1 ml of suspension with an OD_{600} of 1) and heated at 95 °C for 10 min. Samples taken during biochemical assays (protein purification, Co-IP) were mixed with an equal volume of 2 x SDS sample buffer and heated as described before. After the samples were boiled, they were loaded along with a molecular weight marker (PageRuler™ Prestained Protein Ladder; Fermentas, Canada) on an SDS-PAGE consisting of a 5 % stacking gel and a 15 % resolving gel (4.6). Electrophoresis was performed in a Tris/Glycine buffer (25 mM Tris Base, 192 mM glycine, 0.1 % (w/v) SDS) at 15-30 mA per gel using a PerfectBlue™ Twin S system (Peqlab, USA).

For the detection of proteins, SDS-PAGE gels were stained after electrophoresis either for 45 min in Coomassie solution (40 % methanol, 10 % acidic acid, 0.1 % (w/v) Brilliant Blue R 250) and destained (20 % ethanol, 10 % acidic acid) or for 20 min in Instant*Blue*™ (Expedeon, UK) for

faster visualization. For specific protein detection using immunoblot analysis, SDS-PAGE gels were processed further (see subsection 4.5.2).

TABLE 4.6: Composition of a 5 % stacking and a 15 % resolving gel

component	5 % stacking gel (2.5 ml)	15 % resolving gel (5 ml)
ddH_2O	1.43 ml	1.2 ml
4x stacking buffer (0.5 M Tris base, 0.4 % (w/v) SDS, pH 6.8)	625 µl	-
4x resolving buffer (1.5 M Tris base, 0.4 % (w/v) SDS, pH 8.8)	-	1.25 ml
30 % Rotiphorese® Acrylamide/Bis (29:1)	417 µl	2.5 ml
TEMED (N,N,N',N'-Tetramethylethylendiamine)	1.9 µl	3 µl
10 % (w/v) APS (Ammoniumperoxodisulfate)	25 µl	40 µl

4.5.2 Immunoblot analysis

To detect specific proteins using immunoblot analysis, proteins were separated by SDS-PAGE as described before (see subsection 4.5.1) and transferred onto a polyvinylidene fluoride (PVDF) membrane (Millipore, USA) by semi-dry transfer. The first step was the activation of the membrane in 100 % methanol for 15 sec, followed by washing in H_2O for 2 min, and equilibration in 1 x Western transfer buffer (25 mM Tris base, 192 mM glycerol, 10 % methanol) for 5 min. The transfer of the proteins onto the membrane was conducted at 2 mA/cm^2 for 2 h using a PerfectBlue™ Semi-Dry-Electro blotter (Peqlab, USA). To block the membrane, it was incubated with 5 % non-fat milk in 1x TBST (10 mM Tris base, 150 mM NaCl, 0.1 % (w/w) Tween 20, pH 7.5) overnight at 4 °C with gentle agitation. In order to visualize the protein of interest, the membrane was first incubated with a primary antibody (Table 4.7) diluted in 5 % non-fat milk-TBST solution at RT for 1-2 h on a shaker. Before incubating the membrane with a secondary antibody for 1-2 h, it was washed three times in 1x TBST. The secondary antibody is ligated to a horseradish peroxidase (Table 4.7) to visualize the protein of interest. The membrane was rinsed four times with 1x TBST for 5 min and incubated with Western Lightning™ Chemiluminescence Reagent Plus (PerkinElmer, USA) according to the manufacturer's instructions for 1 min. Visualization of the signal was achieved by exposing the membrane to Amersham Hyperfilm™ ECL-Chemiluminescence films (GE Healthcare, UK) followed by development with a LAS-4000 Luminescent Image Analyzer (Fujifilm, Germany). Alternatively, the signal was visualized with the ChemiDoc™ MP Imaging System (Bio-Rad, USA).

TABLE 4.7: Antibodies used for immunoblot analysis

antibody	dilution	reference
Primary antibodies		
α-CedC	1:10,000	this study
α-CtrA	1:10,000	[258]
α-GFP	1:10,000	Sigma-Aldrich, Germany
α-FtsZ	1:20,000	[259]
α-FtsN	1:20,000	[110]
α-mCherry	1:8,000	Millipore, Germany
α-Pbp1A	1:10,000	[260]
α-PbpC	1:10,000	[144]
α-PbpX	1:2,500	[144]
α-PbpY	1:2,500	[144]
α-SpmX	1:50,000	[195]
α-T18	1:100	Santa Cruz Biotechnologies, USA
α-T25	1:1,000	[194]
Secondary antibodies		
α-rabbit-HRP	1:20,000	Perkin Elmer, USA
α-mouse-HRP	1:5,000	Sigma-Aldrich, Germany

4.5.3 Heterologous overproduction in *Escherichia coli*

In order to obtain native CedC, His_6-SUMO-CedC was overproduced and purified. For this purpose, plasmid pWS89 was introduced into *E. coli* Rosetta™ (DE3)/pLysS and cells were grown in 3 l LB medium supplemented with corresponding concentrations of the antibiotics chloramphenicol and ampicillin, at 37 °C with gentle agitation, until an OD_{600} of ∼1 was reached. Overproduction of the protein was started by addition of 0.1 mM IPTG followed by incubation at 37 °C for 3 h with gentle agitation. Cells were harvested by centrifugation at 7,500 x g and 4 °C for 10 min, resuspended in 1/10 volume lysis buffer (50 mM Tris/HCl, pH 8.0, 300 mM NaCl, 10 mM imidazole), pelleted (7,500 x g, 4 °C, 10 min), and weighted before being snap-frozen in liquid nitrogen.

4.5.4 Protein purification

For the purification of native CedC, the cell pellet collected before (see subsection 4.5.3), was resuspended in 2 ml/g lysis buffer, containing 100 µg/ml phenylmethanesulfonyl fluoride (PMSF)

and 10 µg/ml DNaseI followed by cell lysis by three passages through a French Press at 16,000 psi. Cell debris was removed by centrifugation at 30,000 x g for 30 min at 4 °C and the supernatant was applied onto a HisTrap HP 5 ml column (GE Healthcare, UK) that had been equilibrated with 5 CV (column volumes) lysis buffer before. After washing of the column with 5 CV column buffer (50 mM Tris/HCl, pH 8.0, 300 mM NaCl, 20 mM imidazole), the protein was eluted by applying 18 CV of a linear imidazole gradient (20-250 mM imidazole) generated by mixing column buffer and elution buffer (50 mM Tris/HCl, pH 8.0, 300 mM NaCl, 250 mM imidazole). Selected elution fractions were dialyzed against 3 l protease buffer (50 mM Tris/HCl, pH 8.0, 150 mM NaCl, 10 % glycerol) overnight at 4 °C. To cleave off the His_6-SUMO tag, the protein was incubated with His_6-Ulp1 protease at a molar ratio of 1:1,000 (Ulp1:His_6-SUMO-CedC) and 1 mM DTT for 2 h at 4 °C. After centrifugation at 30,000 x g and 4 °C for 30 min, the cleavage reaction was applied onto a HisTrap HP 5 ml column equilibrated with protease buffer. The native CedC protein eluted in the flow-through fraction, whereas the His_6-SUMO tag and the His_6-Ulp1 protease remained bound to the column. The flow-through was collected and the protein was concentrated if necessary, using Amicon® Ultra-15 centrifugal filters (10,000 MWL; Millipore, USA).

For crystallization purposes (see subsection 4.5.6), the native CedC was further purified by size exclusion chromatography. To this end, the protein was concentrated to a maximum volume of 5 ml using Amicon® Ultra-15 centrifugal filters and loaded on a Superdex 200 Prep Grade column (GE Healthcare, USA), which was equilibrated with one CV protease buffer. The protein was eluted with one CV crystallization buffer (20 mM Tris/HCl, pH 8.0, 25 mM NaCl, 1 mM EDTA). Selected elution fractions were collected and snap-frozen in liquid nitrogen.

4.5.5 Antibody synthesis

Purified CedC was sent for antibody generation to the company Eurogentec (Belgium) to produce polyclonal antibodies in rabbits.

4.5.6 Crystallization of CedC

The crystallization of CedC was conducted in collaboration with the MarXtal facility (Philipps University Marburg) and Dr. V. Srinivasan. The condition screen as well as the Hampton additive screen were performed using the high-throughput crystallization robot Honeybee963™ and Formulatrix RockImager™ automated imaging system.

Purified CedC in crystallization buffer (20 mM Tris/HCl, pH 8.0, 25 mM NaCl, 1 mM EDTA) was concentrated up to 25 mg/ml using Amicon® Ultra-15 and Amicon® Ultra-0.5 centrifugal filters (10,000 MWL; Millipore, USA). Crystallization experiments were performed using the hanging drop vapor diffusion method at 18 °C. Drops were prepared by mixing 1 µl of concentrated protein with an equal volume of reservoir solution (4 % PEG6000, 100 mM Bicine, pH 9.0) and transferred on a silicon-covered cover slip, which was put upside down on a well filled with 500 µl reservoir solution. The crystallization approach was incubated at 18 °C for at least 10 days to get crystals formed.

4.5.7 Coimmunoprecipitation and mass-spectrometry

C. crescentus cells of strain SS348 (CB15N *cedC*::*venus-cedC*) and the wild-type strain were grown to exponential phase in 2 x 750 ml M2G and fixed with 0.6 % paraformaldehyde in PBS for 20 min at 37 °C, once they reached an OD_{600} of 0.6. The crosslinking reaction was stopped by adding glycine in PBS to a final concentration of 125 mM. Cells were then harvested by centrifugation at 4 °C, 2,000 x g for 10 min and pellets were washed twice with 200 ml lysis buffer (10mM Tris/HCl pH 7.5, 150 mM NaCl, 0.5 mM EDTA). Afterwards, the cells were resuspended in 20 ml/g cell pellet with lysis buffer and centrifuged at 2,000 x g for 10 min at 4 °C. After addition of 10 mg/ml lysozyme and 5 µg/l DNaseI, the suspension was incubated for 30 min on ice. To disrupt the cells, the suspension was sonicated ten times for 2 min. Subsequently, Triton X-100 was added to a final concentration of 0.5 % and the suspension was incubated for another 1 h at 4 °C. Cell debris were then removed by centrifugation at 13,000 x g for 20 min. 250 µl of the supernatant were incubated overnight at 4 °C under permanent mixing with 25 µl GFP-trap_A beads (Chromotek, USA), which had been equilibrated with dilution buffer before. After incubation, the agarose beads were washed in the following order: one time with wash buffer I (10mM Tris/HCl pH 7.5, 150 mM NaCl, 0.5 mM EDTA), a second time with wash buffer II (10mM Tris/HCl pH 7.5, 325 mM NaCl, 0.5 mM EDTA), and finally with wash buffer III (10mM Tris/HCl pH 7.5, 500 mM NaCl, 0.5 mM EDTA). Each time, the solution was centrifuged at 2,500 x g for 2 min at 4 °C. Bound proteins were eluted by heating the beads for 30 min at 95 °C in 2 x SDS sample buffer. The eluted proteins were then subjected to immunoblot analysis using a α-GFP antibody as described in subsection 4.5.2.

In case the samples were submitted to mass-spectrometry, eluted protein samples were shortly run on a 11 % SDS gel, stained with Coomassie blue, cut out as a single band, and identified using matrix-assisted laser desorption/ionization time-of-flight mass spectrometry (MALDI-MS) analysis. The analysis was performed in collaboration with Dr. Linne from the Chemistry Department at the Philipps University of Marburg.

4.5.8 Gel shift assay

A gel shift assay was used to test for non-specific binding of CedC to DNA. 10 μM purified protein in crystallization buffer (20 mM Tris/HCl pH 8.0, 25 mM NaCl, 1 mM EDTA) were incubated together with 10 nM EcoRI-linearized pMCS-2 at room temperature for 20 min. Then, samples were subjected to standard DNA agarose gel electrophoresis (see subsection 4.3.4). The DNA-protein bands were visualized using 0.5 μg/ml ethidium bromide.

4.6 Bioinformatic analyses

4.6.1 DNA sequence analyses

Nucleotide and genome sequences were obtained from the national center for biotechnology information (NCBI) (http://www.ncbi.nlm.nih.gov/).

4.6.2 Protein analyses

Protein sequences and conserved protein domains were retrieved from NCBI (http://www.ncbi.nlm.nih.gov/) and identified with the help of the SMART (http://smart.embl-heidelberg.de/) or Pfam (http://pfam.xfam.org/search) search. Transmembrane domains and signal sequences were predicted using TMHMM and SignalP (both on http://expasy.org). Protein sequence alignments were generated with ClustalW2 (http://www.ebi.ac.uk/Tools/msa/clustalw2/) and processed with GeneDoc. Immunoblots were analyzed with Image Lab 5.0 (Bio-Rad, USA).

4.6.3 Genomic tree

The genomic iTOL tree of CedC and XerC was prepared in collaboration with Dr. Kristin Wuichet (AG Søgaard-Andersen, Max Planck Institute for Terrestrial Microbiology, Marburg).

Orthologs of CedC were identified from a previously described set of 1611 completely sequenced prokaryotic genomes from the NCBI Refseq database [261], as available on April 4th, 2012 [262], using domain architecture, gene neighborhood, and BLASTP.

The HMMER3 software package [263] was used in conjunction with the Pfam26 domain library [264] for domain architecture analysis with default gathering thresholds. In the case of domain overlaps, the highest scoring domain model was chosen for the final domain architecture. BLASTP from the BLAST$^+$ software package version 2.2.26 [265] was used and hits with e-values of 0.0001 or lower were considered to be significant. Multiple sequence alignments were built using the l-ins-i algorithm of the MAFFT version 6.864b software package [266]. Gblocks version 0.91b was used to extract conserved regions of interest from multiple alignments, using a minimum half of the sequences for identifying conserved and flank positions, eight maximum contiguous non-conserved positions, a ten length minimum for a block, and gaps were allowed, when they were present in less than half of the sequences [267]. Phylogenetic trees were built using FastTree version 2.1.4 with the "slow" option [268] or PhyML version 3.0 with LG + Γ_4 + F parameters and subtree pruning and regrafting topology search with approximate likelihood ratio tests (alRTs) to evaluate branch support [269]. Relevant data was mapped onto phylogenetic trees using iTOL [270].

References

[1] **Liesack, W.**, **König, H.**, **Schlesner, H.**, **Hirsch, P.** (1986) Chemical composition of the peptidoglycan-free cell envelopes of budding bacteria of the *Pirella*/Planctomyces group. *Archives of Microbiology* **145**(4):361–366.

[2] **Razin, S.**, **Glaser, G.**, **Amikam, D.** (1984) Molecular and biological features of *mollicutes* (mycoplasmas). Annales de l'Institut Pasteur/Microbiologie, vol. 135. Elsevier, 9–15.

[3] **Vollmer, W.**, **Seligman, S.J.** (2010) Architecture of peptidoglycan: more data and more models. *Trends in Microbiology* **18**(2):59–66.

[4] **Weidel, W.**, **Pelzer, H.** (1964) Bagshaped macromolecules -a new outlook on bacterial cell walls. *Advances in Enzymology and Related Areas of Molecular Biology* **26**:193–232.

[5] **Höltje, J.V.** (1998) Growth of the stress-bearing and shape-maintaining murein sacculus of *Escherichia coli*. *Microbiology and Molecular Biology Reviews* **62**(1):181–203.

[6] **Glauner, B.** (1988) Separation and quantification of muropeptides with high-performance liquid chromatography. *Analytical Biochemistry* **172**(2):451–464.

[7] **Glauner, B.**, **Höltje, J.**, **Schwarz, U.** (1988) The composition of the murein of *Escherichia coli*. *Journal of Biological Chemistry* **263**(21):10088–10095.

[8] **Vollmer, W.** (2008) Structural variation in the glycan strands of bacterial peptidoglycan. *FEMS Microbiology Reviews* **32**(2):287–306.

[9] **Vollmer, W.**, **Blanot, D.**, **De Pedro, M.A.** (2008) Peptidoglycan structure and architecture. *FEMS Microbiology Reviews* **32**(2):149–167.

[10] **Caparros, M.**, **Torrecuadrada, J.**, **de Pedro, M.** (1991) Effect of D-amino acids on *Escherichia coli* strains with impaired penicillin-binding proteins. *Research in Microbiology* **142**(2):345–350.

[11] **Takacs, C.N.**, **Hocking, J.**, **Cabeen, M.T.**, **Bui, N.K.**, **Poggio, S.**, **Vollmer, W.**, **Jacobs-Wagner, C.** (2013) Growth medium-dependent glycine incorporation into the peptidoglycan of *Caulobacter crescentus*. *PloS One* **8**(2):e57579.

[12] **Lam, H.**, **Oh, D.C.**, **Cava, F.**, **Takacs, C.N.**, **Clardy, J.**, **de Pedro, M.A.**, **Waldor, M.K.** (2009) D-amino acids govern stationary phase cell wall remodeling in bacteria. *Science*

325(5947):1552–1555.

[13] **Royet, J.**, **Dziarski, R.** (2007) Peptidoglycan recognition proteins: pleiotropic sensors and effectors of antimicrobial defences. *Nature Reviews Microbiology* **5**(4):264–277.

[14] **Den Blaauwen, T.**, **De Pedro, M.A.**, **Nguyen-Distèche, M.**, **Ayala, J.A.** (2008) Morphogenesis of rod-shaped sacculi. *FEMS Microbiology Reviews* **32**(2):321–344.

[15] **Koch, A.L.**, **Woeste, S.** (1992) Elasticity of the sacculus of *Escherichia coli*. *Journal of Bacteriology* **174**(14):4811–4819.

[16] **Yao, X.**, **Jericho, M.**, **Pink, D.**, **Beveridge, T.** (1999) Thickness and elasticity of gram-negative murein sacculi measured by atomic force microscopy. *Journal of Bacteriology* **181**(22):6865–6875.

[17] **Oldmixon, E.**, **Glauser, S.**, **Higgins, M.** (1974) Two proposed general configurations for bacterial cell wall peptidoglycans shown by space-filling molecular models. *Biopolymers* **13**(10):2037–2060.

[18] **Virudachalam, R.**, **Rao, V.** (1979) Theoretical studies on peptidoglycans. II. Conformations of the disaccharide–peptide subunit and the three-dimensional structure of peptidoglycan. *Biopolymers* **18**(3):571–589.

[19] **Dworkin, M.**, **Falkow, S.**, **Rosenberg, E.**, **Schleifer, K.H.**, **Stackebrandt, E.** (2006) The Prokaryotes: Vol. 4: Bacteria: Firmicutes, Cyanobacteria. Springer Science & Business Media.

[20] **Mengin-Lecreulx, D.**, **Texier, L.**, **Rousseau, M.**, **van Heijenoort, J.** (1991) The *murG* gene of *Escherichia* coli codes for the UDP-N-acetylglucosamine: N-acetylmuramyl-(pentapeptide) pyrophosphoryl-undecaprenol N-acetylglucosamine transferase involved in the membrane steps of peptidoglycan synthesis. *Journal of Bacteriology* **173**(15):4625–4636.

[21] **Thorne, K.J.**, **Kodicek, E.** (1966) The structure of bactoprenol, a lipid formed by lactobacilli from mevalonic acid. *Biochemical Journal* **99**(1):123.

[22] **Anderson, J.S.**, **Matsuhashi, M.**, **Haskin, M.A.**, **Strominger, J.L.** (1967) Biosynthesis of the Peptidoglycan of Bacterial Cell Walls II. Phospholipid carriers in the reaction sequence. *Journal of Biological Chemistry* **242**(13):3180–3190.

[23] **Higashi, Y.**, **Strominger, J.L.**, **Sweeley, C.C.** (1967) Structure of a lipid intermediate in cell wall peptidoglycan synthesis: a derivative of a C55 isoprenoid alcohol. *Proceedings of the National Academy of Sciences* **57**(6):1878.

[24] **Koyasu, S.**, **Fukuda, A.**, **Okada, Y.** (1980) The penicillin-binding proteins of *Caulobacter crescentus*. *Journal of Biochemistry* **87**(1):363–366.

[25] **Spratt, B.G.** (1977) Properties of the Penicillin-Binding Proteins of *Escherichia coli* K12. *European Journal of Biochemistry* **72**(2):341–352.

[26] **Sauvage, E.**, **Kerff, F.**, **Terrak, M.**, **Ayala, J.A.**, **Charlier, P.** (2008) The penicillin-binding proteins: structure and role in peptidoglycan biosynthesis. *FEMS Microbiology Reviews* **32**(2):234–258.

[27] **Goffin, C.**, **Ghuysen, J.M.** (1998) Multimodular penicillin-binding proteins: an enigmatic family of orthologs and paralogs. *Microbiology and Molecular Biology Reviews* **62**(4):1079–1093.

[28] **Vollmer, W.**, **Joris, B.**, **Charlier, P.**, **Foster, S.** (2008) Bacterial peptidoglycan (murein) hydrolases. *FEMS Microbiology Reviews* **32**(2):259–286.

[29] **Lovering, A.L.**, **De Castro, L.H.**, **Lim, D.**, **Strynadka, N.C.** (2007) Structural insight into the transglycosylation step of bacterial cell-wall biosynthesis. *Science* **315**(5817):1402–1405.

[30] **Cabeen, M.T.**, **Jacobs-Wagner, C.** (2005) Bacterial cell shape. *Nature Reviews Microbiology* **3**(8):601–610.

[31] **Höltje, J.V.** (1993) "Three for one" - a Simple Growth Mechanism that Guarantees a Precise Copy of the Thin, Rod-Shaped Murein Sacculus of *Escherichia coli*. Bacterial Growth and Lysis. Springer, 419–426.

[32] **Cava, F.**, **de Pedro, M.A.** (2014) Peptidoglycan plasticity in bacteria: emerging variability of the murein sacculus and their associated biological functions. *Current Opinion in Microbiology* **18**:46–53.

[33] **Flärdh, K.**, **Buttner, M.J.** (2009) *Streptomyces* morphogenetics: dissecting differentiation in a filamentous bacterium. *Nature Reviews Microbiology* **7**(1):36–49.

[34] **Daniel, R.A.**, **Errington, J.** (2003) Control of cell morphogenesis in bacteria: two distinct ways to make a rod-shaped cell. *Cell* **113**(6):767–776.

[35] **Poindexter, J.S.** (1964) Biological properties and classification of the *Caulobacter* group. *Bacteriological Reviews* **28**(3):231.

[36] **Evinger, M.**, **Agabian, N.** (1977) Envelope-associated nucleoid from *Caulobacter crescentus* stalked and swarmer cells. *Journal of Bacteriology* **132**(1):294–301.

[37] **Marks, M.E.**, **Castro-Rojas, C.M.**, **Teiling, C.**, **Du, L.**, **Kapatral, V.**, **Walunas, T.L.**, **Crosson, S.** (2010) The genetic basis of laboratory adaptation in *Caulobacter crescentus*. *Journal of Bacteriology* **192**(14):3678–3688.

[38] **Nierman, W.C.**, **Feldblyum, T.V.**, **Laub, M.T.**, **Paulsen, I.T.**, **Nelson, K.E.**, **Eisen, J.**, **Heidelberg, J.F.**, **Alley, M.**, **Ohta, N.**, **Maddock, J.R.**, *et al.* (2001) Complete genome sequence of *Caulobacter crescentus*. *Proceedings of the National Academy of Sciences* **98**(7):4136–4141.

[39] **Ely, B.**, **Scott, L.E.** (2014) Correction of the *Caulobacter crescentus* NA1000 genome annotation. *PloS One* **9**(3):e91668.

[40] **Thanbichler, M.**, **Iniesta, A.A.**, **Shapiro, L.** (2007) A comprehensive set of plasmids for vanillate-and xylose-inducible gene expression in *Caulobacter crescentus*. *Nucleic Acids Research* **35**(20):e137–e137.

[41] **Bodenmiller, D.**, **Toh, E.**, **Brun, Y.V.** (2004) Development of surface adhesion in *Caulobacter crescentus*. *Journal of Bacteriology* **186**(5):1438–1447.

[42] **Marczynski, G.T.** (1999) Chromosome Methylation and Measurement of Faithful, Once and Only Once per Cell Cycle Chromosome Replication in *Caulobacter crescentus*. *Journal of Bacteriology* **181**(7):1984–1993.

[43] **Curtis, P.D.**, **Brun, Y.V.** (2010) Getting in the loop: regulation of development in *Caulobacter crescentus*. *Microbiology and Molecular Biology Reviews* **74**(1):13–41.

[44] **Egan, A.J.**, **Vollmer, W.** (2013) The physiology of bacterial cell division. *Annals of the New York Academy of Sciences* **1277**(1):8–28.

[45] **Typas, A.**, **Banzhaf, M.**, **Gross, C.A.**, **Vollmer, W.** (2012) From the regulation of peptidoglycan synthesis to bacterial growth and morphology. *Nature Reviews Microbiology* **10**(2):123–136.

[46] **Glauner, B.**, **Höltje, J.** (1990) Growth pattern of the murein sacculus of *Escherichia coli*. *Journal of Biological Chemistry* **265**(31):18988–18996.

[47] **Burman, L.G.**, **Park, J.T.** (1984) Molecular model for elongation of the murein sacculus of *Escherichia coli*. *Proceedings of the National Academy of Sciences* **81**(6):1844–1848.

[48] **Erickson, H.P.**, **Anderson, D.E.**, **Osawa, M.** (2010) FtsZ in bacterial cytokinesis: cytoskeleton and force generator all in one. *Microbiology and Molecular Biology Reviews* **74**(4):504–528.

[49] **De Pedro, M.**, **Quintela, J.C.**, **Höltje, J.**, **Schwarz, H.** (1997) Murein segregation in *Escherichia coli*. *Journal of Bacteriology* **179**(9):2823–2834.

[50] **Aaron, M.**, **Charbon, G.**, **Lam, H.**, **Schwarz, H.**, **Vollmer, W.**, **Jacobs-Wagner, C.** (2007) The tubulin homologue FtsZ contributes to cell elongation by guiding cell wall precursor synthesis in *Caulobacter crescentus*. *Molecular Microbiology* **64**(4):938–952.

[51] **White, C.L.**, **Kitich, A.**, **Gober, J.W.** (2010) Positioning cell wall synthetic complexes by the bacterial morphogenetic proteins MreB and MreD. *Molecular Microbiology* **76**(3):616–633.

[52] **Kawai, Y.**, **Daniel, R.A.**, **Errington, J.** (2009) Regulation of cell wall morphogenesis in *Bacillus subtilis* by recruitment of PBP1 to the MreB helix. *Molecular Microbiology* **71**(5):1131–1144.

[53] **Vats, P.**, **Shih, Y.L.**, **Rothfield, L.** (2009) Assembly of the MreB-associated cytoskeletal ring of *Escherichia coli*. *Molecular Microbiology* **72**(1):170–182.

[54] **Jones, L.J.**, **Carballido-López, R.**, **Errington, J.** (2001) Control of cell shape in bacteria: helical, actin-like filaments in *Bacillus subtilis*. *Cell* **104**(6):913–922.

[55] **Varley, A.**, **Stewart, G.C.** (1992) The *divIVB* region of the *Bacillus subtilis* chromosome encodes homologs of *Escherichia coli* septum placement (*minCD*) and cell shape (*mreBCD*) determinants. *Journal of Bacteriology* **174**(21):6729–6742.

[56] **Levin, P.A.**, **Margolis, P.S.**, **Setlow, P.**, **Losick, R.**, **Sun, D.** (1992) Identification of *Bacillus subtilis* genes for septum placement and shape determination. *Journal of Bacteriology* **174**(21):6717–6728.

[57] **Doi, M.**, **Wachi, M.**, **Ishino, F.**, **Tomioka, S.**, **Ito, M.**, **Sakagami, Y.**, **Suzuki, A.**, **Matsuhashi, M.** (1988) Determinations of the DNA sequence of the *mreB* gene and of the gene products of the *mre* region that function in formation of the rod shape of *Escherichia coli* cells. *Journal of Bacteriology* **170**(10):4619–4624.

[58] **Kruse, T.**, **Bork-Jensen, J.**, **Gerdes, K.** (2005) The morphogenetic MreBCD proteins of *Escherichia coli* form an essential membrane-bound complex. *Molecular Microbiology* **55**(1):78–89.

[59] **Garner, E.C.**, **Bernard, R.**, **Wang, W.**, **Zhuang, X.**, **Rudner, D.Z.**, **Mitchison, T.** (2011) Coupled, circumferential motions of the cell wall synthesis machinery and MreB filaments in *B. subtilis*. *Science* **333**(6039):222–225.

[60] **Domínguez-Escobar, J.**, **Chastanet, A.**, **Crevenna, A.H.**, **Fromion, V.**, **Wedlich-Söldner, R.**,

Carballido-López, R. (2011) Processive movement of MreB-associated cell wall biosynthetic complexes in bacteria. *Science* **333**(6039):225–228.

[61] **Van Teeffelen, S.**, **Wang, S.**, **Furchtgott, L.**, **Huang, K.C.**, **Wingreen, N.S.**, **Shaevitz, J.W.**, **Gitai, Z.** (2011) The bacterial actin MreB rotates, and rotation depends on cell-wall assembly. *Proceedings of the National Academy of Sciences* **108**(38):15822–15827.

[62] **Shiomi, D.**, **Sakai, M.**, **Niki, H.** (2008) Determination of bacterial rod shape by a novel cytoskeletal membrane protein. *The EMBO Journal* **27**(23):3081–3091.

[63] **Bendezu, F.O.**, **Hale, C.A.**, **Bernhardt, T.G.**, **de Boer, P.A.** (2009) RodZ (YfgA) is required for proper assembly of the MreB actin cytoskeleton and cell shape in *E. coli*. *The EMBO Journal* **28**(3):193–204.

[64] **Van Den Ent, F.**, **Leaver, M.**, **Bendezu, F.**, **Errington, J.**, **De Boer, P.**, **Löwe, J.** (2006) Dimeric structure of the cell shape protein MreC and its functional implications. *Molecular Microbiology* **62**(6):1631–1642.

[65] **Mohammadi, T.**, **Karczmarek, A.**, **Crouvoisier, M.**, **Bouhss, A.**, **Mengin-Lecreulx, D.**, **Den Blaauwen, T.** (2007) The essential peptidoglycan glycosyltransferase MurG forms a complex with proteins involved in lateral envelope growth as well as with proteins involved in cell division in *Escherichia coli*. *Molecular Microbiology* **65**(4):1106–1121.

[66] **Banzhaf, M.**, **van den Berg van Saparoea, B.**, **Terrak, M.**, **Fraipont, C.**, **Egan, A.**, **Philippe, J.**, **Zapun, A.**, **Breukink, E.**, **Nguyen-Distèche, M.**, **den Blaauwen, T.**, *et al.* (2012) Cooperativity of peptidoglycan synthases active in bacterial cell elongation. *Molecular Microbiology* **85**(1):179–194.

[67] **Ursell, T.S.**, **Nguyen, J.**, **Monds, R.D.**, **Colavin, A.**, **Billings, G.**, **Ouzounov, N.**, **Gitai, Z.**, **Shaevitz, J.W.**, **Huang, K.C.** (2014) Rod-like bacterial shape is maintained by feedback between cell curvature and cytoskeletal localization. *Proceedings of the National Academy of Sciences* **111**(11):E1025–E1034.

[68] **Morgenstein, R.M.**, **Bratton, B.P.**, **Nguyen, J.P.**, **Ouzounov, N.**, **Shaevitz, J.W.**, **Gitai, Z.** (2015) RodZ links MreB to cell wall synthesis to mediate MreB rotation and robust morphogenesis. *Proceedings of the National Academy of Sciences* **112**(40):12510–12515.

[69] **Randich, A.M.**, **Brun, Y.V.** (2015) Molecular mechanisms for the evolution of bacterial morphologies and growth modes. *Frontiers in Microbiology* **6**.

[70] **Kühn, J.**, **Briegel, A.**, **Mörschel, E.**, **Kahnt, J.**, **Leser, K.**, **Wick, S.**, **Jensen, G.J.**, **Thanbichler, M.** (2010) Bactofilins, a ubiquitous class of cytoskeletal proteins mediating polar local-

ization of a cell wall synthase in *Caulobacter crescentus*. *The EMBO Journal* **29**(2):327–339.

[71] **Cabeen, M.T.**, **Charbon, G.**, **Vollmer, W.**, **Born, P.**, **Ausmees, N.**, **Weibel, D.B.**, **Jacobs-Wagner, C.** (2009) Bacterial cell curvature through mechanical control of cell growth. *The EMBO Journal* **28**(9):1208–1219.

[72] **Ausmees, N.**, **Kuhn, J.R.**, **Jacobs-Wagner, C.** (2003) The bacterial cytoskeleton: an intermediate filament-like function in cell shape. *Cell* **115**(6):705–713.

[73] **Brown, P.J.**, **Hardy, G.G.**, **Trimble, M.J.**, **Brun, Y.V.** (2008) Complex regulatory pathways coordinate cell-cycle progression and development in *Caulobacter crescentus*. *Advances in Microbial Physiology* **54**:1–101.

[74] **Potluri, L.P.**, **Kannan, S.**, **Young, K.D.** (2012) ZipA is required for FtsZ-dependent preseptal peptidoglycan synthesis prior to invagination during cell division. *Journal of Bacteriology* **194**(19):5334–5342.

[75] **Aarsman, M.E.**, **Piette, A.**, **Fraipont, C.**, **Vinkenvleugel, T.M.**, **Nguyen-Distèche, M.**, **den Blaauwen, T.** (2005) Maturation of the *Escherichia coli* divisome occurs in two steps. *Molecular Microbiology* **55**(6):1631–1645.

[76] **Lutkenhaus, J.** (2007) Assembly dynamics of the bacterial MinCDE system and spatial regulation of the Z ring. *Annual Review of Biochemistry* **76**:539–562.

[77] **Marston, A.L.**, **Thomaides, H.B.**, **Edwards, D.H.**, **Sharpe, M.E.**, **Errington, J.** (1998) Polar localization of the MinD protein of *Bacillus subtilis* and its role in selection of the mid-cell division site. *Genes & Development* **12**(21):3419–30.

[78] **Hale, C.A.**, **Meinhardt, H.**, **de Boer, P.A.** (2001) Dynamic localization cycle of the cell division regulator MinE in *Escherichia coli*. *The EMBO Journal* **20**(7):1563–1572.

[79] **Fu, X.**, **Shih, Y.L.**, **Zhang, Y.**, **Rothfield, L.I.** (2001) The MinE ring required for proper placement of the division site is a mobile structure that changes its cellular location during the *Escherichia coli* division cycle. *Proceedings of the National Academy of Sciences* **98**(3):980–985.

[80] **Raskin, D.M.**, **de Boer, P.A.** (1999) Rapid pole-to-pole oscillation of a protein required for directing division to the middle of *Escherichia coli*. *Proceedings of the National Academy of Sciences* **96**(9):4971–4976.

[81] **Hu, Z.**, **Lutkenhaus, J.** (1999) Topological regulation of cell division in *Escherichia coli* involves rapid pole to pole oscillation of the division inhibitor MinC under the control of

MinD and MinE. *Molecular Microbiology* **34**(1):82–90.

[82] **Raskin, D.M.**, **de Boer, P.A.** (1999) MinDE-dependent pole-to-pole oscillation of division inhibitor MinC in *Escherichia coli*. *Journal of Bacteriology* **181**(20):6419–6424.

[83] **Wu, L.J.**, **Errington, J.** (2004) Coordination of cell division and chromosome segregation by a nucleoid occlusion protein in *Bacillus subtilis*. *Cell* **117**(7):915–925.

[84] **Bernhardt, T.G.**, **De Boer, P.A.** (2005) SlmA, a nucleoid-associated, FtsZ binding protein required for blocking septal ring assembly over chromosomes in *E. coli*. *Molecular Cell* **18**(5):555–564.

[85] **Thanbichler, M.**, **Shapiro, L.** (2006) MipZ, a spatial regulator coordinating chromosome segregation with cell division in *Caulobacter*. *Cell* **126**(1):147–162.

[86] **Kiekebusch, D.**, **Michie, K.A.**, **Essen, L.O.**, **Löwe, J.**, **Thanbichler, M.** (2012) Localized dimerization and nucleoid binding drive gradient formation by the bacterial cell division inhibitor MipZ. *Molecular Cell* **46**(3):245–259.

[87] **Gitai, Z.**, **Dye, N.**, **Shapiro, L.** (2004) An actin-like gene can determine cell polarity in bacteria. *Proceedings of the National Academy of Sciences* **101**(23):8643–8648.

[88] **Figge, R.M.**, **Divakaruni, A.V.**, **Gober, J.W.** (2004) MreB, the cell shape-determining bacterial actin homologue, co-ordinates cell wall morphogenesis in *Caulobacter crescentus*. *Molecular Microbiology* **51**(5):1321–1332.

[89] **Vollmer, W.**, **Bertsche, U.** (2008) Murein (peptidoglycan) structure, architecture and biosynthesis in *Escherichia coli*. *Biochimica et Biophysica Acta (BBA)-Biomembranes* **1778**(9):1714–1734.

[90] **Varma, A.**, **Young, K.D.** (2009) In *Escherichia coli*, MreB and FtsZ direct the synthesis of lateral cell wall via independent pathways that require PBP2. *Journal of Bacteriology* **191**(11):3526–3533.

[91] **Fenton, A.K.**, **Gerdes, K.** (2013) Direct interaction of FtsZ and MreB is required for septum synthesis and cell division in *Escherichia coli*. *The EMBO Journal* **32**(13):1953–65.

[92] **Pinho, M.G.**, **Kjos, M.**, **Veening, J.W.** (2013) How to get (a) round: mechanisms controlling growth and division of coccoid bacteria. *Nature Reviews Microbiology* **11**(9):601–614.

[93] **Erickson, H.P.** (1995) FtsZ, a prokaryotic homolog of tubulin? *Cell* **80**(3):367–370.

[94] **Rothfield, L.**, **Justice, S.**, **Garcia-Lara, J.** (1999) Bacterial cell division. *Annual Review of Genetics* **33**(1):423–448.

[95] **Vaughan, S.**, **Wickstead, B.**, **Gull, K.**, **Addinall, S.G.** (2004) Molecular evolution of FtsZ protein sequences encoded within the genomes of archaea, bacteria, and eukaryota. *Journal of Molecular Evolution* **58**(1):19–29.

[96] **Löwe, J.**, **Amos, L.A.** (1998) Crystal structure of the bacterial cell-division protein FtsZ. *Nature* **391**(6663):203–206.

[97] **RayChaudhuri, D.** (1999) ZipA is a MAP–Tau homolog and is essential for structural integrity of the cytokinetic FtsZ ring during bacterial cell division. *The EMBO Journal* **18**(9):2372–2383.

[98] **Hale, C.A.**, **Rhee, A.C.**, **De Boer, P.A.** (2000) ZipA-induced bundling of FtsZ polymers mediated by an interaction between C-terminal domains. *Journal of Bacteriology* **182**(18):5153–5166.

[99] **Hale, C.A.**, **de Boer, P.A.** (1997) Direct binding of FtsZ to ZipA, an essential component of the septal ring structure that mediates cell division in *E. coli*. *Cell* **88**(2):175–185.

[100] **Hale, C.A.**, **De Boer, P.A.** (2002) ZipA is required for recruitment of FtsK, FtsQ, FtsL, and FtsN to the septal ring in *Escherichia coli*. *Journal of Bacteriology* **184**(9):2552–2556.

[101] **van den Ent, F.**, **Löwe, J.** (2000) Crystal structure of the cell division protein FtsA from *Thermotoga maritima*. *The EMBO Journal* **19**(20):5300–5307.

[102] **Pichoff, S.**, **Lutkenhaus, J.** (2005) Tethering the Z ring to the membrane through a conserved membrane targeting sequence in FtsA. *Molecular Microbiology* **55**(6):1722–1734.

[103] **Pichoff, S.**, **Lutkenhaus, J.** (2002) Unique and overlapping roles for ZipA and FtsA in septal ring assembly in *Escherichia coli*. *The EMBO Journal* **21**(4):685–693.

[104] **Haney, S.A.**, **Glasfeld, E.**, **Hale, C.**, **Keeney, D.**, **He, Z.**, **de Boer, P.** (2001) Genetic Analysis of the *Escherichia coli* FtsZ· ZipA Interaction in the Yeast Two-hybrid System Characterization of FtsZ residues essential for the interactions with ZipA and with FtsA. *Journal of Biological Chemistry* **276**(15):11980–11987.

[105] **Szwedziak, P.**, **Wang, Q.**, **Freund, S.M.**, **Löwe, J.** (2012) FtsA forms actin-like protofilaments. *The EMBO Journal* **31**(10):2249–2260.

[106] **Krupka, M.**, **Rivas, G.**, **Rico, A.I.**, **Vicente, M.** (2012) Key role of two terminal do-

mains in the bidirectional polymerization of FtsA protein. *Journal of Biological Chemistry* **287**(10):7756–7765.

[107] **Busiek, K.K.**, **Eraso, J.M.**, **Wang, Y.**, **Margolin, W.** (2012) The early divisome protein FtsA interacts directly through its 1c subdomain with the cytoplasmic domain of the late divisome protein FtsN. *Journal of Bacteriology* **194**(8):1989–2000.

[108] **Rico, A.I.**, **García-Ovalle, M.**, **Mingorance, J.**, **Vicente, M.** (2004) Role of two essential domains of *Escherichia coli* FtsA in localization and progression of the division ring. *Molecular Microbiology* **53**(5):1359–1371.

[109] **Loose, M.**, **Mitchison, T.J.** (2014) The bacterial cell division proteins FtsA and FtsZ self-organize into dynamic cytoskeletal patterns. *Nature Cell Biology* **16**(1):38–46.

[110] **Möll, A.**, **Thanbichler, M.** (2009) FtsN-like proteins are conserved components of the cell division machinery in proteobacteria. *Molecular Microbiology* **72**(4):1037–1053.

[111] **Goley, E.D.**, **Yeh, Y.C.**, **Hong, S.H.**, **Fero, M.J.**, **Abeliuk, E.**, **McAdams, H.H.**, **Shapiro, L.** (2011) Assembly of the *Caulobacter* cell division machine. *Molecular Microbiology* **80**(6):1680–1698.

[112] **Goley, E.D.**, **Dye, N.A.**, **Werner, J.N.**, **Gitai, Z.**, **Shapiro, L.** (2010) Imaging-based identification of a critical regulator of FtsZ protofilament curvature in *Caulobacter*. *Molecular Cell* **39**(6):975–987.

[113] **Meier, E.L.**, **Razavi, S.**, **Inoue, T.**, **Goley, E.D.** (2016) A novel membrane anchor for FtsZ is linked to cell wall hydrolysis in *Caulobacter crescentus*. *Molecular Microbiology* **101**(2):265–80.

[114] **Gueiros-Filho, F.J.**, **Losick, R.** (2002) A widely conserved bacterial cell division protein that promotes assembly of the tubulin-like protein FtsZ. *Genes & Development* **16**(19):2544–2556.

[115] **Ebersbach, G.**, **Galli, E.**, **Møller-Jensen, J.**, **Löwe, J.**, **Gerdes, K.** (2008) Novel coiled-coil cell division factor ZapB stimulates Z ring assembly and cell division. *Molecular Microbiology* **68**(3):720–735.

[116] **Hale, C.A.**, **Shiomi, D.**, **Liu, B.**, **Bernhardt, T.G.**, **Margolin, W.**, **Niki, H.**, **de Boer, P.A.** (2011) Identification of *Escherichia coli* ZapC (YcbW) as a component of the division apparatus that binds and bundles FtsZ polymers. *Journal of Bacteriology* **193**(6):1393–1404.

[117] **Durand-Heredia, J.M.**, **Helen, H.Y.**, **De Carlo, S.**, **Lesser, C.F.**, **Janakiraman, A.** (2011)

Identification and characterization of ZapC, a stabilizer of the FtsZ ring in *Escherichia coli*. *Journal of Bacteriology* **193**(6):1405–1413.

[118] **Durand-Heredia, J.**, **Rivkin, E.**, **Fan, G.**, **Morales, J.**, **Janakiraman, A.** (2012) Identification of ZapD as a cell division factor that promotes the assembly of FtsZ in *Escherichia coli*. *Journal of Bacteriology* **194**(12):3189–3198.

[119] **Galli, E.**, **Gerdes, K.** (2010) Spatial resolution of two bacterial cell division proteins: ZapA recruits ZapB to the inner face of the Z-ring. *Molecular Microbiology* **76**(6):1514–1526.

[120] **Espéli, O.**, **Borne, R.**, **Dupaigne, P.**, **Thiel, A.**, **Gigant, E.**, **Mercier, R.**, **Boccard, F.** (2012) A MatP divisome-divisome interaction coordinates chromosome segregation with cell division in *E. coli*. *The EMBO Journal* **31**(14):3198–3211.

[121] **Marteyn, B.S.**, **Karimova, G.**, **Fenton, A.K.**, **Gazi, A.D.**, **West, N.**, **Touqui, L.**, **Prevost, M.C.**, **Betton, J.M.**, **Poyraz, O.**, **Ladant, D.**, *et al.* (2014) ZapE is a novel cell division protein interacting with FtsZ and modulating the Z-ring dynamics. *MBio* **5**(2):e00022–14.

[122] **Yang, D.C.**, **Peters, N.T.**, **Parzych, K.R.**, **Uehara, T.**, **Markovski, M.**, **Bernhardt, T.G.** (2011) An ATP-binding cassette transporter-like complex governs cell-wall hydrolysis at the bacterial cytokinetic ring. *Proceedings of the National Academy of Sciences* **108**(45):E1052–E1060.

[123] **Corbin, B.D.**, **Wang, Y.**, **Beuria, T.K.**, **Margolin, W.** (2007) Interaction between cell division proteins FtsE and FtsZ. *Journal of Bacteriology* **189**(8):3026–3035.

[124] **Ploeg, R.**, **Verheul, J.**, **Vischer, N.O.**, **Alexeeva, S.**, **Hoogendoorn, E.**, **Postma, M.**, **Banzhaf, M.**, **Vollmer, W.**, **Blaauwen, T.** (2013) Colocalization and interaction between elongasome and divisome during a preparative cell division phase in *Escherichia coli*. *Molecular Microbiology* **87**(5):1074–1087.

[125] **Buddelmeijer, N.**, **Beckwith, J.** (2004) A complex of the *Escherichia coli* cell division proteins FtsL, FtsB and FtsQ forms independently of its localization to the septal region. *Molecular Microbiology* **52**(5):1315–1327.

[126] **Gonzalez, M.D.**, **Akbay, E.A.**, **Boyd, D.**, **Beckwith, J.** (2010) Multiple interaction domains in FtsL, a protein component of the widely conserved bacterial FtsLBQ cell division complex. *Journal of Bacteriology* **192**(11):2757–2768.

[127] **Mercer, K.L.**, **Weiss, D.S.** (2002) The *Escherichia coli* cell division protein FtsW is required to recruit its cognate transpeptidase, FtsI (PBP3), to the division site. *Journal of Bacteriology* **184**(4):904–912.

[128] **Fraipont, C.**, **Alexeeva, S.**, **Wolf, B.**, **van der Ploeg, R.**, **Schloesser, M.**, **den Blaauwen, T.**, **Nguyen-Disteche, M.** (2011) The integral membrane FtsW protein and peptidoglycan synthase PBP3 form a subcomplex in *Escherichia coli*. *Microbiology* **157**(1):251–259.

[129] **Mohammadi, T.**, **van Dam, V.**, **Sijbrandi, R.**, **Vernet, T.**, **Zapun, A.**, **Bouhss, A.**, **Diepeveen-de Bruin, M.**, **Nguyen-Distèche, M.**, **de Kruijff, B.**, **Breukink, E.** (2011) Identification of FtsW as a transporter of lipid-linked cell wall precursors across the membrane. *The EMBO Journal* **30**(8):1425–1432.

[130] **Boyle, D.S.**, **Khattar, M.M.**, **Addinall, S.G.**, **Lutkenhaus, J.**, **Donachie, W.D.** (1997) *ftsW* is an essential cell-division gene in *Escherichia coli*. *Molecular Microbiology* **24**(6):1263–1273.

[131] **Sham, L.T.**, **Butler, E.K.**, **Lebar, M.D.**, **Kahne, D.**, **Bernhardt, T.G.**, **Ruiz, N.** (2014) MurJ is the flippase of lipid-linked precursors for peptidoglycan biogenesis. *Science* **345**(6193):220–222.

[132] **Meeske, A.J.**, **Sham, L.T.**, **Kimsey, H.**, **Koo, B.M.**, **Gross, C.A.**, **Bernhardt, T.G.**, **Rudner, D.Z.** (2015) MurJ and a novel lipid II flippase are required for cell wall biogenesis in *Bacillus subtilis*. *Proceedings of the National Academy of Sciences* **112**(20):6437–6442.

[133] **Meeske, A.J.**, **Riley, E.P.**, **Robins, W.P.**, **Uehara, T.**, **Mekelanos, J.J.**, **Kahne, D.**, **Walker, S.**, **Kruse, A.C.**, **Bernhardt, T.G.**, **Rudner, D.Z.** (2016) SEDS proteins are a widespread family of bacterial cell wall polymerases. *Nature* .

[134] **Addinall, S.G.**, **Cao, C.**, **Lutkenhaus, J.** (1997) FtsN, a late recruit to the septum in *Escherichia coli*. *Molecular Microbiology* **25**(2):303–309.

[135] **Di Lallo, G.**, **Fagioli, M.**, **Barionovi, D.**, **Ghelardini, P.**, **Paolozzi, L.** (2003) Use of a two-hybrid assay to study the assembly of a complex multicomponent protein machinery: bacterial septosome differentiation. *Microbiology* **149**(12):3353–3359.

[136] **Corbin, B.D.**, **Geissler, B.**, **Sadasivam, M.**, **Margolin, W.** (2004) Z-ring-independent interaction between a subdomain of FtsA and late septation proteins as revealed by a polar recruitment assay. *Journal of Bacteriology* **186**(22):7736–7744.

[137] **Tsang, M.J.**, **Bernhardt, T.G.** (2015) A role for the FtsQLB complex in cytokinetic ring activation revealed by an *ftsL* allele that accelerates division. *Molecular Microbiology* **95**(6):925–944.

[138] **Liu, B.**, **Persons, L.**, **Lee, L.**, **Boer, P.A.** (2015) Roles for both FtsA and the FtsBLQ subcomplex in FtsN-stimulated cell constriction in *Escherichia coli*. *Molecular Microbiology* **95**(6):945–970.

[139] **Yahashiri, A.**, **Jorgenson, M.A.**, **Weiss, D.S.** (2015) Bacterial SPOR domains are recruited to septal peptidoglycan by binding to glycan strands that lack stem peptides. *Proceedings of the National Academy of Sciences* **112**(36):11347–11352.

[140] **Haeusser, D.P.**, **Margolin, W.** (2016) Splitsville: structural and functional insights into the dynamic bacterial Z ring. *Nature Reviews Microbiology* .

[141] **Yang, J.C.**, **Van Den Ent, F.**, **Neuhaus, D.**, **Brevier, J.**, **Löwe, J.** (2004) Solution structure and domain architecture of the divisome protein FtsN. *Molecular Microbiology* **52**(3):651–660.

[142] **Busiek, K.K.**, **Margolin, W.** (2014) A role for FtsA in SPOR-independent localization of the essential *Escherichia coli* cell division protein FtsN. *Molecular Microbiology* **92**(6):1212–1226.

[143] **Gerding, M.A.**, **Liu, B.**, **Bendezú, F.O.**, **Hale, C.A.**, **Bernhardt, T.G.**, **de Boer, P.A.** (2009) Self-enhanced accumulation of FtsN at division sites and roles for other proteins with a SPOR domain (DamX, DedD, and RlpA) in *Escherichia coli* cell constriction. *Journal of Bacteriology* **191**(24):7383–7401.

[144] **Möll, A.** (2011) Anatomy of the divisome during late stages of cell division in the assymetric α-proteobacterium *Caulobacter crescentus*. Ph.D. thesis, Philipps Universität Marburg.

[145] **Derouaux, A.**, **Wolf, B.**, **Fraipont, C.**, **Breukink, E.**, **Nguyen-Distèche, M.**, **Terrak, M.** (2008) The monofunctional glycosyltransferase of *Escherichia coli* localizes to the cell division site and interacts with penicillin-binding protein 3, FtsW, and FtsN. *Journal of Bacteriology* **190**(5):1831–1834.

[146] **Karimova, G.**, **Dautin, N.**, **Ladant, D.** (2005) Interaction network among *Escherichia coli* membrane proteins involved in cell division as revealed by bacterial two-hybrid analysis. *Journal of Bacteriology* **187**(7):2233–2243.

[147] **Bernhardt, T.G.**, **De Boer, P.A.** (2003) The *Escherichia coli* amidase AmiC is a periplasmic septal ring component exported via the twin-arginine transport pathway. *Molecular Microbiology* **48**(5):1171–1182.

[148] **Yeh, Y.C.**, **Comolli, L.R.**, **Downing, K.H.**, **Shapiro, L.**, **McAdams, H.H.** (2010) The *Caulobacter* Tol-Pal complex is essential for outer membrane integrity and the positioning of a polar localization factor. *Journal of Bacteriology* **192**(19):4847–4858.

[149] **Gerding, M.A.**, **Ogata, Y.**, **Pecora, N.D.**, **Niki, H.**, **De Boer, P.A.** (2007) The trans-envelope Tol–Pal complex is part of the cell division machinery and required for proper

outer-membrane invagination during cell constriction in *E. coli*. *Molecular Microbiology* **63**(4):1008–1025.

[150] **Möll, A.**, **Schlimpert, S.**, **Briegel, A.**, **Jensen, G.J.**, **Thanbichler, M.** (2010) DipM, a new factor required for peptidoglycan remodelling during cell division in *Caulobacter crescentus*. *Molecular Microbiology* **77**(1):90–107.

[151] **Poggio, S.**, **Takacs, C.N.**, **Vollmer, W.**, **Jacobs-Wagner, C.** (2010) A protein critical for cell constriction in the Gram-negative bacterium *Caulobacter crescentus* localizes at the division site through its peptidoglycan-binding LysM domains. *Molecular Microbiology* **77**(1):74–89.

[152] **Goley, E.D.**, **Comolli, L.R.**, **Fero, K.E.**, **Downing, K.H.**, **Shapiro, L.** (2010) DipM links peptidoglycan remodelling to outer membrane organization in *Caulobacter*. *Molecular Microbiology* **77**(1):56–73.

[153] **Yu, X.c.**, **Tran, A.H.**, **Sun, Q.**, **Margolin, W.** (1998) Localization of cell division protein FtsK to the *Escherichia coli* septum and identification of a potential N-terminal targeting domain. *Journal of Bacteriology* **180**(5):1296–1304.

[154] **Liu, G.**, **Draper, G.C.**, **Donachie, W.** (1998) FtsK is a bifunctional protein involved in cell division and chromosome localization in *Escherichia coli*. *Molecular Microbiology* **29**(3):893–903.

[155] **Wang, L.**, **Lutkenhaus, J.** (1998) FtsK is an essential cell division protein that is localized to the septum and induced as part of the SOS response. *Molecular Microbiology* **29**(3):731–740.

[156] **Dubarry, N.**, **Possoz, C.**, **Barre, F.X.** (2010) Multiple regions along the *Escherichia coli* FtsK protein are implicated in cell division. *Molecular Microbiology* **78**(5):1088–1100.

[157] **Massey, T.H.**, **Mercogliano, C.P.**, **Yates, J.**, **Sherratt, D.J.**, **Löwe, J.** (2006) Double-stranded DNA translocation: structure and mechanism of hexameric FtsK. *Molecular Cell* **23**(4):457–469.

[158] **Aussel, L.**, **Barre, F.X.**, **Aroyo, M.**, **Stasiak, A.**, **Stasiak, A.Z.**, **Sherratt, D.** (2002) FtsK is a DNA motor protein that activates chromosome dimer resolution by switching the catalytic state of the XerC and XerD recombinases. *Cell* **108**(2):195–205.

[159] **Sivanathan, V.**, **Allen, M.D.**, **de Bekker, C.**, **Baker, R.**, **Arciszewska, L.K.**, **Freund, S.M.**, **Bycroft, M.**, **Löwe, J.**, **Sherratt, D.J.** (2006) The FtsK γ domain directs oriented DNA translocation by interacting with KOPS. *Nature Structural & Molecular Biology* **13**(11):965–972.

[160] **Bigot, S.**, **Saleh, O.A.**, **Cornet, F.**, **Allemand, J.F.**, **Barre, F.X.** (2006) Oriented loading of FtsK on KOPS. *Nature Structural & Molecular Biology* **13**(11):1026–1028.

[161] **Löwe, J.**, **Ellonen, A.**, **Allen, M.D.**, **Atkinson, C.**, **Sherratt, D.J.**, **Grainge, I.** (2008) Molecular mechanism of sequence-directed DNA loading and translocation by FtsK. *Molecular Cell* **31**(4):498–509.

[162] **Levy, O.**, **Ptacin, J.L.**, **Pease, P.J.**, **Gore, J.**, **Eisen, M.B.**, **Bustamante, C.**, **Cozzarelli, N.R.** (2005) Identification of oligonucleotide sequences that direct the movement of the *Escherichia coli* FtsK translocase. *Proceedings of the National Academy of Sciences* **102**(49):17618–17623.

[163] **Bigot, S.**, **Saleh, O.A.**, **Lesterlin, C.**, **Pages, C.**, **El Karoui, M.**, **Dennis, C.**, **Grigoriev, M.**, **Allemand, J.F.**, **Barre, F.X.**, **Cornet, F.** (2005) KOPS: DNA motifs that control *E. coli* chromosome segregation by orienting the FtsK translocase. *The EMBO Journal* **24**(21):3770–3780.

[164] **Graham, J.E.**, **Sherratt, D.J.**, **Szczelkun, M.D.** (2010) Sequence-specific assembly of FtsK hexamers establishes directional translocation on DNA. *Proceedings of the National Academy of Sciences* **107**(47):20263–20268.

[165] **Lesterlin, C.**, **Pages, C.**, **Dubarry, N.**, **Dasgupta, S.**, **Cornet, F.** (2008) Asymmetry of chromosome Replichores renders the DNA translocase activity of FtsK essential for cell division and cell shape maintenance in *Escherichia coli*. *PLoS Genetics* **4**(12):e1000288.

[166] **Blakely, G.**, **May, G.**, **McCulloch, R.**, **Arciszewska, L.K.**, **Burke, M.**, **Lovett, S.T.**, **Sherratt, D.J.** (1993) Two related recombinases are required for site-specific recombination at *dif* and *cer* in *E. coli* K12. *Cell* **75**(2):351–361.

[167] **Blakely, G.**, **Colloms, S.**, **May, G.**, **Burke, M.**, **Sherratt, D.** (1991) *Escherichia coli* XerC recombinase is required for chromosomal segregation at cell division. *The New Biologist* **3**(8):789–798.

[168] **Kuempel, P.**, **Henson, J.**, **Dircks, L.**, **Tecklenburg, M.**, **Lim, D.** (1991) *dif*, a *recA*-independent recombination site in the terminus region of the chromosome of *Escherichia coli*. *The New Biologist* **3**(8):799–811.

[169] **Steiner, W.W.**, **Kuempel, P.L.** (1998) Sister chromatid exchange frequencies in *Escherichia coli* analyzed by recombination at the *dif* resolvase site. *Journal of Bacteriology* **180**(23):6269–6275.

[170] **Hendricks, E.C.**, **Szerlong, H.**, **Hill, T.**, **Kuempel, P.** (2000) Cell division, guillotining of dimer chromosomes and SOS induction in resolution mutants (*dif, xerC and xerD*) of *Es-*

cherichia coli. *Molecular Microbiology* **36**(4):973–981.

[171] **Yates, J.**, **Zhekov, I.**, **Baker, R.**, **Eklund, B.**, **Sherratt, D.J.**, **Arciszewska, L.K.** (2006) Dissection of a functional interaction between the DNA translocase, FtsK, and the XerD recombinase. *Molecular Microbiology* **59**(6):1754–1766.

[172] **Grainge, I.**, **Lesterlin, C.**, **Sherratt, D.J.** (2011) Activation of XerCD-*dif* recombination by the FtsK DNA translocase. *Nucleic Acids Research* **39**(12):5140–5148.

[173] **Bigot, S.**, **Marians, K.J.** (2010) DNA chirality-dependent stimulation of topoisomerase IV activity by the C-terminal AAA+ domain of FtsK. *Nucleic Acids Research* :gkp1243.

[174] **Espeli, O.**, **Lee, C.**, **Marians, K.J.** (2003) A physical and functional interaction between *Escherichia coli* FtsK and topoisomerase IV. *Journal of Biological Chemistry* **278**(45):44639–44644.

[175] **Besprozvannaya, M.**, **Burton, B.M.** (2014) Do the same traffic rules apply? Directional chromosome segregation by SpoIIIE and FtsK. *Molecular Microbiology* **93**(4):599–608.

[176] **Thanbichler, M.** (2010) Synchronization of chromosome dynamics and cell division in bacteria. *Cold Spring Harbor Perspectives in Biology* **2**(1):a000331.

[177] **Reyes-Lamothe, R.**, **Nicolas, E.**, **Sherratt, D.J.** (2012) Chromosome replication and segregation in bacteria. *Annual Review of Genetics* **46**:121–143.

[178] **Dupaigne, P.**, **Tonthat, N.K.**, **Espéli, O.**, **Whitfill, T.**, **Boccard, F.**, **Schumacher, M.A.** (2012) Molecular basis for a protein-mediated DNA-bridging mechanism that functions in condensation of the *E. coli* chromosome. *Molecular Cell* **48**(4):560–571.

[179] **Mercier, R.**, **Petit, M.A.**, **Schbath, S.**, **Robin, S.**, **El Karoui, M.**, **Boccard, F.**, **Espéli, O.** (2008) The MatP/*matS* site-specific system organizes the terminus region of the *E. coli* chromosome into a macrodomain. *Cell* **135**(3):475–485.

[180] **Klein, K.E.** (2008) Die Rolle der Klasse A Penicillin-Bindeproteine bei der Morphogenese von *Caulobacter crescentus*. Diplomarbeit, Philipps Universität Marburg.

[181] **McGrath, P.T.**, **Lee, H.**, **Zhang, L.**, **Iniesta, A.A.**, **Hottes, A.K.**, **Tan, M.H.**, **Hillson, N.J.**, **Hu, P.**, **Shapiro, L.**, **McAdams, H.H.** (2007) High-throughput identification of transcription start sites, conserved promoter motifs and predicted regulons. *Nature Biotechnology* **25**(5):584–592.

[182] **Strobel, W.**, **Möll, A.**, **Kiekebusch, D.**, **Klein, K.E.**, **Thanbichler, M.** (2014) Function and

localization dynamics of bifunctional penicillin-binding proteins in *Caulobacter crescentus*. *Journal of Bacteriology* **196**(8):1627–1639.

[183] **Yakhnina, A.A.**, **Gitai, Z.** (2013) Diverse functions for six glycosyltransferases in *Caulobacter crescentus* cell wall assembly. *Journal of Bacteriology* **195**(19):4527–4535.

[184] **Miyawaki, A.**, **Sawano, A.**, **Kogure, T.** (2003) Lighting up cells: labelling proteins with fluorophores. *Nature Cell Biology* .

[185] **Lippincott-Schwartz, J.**, **Snapp, E.**, **Kenworthy, A.** (2001) Studying protein dynamics in living cells. *Nature Reviews Molecular Cell Biology* **2**(6):444–456.

[186] **Rudner, D.Z.**, **Losick, R.** (2010) Protein subcellular localization in bacteria. *Cold Spring Harbor Perspectives in Biology* **2**(4):a000307.

[187] **Wang, Y.**, **Jones, B.D.**, **Brun, Y.V.** (2001) A set of *ftsZ* mutants blocked at different stages of cell division in *Caulobacter*. *Molecular Microbiology* **40**(2):347–360.

[188] **Müller, P.**, **Ewers, C.**, **Bertsche, U.**, **Anstett, M.**, **Kallis, T.**, **Breukink, E.**, **Fraipont, C.**, **Terrak, M.**, **Nguyen-Distèche, M.**, **Vollmer, W.** (2007) The essential cell division protein FtsN interacts with the murein (peptidoglycan) synthase PBP1B in *Escherichia coli*. *Journal of Biological chemistry* **282**(50):36394–36402.

[189] **Fenton, A.K.**, **Gerdes, K.** (2013) Direct interaction of FtsZ and MreB is required for septum synthesis and cell division in *Escherichia coli*. *The EMBO Journal* **32**(13):1953–65.

[190] **Bertsche, U.**, **Kast, T.**, **Wolf, B.**, **Fraipont, C.**, **Aarsman, M.E.**, **Kannenberg, K.**, **Von Rechenberg, M.**, **Nguyen-Distèche, M.**, **Den Blaauwen, T.**, **Höltje, J.V.**, *et al.* (2006) Interaction between two murein (peptidoglycan) synthases, PBP3 and PBP1B, in *Escherichia coli*. *Molecular Microbiology* **61**(3):675–690.

[191] **Yousif, S.Y.**, **Broome-Smith, J.K.**, **Spratt, B.G.** (1985) Lysis of *Escherichia coli* by β-Lactam Antibiotics: Deletion analysis of the role of penicillin-binding proteins 1A and 1B. *Microbiology* **131**(10):2839–2845.

[192] **Karimova, G.**, **Pidoux, J.**, **Ullmann, A.**, **Ladant, D.** (1998) A bacterial two-hybrid system based on a reconstituted signal transduction pathway. *Proceedings of the National Academy of Sciences* **95**(10):5752–5756.

[193] **Charpentier, X.**, **Chalut, C.**, **Rémy, M.H.**, **Masson, J.M.** (2002) Penicillin-binding proteins 1a and 1b form independent dimers in *Escherichia coli*. *Journal of Bacteriology* **184**(13):3749–3752.

[194] **Robichon, C.**, **Karimova, G.**, **Beckwith, J.**, **Ladant, D.** (2011) Role of leucine zipper motifs in association of the *Escherichia coli* cell division proteins FtsL and FtsB. *Journal of Bacteriology* **193**(18):4988–4992.

[195] **Radhakrishnan, S.K.**, **Thanbichler, M.**, **Viollier, P.H.** (2008) The dynamic interplay between a cell fate determinant and a lysozyme homolog drives the asymmetric division cycle of *Caulobacter crescentus*. *Genes & Development* **22**(2):212–225.

[196] **Quon, K.C.**, **Marczynski, G.T.**, **Shapiro, L.** (1996) Cell cycle control by an essential bacterial two-component signal transduction proteins. *Cell* **84**(1):83–93.

[197] **West, L.**, **Yang, D.**, **Stephens, C.** (2002) Use of the *Caulobacter crescentus* genome sequence to develop a method for systematic genetic mapping. *Journal of Bacteriology* **184**(8):2155–2166.

[198] **Jensen, R.B.** (2006) Analysis of the terminus region of the *Caulobacter crescentus* chromosome and identification of the *dif* site. *Journal of Bacteriology* **188**(16):6016–6019.

[199] **Colloms, S.**, **Sykora, P.**, **Szatmari, G.**, **Sherratt, D.** (1990) Recombination at ColE1 *cer* requires the *Escherichia coli xerC* gene product, a member of the lambda integrase family of site-specific recombinases. *Journal of Bacteriology* **172**(12):6973–6980.

[200] **Geissler, B.**, **Margolin, W.** (2005) Evidence for functional overlap among multiple bacterial cell division proteins: compensating for the loss of FtsK. *Molecular Microbiology* **58**(2):596–612.

[201] **Shibata, T.**, **DasGupta, C.**, **Cunningham, R.P.**, **Radding, C.M.** (1979) Purified *Escherichia coli recA* protein catalyzes homologous pairing of superhelical DNA and single-stranded fragments. *Proceedings of the National Academy of Sciences* **76**(4):1638–1642.

[202] **Cassuto, E.**, **West, S.C.**, **Mursalim, J.**, **Conlon, S.**, **Howard-Flanders, P.** (1980) Initiation of genetic recombination: homologous pairing between duplex DNA molecules promoted by *recA* protein. *Proceedings of the National Academy of Sciences* **77**(7):3962–3966.

[203] **McEntee, K.**, **Weinstock, G.**, **Lehman, I.** (1979) Initiation of general recombination catalyzed in vitro by the *recA* protein of *Escherichia coli*. *Proceedings of the National Academy of Sciences* **76**(6):2615–2619.

[204] **Pérals, K.**, **Capiaux, H.**, **Vincourt, J.B.**, **Louarn, J.M.**, **Sherratt, D.J.**, **Cornet, F.** (2001) Interplay between recombination, cell division and chromosome structure during chromosome dimer resolution in *Escherichia coli*. *Molecular Microbiology* **39**(4):904–913.

[205] **O'Neill, E.A.**, **Hynes, R.H.**, **Bender, R.A.** (1985) Recombination deficient mutant of *Caulobacter crescentus*. *Molecular and General Genetics MGG* **198**(2):275–278.

[206] **Lau, I.F.**, **Filipe, S.R.**, **Søballe, B.**, **Økstad, O.A.**, **Barre, F.X.**, **Sherratt, D.J.** (2003) Spatial and temporal organization of replicating *Escherichia coli* chromosomes. *Molecular Microbiology* **49**(3):731–743.

[207] **Viollier, P.H.**, **Thanbichler, M.**, **McGrath, P.T.**, **West, L.**, **Meewan, M.**, **McAdams, H.H.**, **Shapiro, L.** (2004) Rapid and sequential movement of individual chromosomal loci to specific subcellular locations during bacterial DNA replication. *Proceedings of the National Academy of Sciences* **101**(25):9257–9262.

[208] **Malakhov, M.P.**, **Mattern, M.R.**, **Malakhova, O.A.**, **Drinker, M.**, **Weeks, S.D.**, **Butt, T.R.** (2004) SUMO fusions and SUMO-specific protease for efficient expression and purification of proteins. *Journal of Structural and Functional Genomics* **5**(1-2):75–86.

[209] **Mason, J.M.**, **Arndt, K.M.** (2004) Coiled coil domains: stability, specificity, and biological implications. *ChemBioChem* **5**(2):170–176.

[210] **Crick, F.H.** (1953) The Fourier transform of a coiled-coil. *Acta Crystallographica* **6**(8-9):685–689.

[211] **Glover, J.M.**, **Harrison, S.C.** (1995) Crystal structure of the heterodimeric bZIP transcription factor c-Fos–c-Jun bound to DNA. *Nature* .

[212] **Zhang, Y.** (2008) I-TASSER server for protein 3D structure prediction. *BMC Bioinformatics* **9**(1):40.

[213] **Yang, J.**, **Yan, R.**, **Roy, A.**, **Xu, D.**, **Poisson, J.**, **Zhang, Y.** (2015) The I-TASSER Suite: protein structure and function prediction. *Nature Methods* **12**(1):7–8.

[214] **Roy, A.**, **Kucukural, A.**, **Zhang, Y.** (2010) I-TASSER: a unified platform for automated protein structure and function prediction. *Nature Protocols* **5**(4):725–738.

[215] **Kato, J.i.**, **Suzuki, H.**, **Hirota, Y.** (1985) Dispensability of either penicillin-binding protein -1a or -1b involved in the essential process for cell elongation in *Escherichia coli*. *Molecular and General Genetics MGG* **200**(2):272–277.

[216] **Weiss, D.S.** (2015) Last but not least: new insights into how FtsN triggers constriction during *Escherichia coli* cell division. *Molecular Microbiology* **95**(6):903–909.

[217] **Laub, M.T.**, **McAdams, H.H.**, **Feldblyum, T.**, **Fraser, C.M.**, **Shapiro, L.** (2000) Global anal-

ysis of the genetic network controlling a bacterial cell cycle. *Science* **290**(5499):2144–2148.

[218] **Simm, A.M.**, **Higgins, C.S.**, **Pullan, S.T.**, **Avison, M.B.**, **Niumsup, P.**, **Erdozain, O.**, **Bennett, P.M.**, **Walsh, T.R.** (2001) A novel metallo-β-lactamase, Mbl1b, produced by the environmental bacterium *Caulobacter crescentus*. *FEBS Letters* **509**(3):350–354.

[219] **Hocking, J.**, **Priyadarshini, R.**, **Takacs, C.N.**, **Costa, T.**, **Dye, N.A.**, **Shapiro, L.**, **Vollmer, W.**, **Jacobs-Wagner, C.** (2012) Osmolality-dependent relocation of penicillin-binding protein PBP2 to the division site in *Caulobacter crescentus*. *Journal of Bacteriology* **194**(12):3116–3127.

[220] **Dye, N.A.**, **Pincus, Z.**, **Theriot, J.A.**, **Shapiro, L.**, **Gitai, Z.** (2005) Two independent spiral structures control cell shape in *Caulobacter*. *Proceedings of the National Academy of Sciences* **102**(51):18608–18613.

[221] **Divakaruni, A.V.**, **Loo, R.R.O.**, **Xie, Y.**, **Loo, J.A.**, **Gober, J.W.** (2005) The cell-shape protein MreC interacts with extracytoplasmic proteins including cell wall assembly complexes in *Caulobacter crescentus*. *Proceedings of the National Academy of Sciences* **102**(51):18602–18607.

[222] **Schiffer, G.**, **Höltje, J.V.** (1999) Cloning and characterization of PBP1C, a third member of the multimodular class A penicillin-binding proteins of *Escherichia coli*. *Journal of Biological Chemistry* **274**(45):32031–32039.

[223] **Vollmer, W.**, **von Rechenberg, M.**, **Höltje, J.V.** (1999) Demonstration of molecular interactions between the murein polymerase PBP1B, the lytic transglycosylase MltA, and the scaffolding protein MipA of *Escherichia coli*. *Journal of Biological Chemistry* **274**(10):6726–6734.

[224] **Paradis-Bleau, C.**, **Markovski, M.**, **Uehara, T.**, **Lupoli, T.J.**, **Walker, S.**, **Kahne, D.E.**, **Bernhardt, T.G.** (2010) Lipoprotein cofactors located in the outer membrane activate bacterial cell wall polymerases. *Cell* **143**(7):1110–1120.

[225] **Typas, A.**, **Banzhaf, M.**, **van Saparoea, B.v.d.B.**, **Verheul, J.**, **Biboy, J.**, **Nichols, R.J.**, **Zietek, M.**, **Beilharz, K.**, **Kannenberg, K.**, **von Rechenberg, M.**, *et al.* (2010) Regulation of peptidoglycan synthesis by outer-membrane proteins. *Cell* **143**(7):1097–1109.

[226] **Markovski, M.**, **Bohrhunter, J.L.**, **Lupoli, T.J.**, **Uehara, T.**, **Walker, S.**, **Kahne, D.E.**, **Bernhardt, T.G.** (2016) Cofactor bypass variants reveal a conformational control mechanism governing cell wall polymerase activity. *Proceedings of the National Academy of Sciences* **113**(17):4788–4793.

[227] **Lupoli, T.J.**, **Lebar, M.D.**, **Markovski, M.**, **Bernhardt, T.**, **Kahne, D.**, **Walker, S.** (2013) Lipoprotein activators stimulate *Escherichia coli* penicillin-binding proteins by different mechanisms. *Journal of the American Chemical Society* **136**(1):52–55.

[228] **Mercer, R.G.**, **Callister, S.J.**, **Lipton, M.S.**, **Pasa-Tolic, L.**, **Strnad, H.**, **Paces, V.**, **Beatty, J.T.**, **Lang, A.S.** (2010) Loss of the response regulator CtrA causes pleiotropic effects on gene expression but does not affect growth phase regulation in *Rhodobacter capsulatus*. *Journal of Bacteriology* **192**(11):2701–2710.

[229] **Buttigieg, P.L.**, **Hankeln, W.**, **Kostadinov, I.**, **Kottmann, R.**, **Yilmaz, P.**, **Duhaime, M.B.**, **Glöckner, F.O.** (2013) Ecogenomic perspectives on domains of unknown function: correlation-based exploration of marine metagenomes. *PloS One* **8**(3):e50869.

[230] **Narayanan, S.**, **Janakiraman, B.**, **Kumar, L.**, **Radhakrishnan, S.K.** (2015) A cell cycle-controlled redox switch regulates the topoisomerase IV activity. *Genes & Development* **29**(11):1175–1187.

[231] **Ptacin, J.L.**, **Lee, S.F.**, **Garner, E.C.**, **Toro, E.**, **Eckart, M.**, **Comolli, L.R.**, **Moerner, W.**, **Shapiro, L.** (2010) A spindle-like apparatus guides bacterial chromosome segregation. *Nature Cell Biology* **12**(8):791–798.

[232] **Goehring, N.W.**, **Beckwith, J.** (2005) Diverse paths to midcell: assembly of the bacterial cell division machinery. *Current Biology* **15**(13):R514–R526.

[233] **Harry, E.**, **Monahan, L.**, **Thompson, L.** (2006) Bacterial cell division: the mechanism and its precison. *International Review of Cytology* **253**:27–94.

[234] **Wang, S.C.**, **West, L.**, **Shapiro, L.** (2006) The bifunctional FtsK protein mediates chromosome partitioning and cell division in *Caulobacter*. *Journal of Bacteriology* **188**(4):1497–1508.

[235] **Radhakrishnan, S.K.**, **Pritchard, S.**, **Viollier, P.H.** (2010) Coupling prokaryotic cell fate and division control with a bifunctional and oscillating oxidoreductase homolog. *Developmental Cell* **18**(1):90–101.

[236] **Baba, T.**, **Ara, T.**, **Hasegawa, M.**, **Takai, Y.**, **Okumura, Y.**, **Baba, M.**, **Datsenko, K.A.**, **Tomita, M.**, **Wanner, B.L.**, **Mori, H.** (2006) Construction of *Escherichia coli* K-12 in-frame, single-gene knockout mutants: the Keio collection. *Molecular Systems Biology* **2**(1).

[237] **Aravind, L.**, **Ponting, C.P.** (1997) The GAF domain: an evolutionary link between diverse phototransducing proteins. *Trends in Biochemical Sciences* **22**(12):458–459.

[238] **Joerger, R.D.**, **Jacobson, M.R.**, **Bishop, P.E.** (1989) Two *nifA*-like genes required for expression of alternative nitrogenases by *Azotobacter vinelandii*. *Journal of Bacteriology* **171**(6):3258–3267.

[239] **Kanacher, T.**, **Schultz, A.**, **Linder, J.U.**, **Schultz, J.E.** (2002) A GAF-domain-regulated adenylyl cyclase from *Anabaena* is a self-activating cAMP switch. *The EMBO Journal* **21**(14):3672–3680.

[240] **Bramkamp, M.**, **Emmins, R.**, **Weston, L.**, **Donovan, C.**, **Daniel, R.A.**, **Errington, J.** (2008) A novel component of the division-site selection system of *Bacillus subtilis* and a new mode of action for the division inhibitor MinCD. *Molecular Microbiology* **70**(6):1556–1569.

[241] **De Boer, P.**, **Crossley, R.E.**, **Rothfield, L.I.** (1992) Roles of MinC and MinD in the site-specific septation block mediated by the MinCDE system of *Escherichia coli*. *Journal of Bacteriology* **174**(1):63–70.

[242] **Little, J.W.** (1991) Mechanism of specific LexA cleavage: autodigestion and the role of RecA coprotease. *Biochimie* **73**(4):411–21.

[243] **Erill, I.**, **Campoy, S.**, **Barbé, J.** (2007) Aeons of distress: an evolutionary perspective on the bacterial SOS response. *FEMS Microbiology Reviews* **31**(6):637–56.

[244] **Huisman, O.**, **D'Ari, R.** (1981) An inducible DNA replication-cell division coupling mechanism in *E. coli*. *Nature* **290**(5809):797–799.

[245] **Mukherjee, A.**, **Cao, C.**, **Lutkenhaus, J.** (1998) Inhibition of FtsZ polymerization by SulA, an inhibitor of septation in *Escherichia coli*. *Proceedings of the National Academy of Sciences* **95**(6):2885–90.

[246] **Modell, J.W.**, **Hopkins, A.C.**, **Laub, M.T.** (2011) A DNA damage checkpoint in *Caulobacter crescentus* inhibits cell division through a direct interaction with FtsW. *Genes & Development* **25**(12):1328–43.

[247] **Modell, J.W.**, **Kambara, T.K.**, **Perchuk, B.S.**, **Laub, M.T.** (2014) A DNA damage-induced, SOS-independent checkpoint regulates cell division in *Caulobacter crescentus*. *PLoS Biology* **12**(10):e1001977.

[248] **Geissler, B.**, **Shiomi, D.**, **Margolin, W.** (2007) The *ftsA** gain-of-function allele of *Escherichia coli* and its effects on the stability and dynamics of the Z ring. *Microbiology* **153**(3):814–825.

[249] **Ausubel, F.M.** (1988) Current protocols in molecular biology. *Greene Pub Associates, Wiley-Interscience* :New York.

[250] **Sambrook, J.**, **Fritsch, E.F.**, **Maniatis, T.** (1989) Molecular cloning: a laboratory manual. *Cold Spring Harbor Laboratory Press* :Cold Spring Harbor, N.Y.

[251] **Miller, J.H.** (1972) Experiments in molecular genetics. *Cold Spring Harbor Laboratory Press* :Cold Spring Harbor, N.Y.

[252] **Ely, B.** (1990) Genetics of *Caulobacter crescentus*. *Methods in Enzymology* **204**:372–384.

[253] **Ueki, T.**, **Inouye, S.**, **Inouye, M.** (1996) Positive-negative KG cassettes for construction of multi-gene deletions using a single drug marker. *Gene* **183**(1):153–157.

[254] **Tivol, W.F.**, **Briegel, A.**, **Jensen, G.J.** (2008) An improved cryogen for plunge freezing. *Microscopy and Microanalysis* **14**(05):375–379.

[255] **Zheng, S.Q.**, **Keszthelyi, B.**, **Branlund, E.**, **Lyle, J.M.**, **Braunfeld, M.B.**, **Sedat, J.W.**, **Agard, D.A.** (2007) UCSF tomography: an integrated software suite for real-time electron microscopic tomographic data collection, alignment, and reconstruction. *Journal of Structural Biology* **157**(1):138–147.

[256] **Kremer, J.R.**, **Mastronarde, D.N.**, **McIntosh, J.R.** (1996) Computer visualization of three-dimensional image data using IMOD. *Journal of Structural Biology* **116**(1):71–76.

[257] **Lämmli, U.K.** (1970) Cleavage of structural proteins during the assembly of the head of bacteriophage T4. *Nature* **227**:680–685.

[258] **Domian, I.J.**, **Quon, K.C.**, **Shapiro, L.** (1997) Cell type-specific phosphorylation and proteolysis of a transcriptional regulator controls the G1-to-S transition in a bacterial cell cycle. *Cell* **90**(3):415–424.

[259] **Mohl, D.A.**, **Easter, Jr, J.**, **Gober, J.W.** (2001) The chromosome partitioning protein, ParB, is required for cytokinesis in *Caulobacter crescentus*. *Molecular Microbiology* **42**(3):741–55.

[260] **Strobel, W.** (2012) Funktionelle Charakterisierung der Klasse A Penicillin-Bindeproteine in *Caulobacter crescentus*. Master's thesis, Philipps Universität Marburg.

[261] **Pruitt, K.D.**, **Tatusova, T.**, **Maglott, D.R.** (2007) NCBI reference sequences (RefSeq): a curated non-redundant sequence database of genomes, transcripts and proteins. *Nucleic Acids Research* **35**(suppl 1):D61–D65.

[262] **Keilberg, D.**, **Wuichet, K.**, **Drescher, F.**, **Søgaard-Andersen, L.** (2012) A response regulator interfaces between the Frz chemosensory system and the MglA/MglB GTPase/GAP module to regulate polarity in *Myxococcus xanthus*. *PLoS Genetics* **8**(9):e1002951.

[263] **Finn, R.D.**, **Mistry, J.**, **Tate, J.**, **Coggill, P.**, **Heger, A.**, **Pollington, J.E.**, **Gavin, O.L.**, **Gunasekaran, P.**, **Ceric, G.**, **Forslund, K.**, *et al.* (2010) The Pfam protein families database. *Nucleic Acids Research* **38**(suppl 1):D211–D222.

[264] **Punta, M.**, **Coggill, P.**, **Eberhardt, R.**, **Mistry, J.**, **Tate, J.**, **Boursnell, C.**, **Pang, N.**, **Forslund, K.**, **Ceric, G.**, **Clements, J.**, *et al.* (2012) The Pfam protein families database Nucleic Acids Res. 40. *D290–D301 Atom-1 Force Constant Equilibrium Atom-2 Residue Atom (kcal· mol- 1· Å- 2) Distance (Å) Residue Atom Y* **397**.

[265] **Camacho, C.**, **Coulouris, G.**, **Avagyan, V.**, **Ma, N.**, **Papadopoulos, J.**, **Bealer, K.**, **Madden, T.L.** (2009) BLAST+: architecture and applications. *BMC Bioinformatics* **10**(1):1.

[266] **Katoh, K.**, **Kuma, K.i.**, **Toh, H.**, **Miyata, T.** (2005) MAFFT version 5: improvement in accuracy of multiple sequence alignment. *Nucleic Acids Research* **33**(2):511–518.

[267] **Castresana, J.** (2000) Selection of conserved blocks from multiple alignments for their use in phylogenetic analysis. *Molecular Biology and Evolution* **17**(4):540–552.

[268] **Price, M.N.**, **Dehal, P.S.**, **Arkin, A.P.** (2010) FastTree 2–approximately maximum-likelihood trees for large alignments. *PloS One* **5**(3):e9490.

[269] **Guindon, S.**, **Gascuel, O.** (2003) A simple, fast, and accurate algorithm to estimate large phylogenies by maximum likelihood. *Systematic Biology* **52**(5):696–704.

[270] **Letunic, I.**, **Bork, P.** (2007) Interactive Tree Of Life (iTOL): an online tool for phylogenetic tree display and annotation. *Bioinformatics* **23**(1):127–128.

Appendix

TABLE A1: Used strains

Strain	Genotype	Reference/Source
Caulobacter crescentus		
CB15N	synchronizable derivative of wild-type *C. crescentus*	[36]
CJW1715	CB15N *mreB*$_{Q26P}$	[50]
CS606	CB15N Δ*bla*	[197]
AM52	CB15N Δ*vanA* P_{van}::P_{van}-*ftsN* Δ*ftsN*	[110]
AM160	CB15N *ftsN*::*ecfp-ftsN* P_{xyl}-*ftsZ-eyfp*	[144]
AM372	CB15N Δ*pbp1a* Δ*pbpY*	[144]
AM373	CB15N Δ*pbp1a* Δ*pbpZ*	[144]
AM457	CB15N P_{xyl}-*venus-pbpY*	[182]
AM458	CB15N P_{xyl}-*venus-pbpZ*	[182]
AM472	CB15N Δ*vanA* P_{van}::P_{van}-*ftsN* Δ*ftsN* P_{xyl}::P_{xyl}-*venus-pbpY*	[144]
AM473	CB15N Δ*vanA* P_{van}::P_{van}-*ftsN* Δ*ftsN* P_{xyl}::P_{xyl}-*venus-pbpX*	[144]
DK60	CB15N *ftsZ*::P_{iolC}-*ftsZ*	[182]
JK305	CB15N Δ*pbp1a* Δ*pbpC* Δ*pbpY* Δ*pbpZ*	[182]
KK1	CB15N Δ*pbpX*	[180]
KK12	CB15N Δ*pbp1a* Δ*pbpY* Δ*pbpZ*	[180]
KK16	CB15N Δ*pbpY*	[180]
KK17	CB15N Δ*pbpZ*	[180]
KK18	CB15N Δ*pbp1a*	[180]
KK24	CB15N Δ*pbpX* Δ*pbpZ*	[180]
KK33	CB15N P_{xyl}::P_{xyl}-*venus-pbp1a*	[180]
KK37	CB15N Δ*pbpY* Δ*pbpZ*	[180]
MT56	CB15N *ftsN*::*ecfp-ftsN* P_{xyl}::P_{xyl}-*mreB-eyfp*	[182]
MT258	CB15N Δ*dipM*	[150]
MT278	CB15N P_{xyl}::P_{xyl}-*venus-pbpX*	[182]
MT279	CB15N P_{xyl}::P_{xyl}-*venus-pbpC*	[70]
MT282	CB15N Δ*pbpC*	[182]
SS310	CB15N P_{xyl}::P_{xyl}-*cedD-mCherry*	S. Schlimpert, unpublished
SS313	CB15N Δ*bla* P_{xyl}::P_{xyl}-*cedD-bla*	S. Schlimpert, unpublished
SS330	CB15N P_{xyl}::P_{xyl}-*venus-cedC*	S. Schlimpert, unpublished
SS347	CB15N Δ*cedC*	S. Schlimpert, unpublished
SS348	CB15N *cedC*::*venus-cedC*	S. Schlimpert, unpublished
SS356	CB15N Δ*cedC* Δ*xerC*	S. Schlimpert, unpublished
SS362	CB15N P_{xyl}::P_{xyl}-*yigA-venus*	S. Schlimpert, unpublished
SS363	CB15N Δ*cedD* Δ*xerD*	S. Schlimpert, unpublished
SS367	CB15N Δ*xerD*	S. Schlimpert, unpublished
SS371	CB15N Δ*xerC*	S. Schlimpert, unpublished

TABLE A1: used strains: continued

Strain	Genotype	Reference/Source
SS372	CB15N Δ*xerC* Δ*xerD*	S. Schlimpert, unpublished
SS374	CB15N Δ*cedC* Δ*cedD* Δ*xerC* Δ*xerD*	S. Schlimpert, unpublished
SS376	CB15N Δ*cedC* P_{xyl}::P_{xyl}-*cedC*	S. Schlimpert, unpublished
SS426	CB15N Δ$cedD_{\Delta aa68\text{-}508}$	S. Schlimpert, unpublished
SS455	CB15N Δ*cedC* Δ$cedD_{\Delta aa68\text{-}508}$	S. Schlimpert, unpublished
WS041	CB15N Δ*pbp1a* Δ*pbpX* P_{xyl}::P_{xyl}-*venus-pbpX*	[182]
WS044	CB15N Δ*pbpX* Δ*pbpY* P_{xyl}::P_{xyl}-*venus-pbpX*	[182]
WS045	CB15N *pbpY*::*venus-pbpY*	[182]
WS055	CB15N *pbpX*::*venus-pbpX*	[182]
WS056	CB15N Δ*pbp1a* Δ*pbpC* Δ*pbpX* Δ*pbpY* Δ*pbpZ* P_{xyl}::P_{xyl}-*pbpX*	[182]
WS057	CB15N Δ*dipM* P_{xyl}::P_{xyl}-*venus-pbpY*	[182]
WS058	CB15N Δ*dipM* P_{xyl}::P_{xyl}-*venus-pbpX*	[182]
WS062	CB15N *ftsZ*::P_{iolC}-*ftsZ* P_{xyl}::P_{xyl}-*venus-pbpX*	[182]
WS063	CB15N *ftsZ*::P_{iolC}-*ftsZ* P_{xyl}::P_{xyl}-*venus-pbpY*	[182]
WS070	CB15N Δ*pbp1a* Δ*pbpC* Δ*pbpX* Δ*pbpY* Δ*pbpZ* P_{xyl}::P_{xyl}-*pbpX* P_{iolC}::P_{iolC}-*pbpX*	[182]
WS071	CB15N Δ*pbp1a* Δ*pbpC* Δ*pbpX* Δ*pbpY* Δ*pbpZ* P_{xyl}::P_{xyl}-*pbpX* P_{iolC}::P_{iolC}-*pbpY*	[182]
WS072	CB15N Δ*pbp1a* Δ*pbpC* Δ*pbpX* Δ*pbpY* Δ*pbpZ* P_{xyl}::P_{xyl}-*pbpX* P_{iolC}::P_{iolC}-*pbp1a*	[182]
WS073	CB15N Δ*pbp1a* Δ*pbpC* Δ*pbpX* Δ*pbpY* Δ*pbpZ* P_{xyl}::P_{xyl}-*pbpX* P_{iolC}::P_{iolC}-*pbpC*	[182]
WS074	CB15N Δ*pbp1a* Δ*pbpC* Δ*pbpX* Δ*pbpY* Δ*pbpZ* P_{xyl}::P_{xyl}-*pbpX* P_{iolC}::P_{iolC}-*pbpZ*	[182]
WS076	CB15N Δ*pbp1a* Δ*pbpC* Δ*pbpX* Δ*pbpY* Δ*pbpZ* P_{xyl}::P_{xyl}-*pbpX* P_{iolC}::pAMIOL-4	[182]
WS084	CB15N $mreB_{Q26P}$ P_{xyl}::P_{xyl}-*venus-pbpX*	[182]
WS085	CB15N $mreB_{Q26P}$ P_{xyl}::P_{xyl}-*venus-pbpY*	[182]
WS090	CB15N Δ*pbp1a* Δ*pbpX* Δ*pbpY* Δ*pbpZ* P_{xyl}::P_{xyl}-*pbpX*	[182]
WS093	CB15N *ftsZ*::P_{iolC}-*ftsZ* P_{xyl}::P_{xyl}-*venus-cedD*	This work
WS102	CB15N Δ*cedD* Δ*xerC* Δ*xerD*	This work
WS103	CB15N *cedC*::*venus-cedC* P_{van}::P_{van}-*ftsZ-ecfp*	This work
WS104	CB15N *cedC*::*venus-cedC* P_{xyl}::P_{xyl}-*ftsK-ecfp*	This work
WS105	CB15N Δ*recA*	This work
WS112	CB15N P_{xyl}::P_{xyl}-$yigA_{sup}$-*venus*	This work
WS113	CB15N Δ*cedD* Δ*xerC*	This work
WS116	CB15N Δ*cedC* Δ*cedD* Δ*xerC*	This work
WS117	CB15N P_{xyl}::P_{xyl}-*cedC*	This work
WS119	CB15N Δ*cedC* Δ*cedD* Δ*xerD*	This work
WS120	CB15N Δ*cedC* P_{xyl}::P_{xyl}-*cedC*	This work
WS121	CB15N Δ*cedC* Δ*xerC* Δ*xerD*	This work
WS123	CB15N *cedC*::*venus-cedC* P_{van}::P_{van}-*mCherry-ftsN*	This work
WS125	CB15N Δ*cedC* Δ*recA* P_{xyl}::P_{xyl}-*cedC*	This work
WS129	CB15N P_{xyl}::P_{xyl}-$cedC_{aa1\text{-}50}$	This work

TABLE A1: used strains: continued

Strain	Genotype	Reference/Source
WS130	CB15N P_{xyl}::P_{xyl}-*cedC*$_{aa1-98}$	This work
WS131	CB15N P_{xyl}::P_{xyl}-*cedC*$_{aa51-225}$	This work
WS132	CB15N P_{xyl}::P_{xyl}-*cedC*$_{aa99-225}$	This work
WS133	CB15N P_{xyl}::P_{xyl}-*cedC*$_{aa51-98}$	This work
WS134	CB15N *ftsA*::*ftsA*$_{T17M}$	This work
WS135	CB15N *ftsA*::*ftsA*$_{T17M}$ P_{xyl}::P_{xyl}-*yigA-venus*	This work
WS144	CB15N Δ*ftsA* P_{van}::P_{van}-*ftsA* P_{xyl}::P_{xyl}-*venus-cedC*	This study
WS145	CB15N Δ*ftsA* P_{van}::P_{van}-*ftsA* P_{xyl}::P_{xyl}-*yigA-venus*	This study
Escherichia coli		
BTH101	F^- *cya-99 araD139 galE15 galK16 rpsL1 hsdR2 mcrA1 mcrB1*, Str^R	Euromedex (France)
Rosetta™ (DE3) pLysS	F^- *ompT hsdSB*(*rB- mB-*) *gal dcm* (DE3) pLysSRARE2, Cam^R	Novagen (Germany)
TOP10	F^- *mcrA* Δ(*mrr-hsdRMS-mcrBC*) ϕ80*lacZ*ΔM15 Δ*lacX74 nupG recA1 araD139* Δ(ara-leu)7697 *galE15 galK16 rpsL*(Str^R) *endA1* λ-	Invitrogen (Germany)
XL1-blue	*recA1 endA1 gyrA96 thi-1 hsdR17 supE44 relA1 lac*	Stratagene (USA)
WS111	Rosetta™ (DE3) pLysS His_6-*sumo-cedC*	This study

TABLE A2: Used plasmids

Plasmid	Genotype/description	Reference/Source
pAMIOL-4	Integrating plasmid used for the expression of genes under the control of P_{iolC}, $Gent^R$	[182]
pKT25	Plasmid for constructing N-terminal fusions to T25, Kan^R	[192]
pKNT25	Plasmid for constructing C-terminal fusions to T25, Kan^R	[192]
pKT25-zip	Derivative of pKT25 in which the leucine zipper of GCN4 is genetically fused *in frame* to the T25 fragment, Kan^R	[192]
pUT18C	Plasmid for constructing N-terminal fusions to T18, Amp^R	[192]
pUT18	Plasmid for constructing C-terminal fusions to T18, Amp^R	[192]
pUT18C-zip	Derivative of pUT18C in which the leucine zipper of GCN4 is genetically fused *in frame* to the T18 fragment, Amp^R	[192]
pNPTS138	*sacB*-containing suicide vector for double homologous recombination, Kan^R	M. R. K. Alley, unpublished
pTB146	Plasmid for overexpression of N-terminally His_6-Sumo-tagged proteins, Amp^R	[63]
pVCERC-6	Integrating plasmid for constructing C-terminal fusions to Cerulean under the control of P_{van}, Cam^R	M. Thanbichler, unpublished
pVCHYN-1	Integrating plasmid for constructing N-terminal fusions to mCherry under the control of P_{van}, $Spec^R$	[40]
pXCFPC-2	Integrating plasmid for constructing C-terminal fusions to CFP under the control of P_{xyl}, Kan^R	[40]
pXVENC-2	Integrating plasmid for constructing C-terminal fusions to Venus under the control of P_{xyl}, Kan^R	[40]
pXVENN-1	Integrating plasmid for constructing N-terminal fusions to Venus under the control of P_{xyl}, $Spec^R$	[40]
pXVENN-2	Integrating plasmid for constructing N-terminal fusions to Venus under the control of P_{xyl}, Kan^R	[40]
pAM087	pXCFPC-2 carrying *ftsK*	A. Möll
pMT825	pVCHYN-1 carrying *ftsN*	M. Thanbichler
pSS249	pXVENN-2 carrying *cedC*	S. Schlimpert
pSS254	pNPTS138-based plasmid for generating an *in frame* deletion in *cedC*	S. Schlimpert
pSS269	pNPTS138-based plasmid for generating an *in frame* deletion in *cedC-xerC*	S. Schlimpert
pSS270	pNPTS138-based plasmid for generating an *in frame* deletion in *cedD-xerD*	S. Schlimpert
pSS271	pNPTS138-based plasmid for generating an *in frame* deletion in *xerC*	S. Schlimpert
pSS290	pXVENC-2 carrying *yigA*	S. Schlimpert
pSS316	pNPTS138-based plasmid for generating an *in frame* deletion in $cedD_{aa38\text{-}508}$	S. Schlimpert
pSS321	pKNT25 carrying $ftsK_{aa333\text{-}493}$	S. Schlimpert
pSS322	pUT18C carrying *cedC*	S. Schlimpert
pSS323	pKT25 carrying *cedC*	S. Schlimpert
pSS324	pUT18 carrying $ftsK_{aa333\text{-}493}$	S. Schlimpert
pSS341	pUT18 carrying *xerC*	S. Schlimpert

TABLE A2: used plasmids: continued

Strain	Genotype/description	Reference/Source
pSS342	pUT18 caryying *xerD*	S. Schlimpert
pSS343	pKNT25 carrying *xerC*	S. Schlimpert
pSS344	pKNT25 carrying *xerD*	S. Schlimpert
pSW15	pVCERC-6 carrying *ftsZ*	S. Wick
pTB146	Vector for overexpression of N-terminally His_6-SUMO-tagged proteins, Amp^R	[63]
pWS79	pNPTS138-based plasmid for generating an *in frame* deletion in *recA*	This study
pWS89	pTB146 carrying *cedC*	This study
pWS90	pXVENN-1 carrying *cedC* without *venus*	This study
pWS99	pXVENN-1 carrying $cedC_{aa1\text{-}50}$	This study
pWS100	pXVENN-1 carrying $cedC_{aa1\text{-}98}$	This study
pWS101	pXVENN-1 carrying $cedC_{aa51\text{-}225}$	This study
pWS102	pXVENN-1 carrying $cedC_{aa99\text{-}225}$	This study
pWS103	pXVENN-1 carrying $cedC_{aa51\text{-}98}$	This study
pWS105	pNPTS138-based plasmid for replacing *ftsA* with $ftsA_{T17M}$	This study

Table A3: Used oligonucleotides

Name	Sequence (5' - 3')
IntSpec-1	atgccgtttgtgatggcttccatgtcg
IntXyl-2	tcttccggcaggaattcactcacgcc
M13for	gccagggttttcccagtcacga
M13rev	gagcggataacaatttcacacagg
eGYC-up	cttgccgtaggtggcatcgccctcg
eGYC-down	gctgctgcccgacaaccactacctgag
mCherry-up	ctcgccctcgccctcgatctcgaac
mCherry-down	ggcgcctacaacgtcaacatcaagttgg
REV-uni	ggggatgtgctgcaaggcgattaagttg
RecVan-2	cagccttggccacggtttcggtacc
RecIol-2	tcaagggtctttgcgtcctgggcc
Pxyl-for	tgtcggcggcttctagcatggaccg
Pvan-for	tggactctagccgaccgactgagacgc
Piol-for	aaggaagaacgcaaggcccagaagg
pUT18C-rev	tcagcgggtgttggcgggtgtc
pUT18-for	ccaggctttacactttatgcttcc
pUT18-rev	gacgcgcctcggtgcccactgc
pKT25-for	ccgccggacatcagcgccattc
pKT25-rev	ccgccggacatcagcgccattc
pKNT25-for	cccaggctttacactttatgcttcc
pKNT25-rev	gtttttttccttcgccacggccttg
oSS470	attaattcatatgagcgacgcgacgcgagcgacc
oSS471	tagagctcccaggacgggccagcgttcggccg
oSS473	tagagctctcacaggacgggccagcgttcgg
oWS62	atataagcttgagatgcggccttgattctcggg
oWS64	ctcgtggccctggtcggcggcccggaag
oWS65	atatgaattcgagcagcgaggggtggtgagttg
oWS66	atgctcttcaggtatgagcgacgcgacgcg
oWS67	atatggatcctcacaggacgggccagcgttc
oWS70	gcgcgcgttcccgccc
oWS71	caacgccctgatgcggtaaaatcg
oWS72	gacccgctccagcaccggc
oWS73	gccacggcgttgtccttgaacac
oWS74	gacctgcacgaagtcgatgccg
oWS75	cgggtttcttcggacatgggagg
oWS76	ggcctgcgcgttgcaggac
oWS77	cttgagctcatcctcggcctccttg
oWS95	atatggtaccatgagcgacgcgacgcg
oWS96	atatgagctctcagtcgacgacgttggccgc
oWS97	atatgagctctcagcgggcgtcgagcatgtc
oWS98	atatggtaccatgtttggcccgcgcgcc
oWS99	atatggtaccatgaaccactccgatctcgcccg
oWS100	atatgagctctcacaggacgggccagcg
oWS109	atataagcttcacgcagcctggcatgacg
oWS110	atatggatccggacgacccaggcgaacg

TABLE A3: used oligonucleotides: continued

Name	Sequence (5' - 3')
oWS121	atatggtaccatgtttggcccgcgcgcc
oWS122	atatgagctctcagcgggcgtcgagcatgtc

TABLE A4: Construction of strains and plasmids

Strain	Genotype
Strains	
WS093	Integration of pSS249 at the *xylX* locus of DK60
WS102	Double homologous recombination for *in-frame* deletion of *ceD-xerD* by use of pSS270 in SS371
WS103	Integration of pSW15 at the *vanA* locus of SS348
WS104	Integration of pAM087 at the *xyl* locus of SS348
WS105	Double homologous recombination for *in-frame* deletion of *recA* by use of pWS79 in CB15N
WS111	Transformation of pWS89 in *E. coli* Rosetta™
WS112	Overexpression of YigA-Venus for four days to obtain suppressor mutants
WS113	Double homologous recombination for *in-frame* deletion of *xerC* by use of pSS271 in SS426
WS116	Double homologous recombination for *in-frame* deletion of *cedD* by use of pSS316 in SS356
WS117	Integration of pWS90 at the *xylX* locus of CB15N
WS119	Double homologous recombination for *in-frame* deletion of *cedC* by use of pSS254 in SS363
WS120	Double homologous recombination for *in-frame* deletion of *cedC* by use of pSS254 in WS117
WS121	Double homologous recombination for *in-frame* deletion of *cedC-xerC* by use of pSS269 in SS367
WS123	Integration of pMT825 at the *vanA* locus of SS348
WS125	Double homologous recombination for *in-frame* deletion of *recA* by use of pWS79 in WS120
WS129	Integration of pWS99 at the *xylX* locus of CB15N
WS130	Integration of pWS100 at the *xylX* locus of CB15N
WS131	Integration of pWS101 at the *xylX* locus of CB15N
WS132	Integration of pWS102 at the *xylX* locus of CB15N
WS133	Integration of pWS103 at the *xylX* locus of CB15N
WS134	Double homologous recombination for point mutation in *ftsA* by use of pWS105 in CB15N
WS135	Integration of pSS290 at the *xylX* locus of WS134
Plasmids	
pWS79	Amplification of ∼600 bp of the upstream and downstream region of *recA* from CB15N chrom. DNA using oligos oWS62/oWS65 and oWS64/oWS65, overlap-extension PCR using primers oWS62/oWS65 and restriction digest of the PCR product using HindIII / EcoR with subsequent ligation into equally treated pNPTS138.
pWS89	Amplification of *cedC* from CB15N chrom. DNA using oligos oWS66 and oWS67, sequential restriction with SapI / BamHI and ligation into pTB146 treated with SapI / BamHI.
pWS90	Amplification of *cedC* from CB15N chrom. DNA using oligos oSS470 and oSS473, restriction with NdeI / SacI and ligation into pXVENN-1 treated with NdeI / SacI.
pWS99	Amplification of $cedC_{aa1\text{-}50}$ from CB15N chrom. DNA using oligos oWS95 and oWS96, restriction with KpnI / SacI and ligation into pXVENN-1 treated with KpnI / SacI.

TABLE A4: construction of strains and plasmids: continued

Strain	Genotype
pWS100	Amplification of $cedC_{aa1\text{-}98}$ from CB15N chrom. DNA using oligos oWS95 and oWS97, restriction with KpnI / SacI and ligation into pXVENN-1 treated with KpnI / SacI.
pWS101	Amplification of $cedC_{aa51\text{-}225}$ from CB15N chrom. DNA using oligos oWS98 and oWS100, restriction with KpnI / SacI and ligation into pXVENN-1 treated with KpnI / SacI.
pWS102	Amplification of $cedC_{aa99\text{-}225}$ from CB15N chrom. DNA using oligos oWS99 and oWS100, restriction with KpnI / SacI and ligation into pXVENN-1 treated with KpnI / SacI.
pWS103	Amplification of $cedC_{aa51\text{-}98}$ from CB15N chrom. DNA using oligos oWS121 and oWS122, restriction with KpnI / SacI and ligation into pXVENN-1 treated with KpnI / SacI.
pWS105	Amplification of the *ftsQA*' operon from WS112 (clone 7) using oligos oWS109 and oWS110, restriction with HindIII / BamHI and ligation into equally treated pNPTS138.

TABLE A5: Co-immunoprecipitation results of CedC (hits which occur both in the control [WT] and strain SS348 were omitted.

Protein name	Protein MW [kDa]	Peptide count	Total ion score
5-methyltetrahydropteroyltriglutamate-homocysteine methyltransferase [*Caulobacter crescentus* NA1000]	84.3	14	1217
hypothetical protein CCNA_00350 (CedC) [*Caulobacter crescentus* NA1000]	24,9	8	472
ATP synthase alpha chain [*Caulobacter crescentus* NA1000]	55.3	6	353
S-adenosylmethionine synthetase [*Caulobacter crescentus* NA1000]	43.8	5	223
chaperonin GroEL [*Caulobacter crescentus* NA1000]	57.4	5	218
TonB accessory protein ExbB [*Caulobacter crescentus* NA1000]	30.8	1	125
hypothetical cytosolic protein [*Caulobacter crescentus* NA1000]	28.9	2	123
pyruvate dehydrogenase complex, dihydrolipoamide acetyl-transferase component [*Caulobacter crescentus*]	44	2	122
phosphogluconate dehydratase [*Caulobacter crescentus* NA1000]	63.1	3	119
citrate synthase [*Caulobacter crescentus* NA1000]	47.9	2	110
ATP synthase beta chain [*Caulobacter crescentus* NA1000]	56.8	2	109
sulfate adenylyltransferase subunit 1/adenylylsulfate kinase [*Caulobacter crescentus* NA1000]	69.8	1	92
GTP-binding protein TypA/BipA [*Caulobacter crescentus* NA1000]	67	3	85
pyruvate phosphate dikinase [*Caulobacter crescentus* NA1000]	97.1	2	82
SSU ribosomal protein S4P [*Caulobacter crescentus* NA1000]	23.3	2	78
3-isopropylmalate dehydratase large subunit [*Caulobacter crescentus* NA1000]	50.7	2	77
LSU ribosomal protein L19P [*Caulobacter crescentus* NA1000]	14.8	1	75
methionine synthase I metH [*Caulobacter crescentus* NA1000]	99	2	74
DNA-directed RNA polymerase beta chain [*Caulobacter crescentus* NA1000]	15.1	3	70
RecA protein [*Caulobacter crescentus* NA1000]	37.9	2	68

TABLE A6: Suppressor mutations identified by whole-genome sequencing

Gene	Description	Mutation	Annotation
CCNA_00945	chemotaxis protein MotD	C→G	T112T (ACC→ACG)
CCNA_02578	hypothetical protein	Δ210bp	/
ftsA	cell division protein	G→A	T17M (ACG→ATG)
serS	seryl-tRNA synthetase	$(C)_{6\rightarrow5}$	coding (1435/1449 nt)
cspC	cold shock protein CspC	A→C	D46E (GAT→GAG)

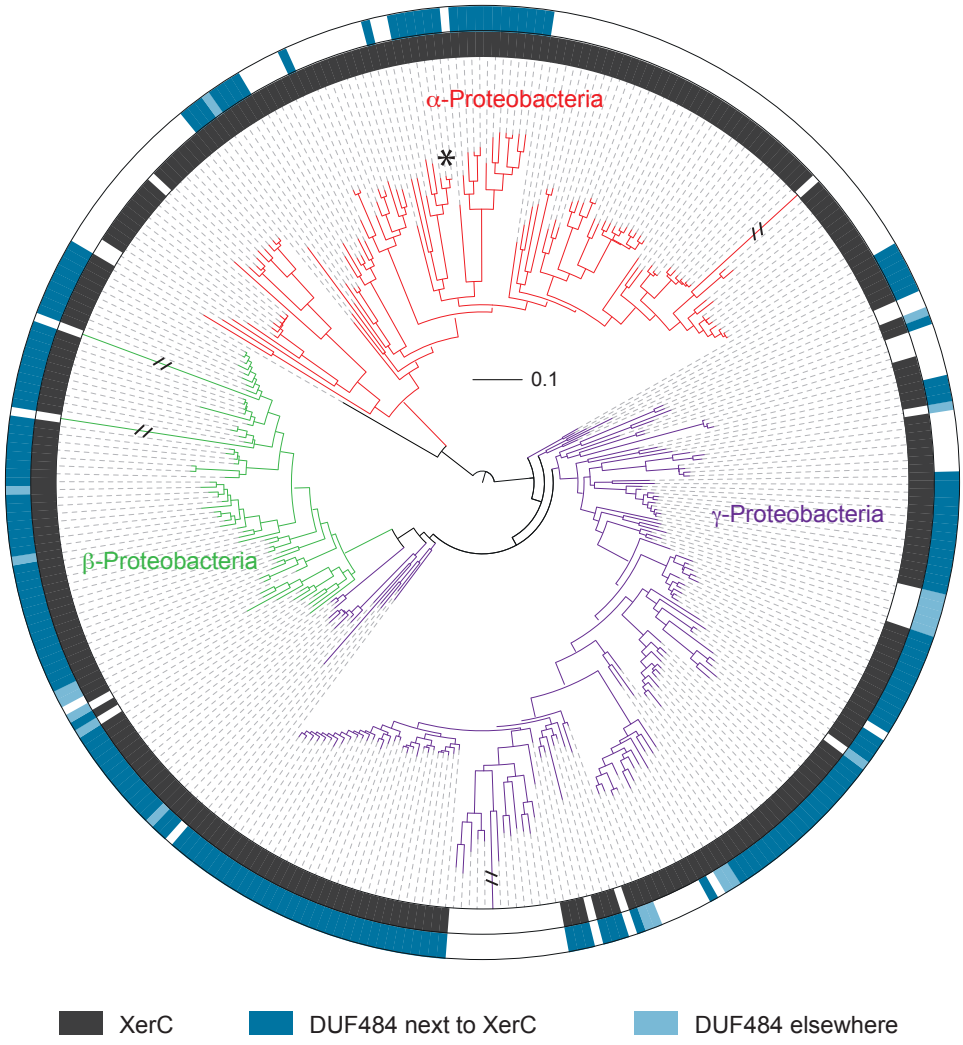

FIGURE A1: Distribution of XerC and CedC homologs. The phylogenetic tree harbors 338 representatives of α-, β-, γ-proteobacteria and *Magnetococcus* from a concatenated multiple sequence alignment of 16S and 23S rRNA sequences. Red, green, and purple branches indicate sequences encoded in α-, β-, γ-proteobacterial genomes, respectively. The black branch basal to the α-proteobacteria clade represents *Magnetococcus*. The asterisk indicates the location of *C. crescentus*. The four branches crossed by black lines correspond to divergent sequences encoded in endosymbiont genomes (*Carsonella ruddii, Hodgkinia cicadicola, Tremblaya princeps*, and *Zinderia insecticola*) and are not shown at their full length for presentation purposes. Bioinformatic analyses were performed and the phylogenetic tree was generated by Dr. K. Wuichet, Søgaard-Andersen lab.

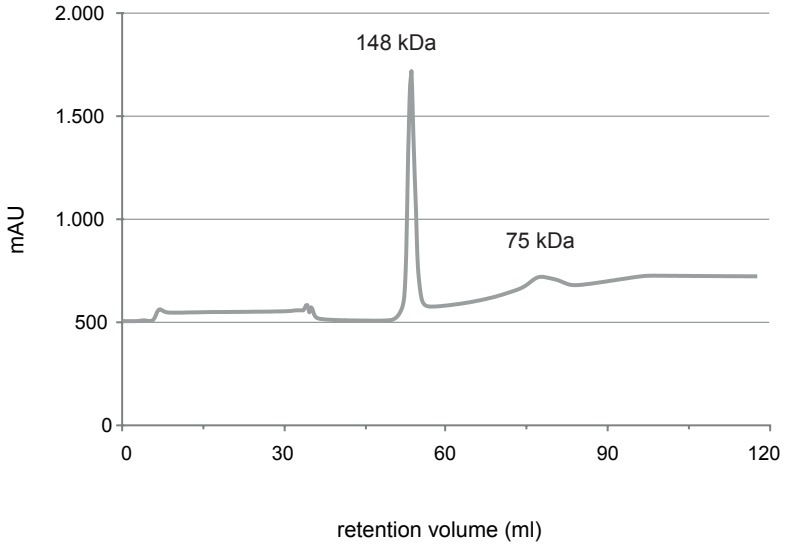

FIGURE A2: Size exclusion chromatography to assess the oligomerization state of purified CedC. The gel filtration was performed using an Äkta Purifier System 10 and Superdex200 column. The injection volume was 4 ml. The protein mass was evaluated using a calibration curve, which was recorded before. The major peak corresponds to a molecular mass of 148 kDa, which is equivalent to the exact size of four (tetramer) CedC monomers ($\sim$ 37 kDa), whereas the small peak corresponds to dimer formation.

Acknowledgements

Curriculum vitae

Erklärung

Ich versichere, dass ich meine Dissertation:

“Last but not least - Late cell division proteins in *Caulobacter crescentus*”

selbständig, ohne unerlaubte Hilfe angefertigt und mich dabei keiner anderen als der von mir ausdrücklich bezeichneten Quellen und Hilfen bedient habe. Die Dissertation wurde in der jetzigen oder einer ähnlichen Form noch bei keiner anderen Hochschule eingereicht und hat noch keinen sonstigen Prüfungszwecken gedient.

Marburg, den .....

.....
Wolfgang Strobel